

DEVELOPMENT OF PARTICLE SIZING BASED ON DYNAMIC
IMAGE ANALYSIS

Thesis submitted for the degree of
Doctor of Philosophy
at the University of Leicester

by

Mohd Farid bin Muhamad Said

Thermal & Fluid Engineering /Department of Engineering
University of Leicester

March 2011

Mohd Farid bin Muhamad Said

Development of Particle Sizing Based on Dynamic Image Analysis

Abstract

Dispersion of particles in multiphase-flows can be both quantitatively and qualitatively characterised using modern optical or nonintrusive devices. The development of a non-intrusive particle sizer (NPS) is performed. This device employs a high intensity pulsed laser as a light source and a digital camera to capture the particle images. The dynamic image analysis (DIA) software is designed to analyse the captured images and control the inputs and outputs of the data. The NPS has the ability to operate using shadow sizing, direct illumination (DI) and particle mixture shadow (PMS) techniques. The architecture and working principles of each technique are described in detail. A novel technique, which is Particle Mixture Shadow has been developed for the characterisation of solid/liquid mixture dispersed in air. The capability of the technique to distinguish and size the solid and liquid particles is demonstrated. The sensitivities of laser intensity, image magnification factor and scattering angle on the accuracy of particle size have been investigated. In order to evaluate the repeatability and the accuracy of the NPS device, the measurements of certified microsphere particle sizes are repeated several times. The results are then validated against proprietary particles with specification data provided by the manufacturer. The particle size error of the developed device confirms that it has a good repeatability in sizing the particles. The device is applied to solid and liquid particles dispersed in fluid media using shadow and DI techniques. The results comparison between these techniques is also demonstrated.

Acknowledgements

First of all, I would like to express my gratitude to my supervisor, Professor Abdelwahab Aroussi for his encouragement, supervision, support, patience and tolerant throughout the years. This thesis would not have been possible without his kindness and guidance to work on such interesting project. I wish to thank to the Ministry of Higher Education Malaysia and Universiti Teknologi Malaysia for the financial support throughout the study.

I would like to acknowledge Dr. Chris Coats for his valuable advice in preparing my thesis as well as my experimental work. I also would like to thank the staff of the Department of Engineering at the University of Leicester for their help and assistance, especially Dipak Raval and Paul Williams. I also wish to acknowledge my colleagues for their assistance and support during this project.

Most importantly, I would like to thank my parents and in-laws for theirs love, support and constant encouragement. Finally, special thank to my wife, Fara Rahman who put her career on hold to accompany me here. Her understanding and moral support has made the difficult times during my study bearable.

List of Contents

Abstract	ii
Acknowledgements	iii
List of Contents	iv
List of Figures	ix
List of Tables	xvi
Abbreviations	xvii
Symbols	xix
Chapter 1 Introduction	1
1.1 Background	1
1.2 Problem Definition.....	2
1.3 Objective	3
1.4 Methodology	4
1.5 Thesis Layout.....	4
Chapter 2 Literature Review.....	6
2.1 Introduction	6
2.2 Review of Particle Size Measurement Techniques.....	8
2.2.1 Intrusive - Solid Particles	9
2.2.2 Intrusive - Liquid Particles	11
2.2.3 Non-intrusive/Optical.....	12
2.3 Light Scattering Techniques	13

2.3.1	Laser Diffraction	13
2.3.2	Phase Doppler Anemometry.....	15
2.4	Imaging Techniques	16
2.4.1	Shadow Sizing	17
2.4.2	Direct Illumination	19
2.4.3	Interferometric Particle Imaging	21
2.5	Summary of Particle Size Measurement Techniques.....	22
2.6	Representation of Particle Size	25
2.6.1	Size Distribution.....	26
2.6.2	Frequently Used Size Distribution Functions	30
2.6.3	Statistical Parameters.....	33
Chapter 3	Fundamental of Image Processing	36
3.1	Introduction	36
3.2	Parameters of an Imaging System.....	36
3.3	Electronic Imaging	39
3.3.1	Charge Coupled Device.....	39
3.3.2	Charge Coupled Device Size.....	39
3.3.3	Monochrome CCD Camera.....	40
3.3.4	Interlaced and Progressive Scan.....	40
3.3.5	Frame Rate and Shutter Speed	40
3.4	Illumination	41
3.4.1	White Light.....	41

3.4.2	Laser	43
3.5	Image Processing Fundamentals	44
3.5.1	Digital Image Representation	44
3.5.2	Grey Level Histogram	45
3.5.3	Lookup Tables	46
3.5.4	Convolution Kernels.....	46
3.5.5	Spatial Filtering	48
3.5.6	Segmentation and Thresholding.....	49
3.5.7	Morphological Functions	50
3.6	Summary	51
Chapter 4	Development of the Dynamic Image Analysis Software.....	52
4.1	Introduction	52
4.2	Shadow Module	53
4.2.1	Algorithm for Solid Particles	54
4.2.2	Algorithm for Liquid Particles	61
4.2.3	Algorithm for a Mixture of Solid and Liquid Particles	64
4.3	Direct Illumination Module.....	70
4.3.1	Algorithms for Solid Particles	70
4.3.2	Algorithm for Liquid Particles	74
4.4	Measured Parameters from the Image.....	80
4.4.1	Particle Size	81
4.4.2	Particle Shape	81

4.4.3	Particle Concentration	81
4.5	Conclusions	82
Chapter 5	The Non-Intrusive Particle Sizer.....	84
5.1	Introduction	84
5.2	Instrument Design	85
5.2.1	Requirement Specification	85
5.2.2	Operating Principle.....	87
5.3	Calibration of the NPS	88
5.4	Particle Sizing by the Shadow Technique.....	90
5.4.1	Measurement of the Certified Microsphere Particle Size Standard	92
5.4.2	Measurement of Fillite particles	97
5.4.3	Evaluation of the Measurements of Liquid Particles	103
5.5	Parametric Study with the Shadow Technique	105
5.5.1	Certified Microsphere - Laser Intensity	106
5.5.2	Certified Microsphere - Image Magnification.....	109
5.5.3	Fillite Particles - Laser Intensity.....	113
5.5.4	Fillite Particles - Image Magnification.....	116
5.6	Particle Sizing by Direct Illumination Technique.....	119
5.7	Parametric Study on DI Technique	121
5.7.1	Fillite Particles - Laser Intensity.....	122
5.7.2	Fillite Particles - Scattering Angle	125
5.7.3	Liquid Particles - Laser Intensity	127

5.7.4	Liquid Particles - Scattering Angle	130
5.8	Characterisation of Solid and Liquid Particles Dispersed in Air	135
5.9	Conclusions	138
Chapter 6	Conclusions and Suggestions for Future Work.....	140
6.1	Conclusions	140
6.2	Recommendations for further work:	142
	References	145
Appendix A	Publications, Recognitions, Conferences	153
Appendix B	Dynamic Image Analysis Software	156
Appendix C	Certificate of Size Calibration	159

List of Figures

Figure 2.1: Particle size range of some particulate material [2].	7
Figure 2.2: Particle characterisation techniques.	9
Figure 2.3: Working principle of imaging technique.	17
Figure 2.4: Schematic representation of the experimental setup for the shadow sizing technique [40].	18
Figure 2.5: Two different setups produced by Carter et al. in sizing the particles by DI technique (a) Scattering angle at 90° [36], (b) Scattering angle at about 135° [46].	20
Figure 2.6: Schematic of the optical paths of reflection and refraction points through transparent spherical particle [50].	21
Figure 2.7: Focus and defocus images from a spherical particle [54].	22
Figure 2.8: Number size distribution of particles based on linear abscissa.	27
Figure 2.9: Number size distribution of particles based on logarithmic abscissa.	28
Figure 2.10: Relation between number and volume distribution.	29
Figure 2.11: Comparison between number and volume size distribution.	30
Figure 2.12: Number based distribution of (a) Normal and (b) Log-normal distributions.	32
Figure 2.13: Rosin-Rammler distribution.	32
Figure 2.14: Locations of representative particle size.	35
Figure 3.1: Fundamental parameters of an imaging system.	37
Figure 3.2: Illustration of the ratio between CCD sensor size with FOV.	38
Figure 3.3: Illustration of the dimensions in (mm) of CCD standard sizes camera.	39
Figure 3.4: Electromagnetic spectrum [71].	42
Figure 3.5: Spectral sensitivity of the XCD-SX90 SONY camera [72].	42

Figure 3.6: Properties of laser light [73].....	43
Figure 3.7: (a) Greyscale image representation. (b) Grey levels for 8-bit image.	45
Figure 3.8: Sample of particles image with its associated grey level histogram.	46
Figure 3.9: Examples of kernels.	47
Figure 3.10: Mechanics of filtering [74]	48
Figure 4.1: A schematic diagram of the DIA software.....	52
Figure 4.2: The flowchart of the DIA software for the shadow technique module.....	54
Figure 4.3: Sequence of solid particles image analysis in shadow module.....	55
Figure 4.4: Images of the sequence of solid particle image analysis by the shadow module.	58
Figure 4.5: An edge and hole area of single solid particle image analysed by the shadow module.	59
Figure 4.6: Detected %Area in relation to solid particle size and image magnification factor.	60
Figure 4.7: Sequence of liquid or transparent particles image analysis in the shadow module.	61
Figure 4.8: Images of the sequence of liquid particle analysis by the shadow module..	63
Figure 4.9: An edge and hole area of single liquid particle image.	64
Figure 4.10: Detected %Area in relation to liquid particle size and IMF.....	64
Figure 4.11: Method to differentiate between solid and liquid particles in the shadow module.	65
Figure 4.12: Image processing sequence for the solid and liquid particles recognition.	69
Figure 4.13: Sequence of steps used in analysing the solid particles images in DI module.	71

Figure 4.14: Image Processing Sequence for solid particles analysis by the DI module.	73
Figure 4.15: Sequence of steps used in the DI module to analyse the liquid particles images.....	75
Figure 4.16: Processed images of each step of the liquid particles analysis by the DI module.....	77
Figure 4.17: Extraction of liquid particles from the Removed Border image.....	78
Figure 4.18: (a) Produced image after particle analysis function, (b) Method to determine single particle size from two glare points.....	78
Figure 4.19: Successfully detected particles are plotted with their diameter size on the acquired image.....	80
Figure 5.1: General diagram of the NPS.....	87
Figure 5.2: The objective Micrometer Plate.....	88
Figure 5.3: Calibrated image acquired from the objective micrometer plate.....	89
Figure 5.4: NPS setup for the shadow technique.....	90
Figure 5.5: The geometrical configuration of the shadow imaging technique.....	91
Figure 5.6: Examples of acquired raw images by NPS. (a) solid particles dispersed in air, (b) liquid particles dispersed in air.....	92
Figure 5.7: The Microsphere particles used for validation purposes.....	93
Figure 5.8: Experimental setup of size measurement for particles suspended in water using the shadow technique.....	94
Figure 5.9: Image of certified particles dispersed in water by the NPS. (a) acquired raw image, (b) Processed image.....	95
Figure 5.10: Number based size distribution of certified particles.....	96
Figure 5.11: Mean size and standard deviation of certified particles.....	96

Figure 5.12: Mean size and standard deviation error of certified particles.	96
Figure 5.13: Image of Fillite particles measured by SEM.	98
Figure 5.14: Number size distribution of Fillite particles measured by SEM.	98
Figure 5.15: Different types of mean values measured by SEM that represent the Fillite particle size.	99
Figure 5.16: An image of Fillite particles dispersed in water. (a) acquired raw image, (b) Processed image.	100
Figure 5.17: Number based size distribution of Fillite particles.	102
Figure 5.18: Mean size and standard deviation of Fillite particles.	102
Figure 5.19: Mean size and standard deviation error of Fillite particles.	102
Figure 5.20: Particle size and its error at 10, 50 and 90% of cumulative distribution..	103
Figure 5.21: Image of liquid particles dispersed in air. (a) acquired raw image, (b) Processed image.	103
Figure 5.22: Number density and cumulative distribution of spray droplets.	104
Figure 5.23: Mean size and size at 10, 50 and 90% of cumulative distribution.	104
Figure 5.24: Particle shape of spray droplets.	105
Figure 5.25: Acquired and processed images of the certified microsphere for IMF = 0.8 at different LI.	107
Figure 5.26: Numbered density and cumulative size distribution of the certified microspheres for IMF = 0.8 at different LI.	108
Figure 5.27: Mean sizes of the certified microspheres and their errors for IMF = 0.8 at different LI.	109
Figure 5.28: Optimum LI of the certified microspheres at different IMF.	109
Figure 5.29: Numbered density and cumulative size distribution of the certified microspheres for optimum LI at different IMF.	111

Figure 5.30: Mean sizes of the certified microspheres and their standard distribution for optimum LI at different IMF.	111
Figure 5.31: Mean size errors of the certified microspheres and their standard deviation errors for optimum LI at different IMF.	112
Figure 5.32: Particle shape and detected number of particle of the certified microspheres.	112
Figure 5.33: Particle area in pixels and the dimension of single pixels size of the certified microspheres.	113
Figure 5.34: Acquired and processed images of the Fillite particles for IMF of 0.8 at different LI.	114
Figure 5.35: Numbered density and cumulative size distribution of Fillite for IMF of 0.8 at different LI.	115
Figure 5.36: Mean sizes of the Fillite and their errors for IMF = 0.8 at different LI. ..	115
Figure 5.37: Optimum LI of the Fillite at different IMF.	116
Figure 5.38: Numbered density and cumulative size distribution of the Fillite particles for optimum LI at different IMF.	117
Figure 5.39: Mean sizes of the Fillite particles and their standard distribution for optimum LI at different IMF.	118
Figure 5.40: Mean size errors of the Fillite particles and their standard deviation errors for optimum LI at different IMF.	118
Figure 5.41: Particle shape and detected number of particle of the Fillite particles.	119
Figure 5.42: Particle area in pixels and dimension of single pixels size of the Fillite particles.	119
Figure 5.43: NPS setup for the direct illumination technique.	120

Figure 5.44: Examples of acquired raw images by DI technique. (a) solid particles dispersed in air ($SA = 90^0$), (b) liquid particles dispersed in air ($SA = 70^0$).	121
Figure 5.45: Experimental setup of size measurement for particles suspended in water using DI technique.	123
Figure 5.46: Acquired and processed images of the Fillite particles for $IMF = 0.8$ at different LI.	124
Figure 5.47: Mean particle size and its error at different LI.	125
Figure 5.48: Particle size and its error at 10, 50 and 90% of cumulative distribution..	125
Figure 5.49: Mean particle size and its error at different SA.	126
Figure 5.50: Particle size and its error at 10, 50 and 90% of cumulative distribution..	126
Figure 5.51: Experimental setup of droplet sizing by DI technique.	127
Figure 5.52: Acquired and processed images of the liquid particles for $IMF = 0.8$ at different LI.	128
Figure 5.53: Mean particle size and its error at different LI.	129
Figure 5.54: Particle size and its error at 10, 50 and 90% of cumulative distribution..	129
Figure 5.55: Schematic configuration of the DI method	131
Figure 5.56: In-focus image of two glare points of a droplet	132
Figure 5.57: Acquired images and greyscale plots of liquid particles at 30^0 , 50^0 , 70^0 and 90^0 scattering angle.	133
Figure 5.58: Greyscale ratio between reflection and refraction points.....	134
Figure 5.59: Comparison of numbered size distribution between DI, Shadow and work done by Hess [48] using Equation 5.1.	134
Figure 5.60: (a) Particle size at 10, 50 and 90% of cumulative distribution obtained DI, Shadow and work done by Hess [48] using Equation 5.1. (b) Particle size error obtained by DI compared to the shadow technique.	135

Figure 5.61: Acquired image by PMS technique that contain solid and liquid particles.	136
Figure 5.62: Processed image by PMS technique that contain solid and liquid particles.	136
Figure 5.63: Size distribution of liquid and solid particles dispersed in air measured by PMS technique.....	137
Figure 5.64: %Area that represents solid and liquid particles.....	138
Figure B.1: Front panel of the DIA software shows the captured and processed images.	155
Figure B.2: Front panel of the DIA software shows the size number distribution of local and average values.....	156
Figure B.3: Front panel of the DIA software shows the size volume distribution of local and average values.....	157
Figure B.4: Front panel of the DIA software shows the distribution of circularity factor and particle concentration for local and average values.....	158

List of Tables

Table 2.1: Examples of particulate material (adapted from [2]).....	6
Table 2.2: Types of equivalent spherical diameters [2].....	26
Table 2.3: Symbols that represent size distribution [66].	28
Table 2.4: Definition of the term that represents particle sizes [1].....	34
Table 3.1: Types of spatial filters.	49
Table 5.1: Static image calibration results.....	90
Table 5.2: Properties of the certified particles.....	93
Table 5.3: Data of Fillite size distribution provided by the manufacturer.....	97
Table 5.4: Matrix of experiments to identify the optimum value of IMF and LI.....	106
Table 5.5: Matrix of experiments to identify the optimum value of LI and SA.....	122

Abbreviations

CCD	Charge Coupled Device
CF	Circularity Factor
CVS	Compact Vision System
DI	Direct Illumination
DIA	Dynamic Image Analysis
DOF	Depth of Field
FOV	Field of View
IMF	Image Magnification Factor
IPI	Interferometric Particle Imaging
LALLS	Low-Angle Laser Light Scattering
LD	Laser Diffraction
LI	Laser Intensity
LUT	LookUp Table
MSI	Mie Scattering Imaging
NIST	National Institute of Standards and Technology
NPS	Nonintrusive Particle Sizer
PDA	Phase Doppler Anemometry
PMS	Particle Mixture Shadow
PSD	Particle Size Distribution
RI	Refractive Index
RR	Rosin Rammler
SA	Scattering Angle
SEM	Scanning Electron Microscopy

SLS	Static Light Scattering
SMD	Sauter Mean Diameter

Symbols

$\%Area$	Percentage Area
A_E	Edge Area
A_{g1}	Area of Glare Point 1
A_{g2}	Area of Glare Point 2
A_H	Hole Area
A_p	Area of the Particle
c	Distribution Constant (Rosin Rammler)
C_{12}	Distance Between Two Glare Points
d	Equivalent Spherical Diameter
D	Particle Diameter of Size
$d_{0.1}$	The size indicates that 10% of total particle are below its size.
$d_{0.5}$	The size indicates that 50% of total particle are below its size.
$d_{0.9}$	The size indicates that 90% of total particle are below its size.
d_{32}	Sauter Mean Diameter
d_A	Equivalent Projected Area Diameter
D_e	Reference Size Constant (Rosin Rammler)
d_{g1}	Diameter of Glare Point 1
d_{g2}	Diameter of Glare Point 2
D_{gp}	Droplet Size Based on Glare Point Technique
D_i	Mid-point of Size Interval
d_{mean}	Mean Particle Size
d_{peak}	Peak Size of the Histogram or Density Distribution.
d_S	Equivalent Surface Area Diameter
d_{Si}	Equivalent Sieve Diameter

d_V	Equivalent Volume Diameter
GP	Separation Between Glare Points
m	Mass of Particle
N	Number of Particles
P_{act}	Actual Perimeter
PC	Particle Concentration
P_{eq}	Equivalent Spherical Perimeter
$q_0(d)$	Number Based Density Size Distribution
$Q_0(d)$	Number Based Cumulative Size Distribution
$q_1(d)$	Length Based Density Size Distribution
$Q_1(d)$	Length Based Cumulative Size Distribution
$q_2(d)$	Area Based Density Size Distribution
$Q_2(d)$	Area Based Cumulative Size Distribution
$q_3(d)$	Volume or Mass Based Density Size Distribution
$Q_3(d)$	Volume or Mass Based Cumulative Size Distribution
\bar{q}_r	Density Distribution on Each Interval
$q_r(d)$	General Symbol for Density Size Distribution
$Q_r(d)$	General Symbol for Cumulative Size Distribution
V	Volume of Particle
ΔD	Size Interval
θ	Scattering Angle
μ	Mean Size
μ_g	Geometric Mean Size
σ	Standard Deviation
σ_g	Geometric Standard Deviation

Chapter 1

Introduction

1.1 Background

Multi-phase flows invariably mean a carrier fluid in which particles are embedded. The carrier fluid is either gas or a liquid and the particles are either droplets, bubbles, solid particles or a combination of these. In each application, the particles are characterised to determine the performance and quality of the products. Particle characterisation is very important in applications such as fuel sprays combustion, pulverised coal combustion, control of particulate emissions, powder manufacturing, agricultural sprays, pharmaceuticals, domestic sprays and spray drying of food industry.

Generally, the main purpose of a particle characterisation is to determine its size. Other important parameters include its concentration and shape. Accurate size information is an important factor in the overall effectiveness of particle production. However, there are several difficulties in obtaining accurate size due to the particle behaviour in the plethora of applications [1]. These include the high concentration of particles in the flow system, high and changing velocity of the particles, the wide range of sizes and the changes of sizes with time through evaporation and coalescence processes.

In order to obtain an accurate and reliable measurement of particle size, it is important to take into consideration the above difficulties when dealing with any new development of a particle characterisation device.

There are various techniques available to characterise a particle system in terms of its size. All techniques differ from each other in terms of the principle that forms the basis of the technique. Other differences include the method to quantify the relative amounts of various particle sizes, the type of sample to be used; i.e., solid or liquid, the amount of sample that is taken into account and the concentration required during the measurement [2].

1.2 Problem Definition

In this modern technology era, instruments and/or devices that characterise particles tend to be optically based and therefore non intrusive. These techniques are proven by previous researchers in characterising two-phase flows especially in determining the size of particles. Generally, these are developed to cater for specific applications and therefore lack universality. For example, a technique can only be used for sizing static particles and not moving particles. Other techniques are only suitable for sizing solid particles and not the liquid droplets. Thus, it is important to use an appropriate technique that is suitable for the specific application.

It is clear that current optical techniques are capable of measuring a particle size at different types of dispersion media. The available instruments or devices are based on a Laser Diffraction (LD), Phase Doppler Anemometry (PDA), shadow sizing, Direct Illumination (DI) and Interferometric Particle Imaging (IPI) techniques. These have been widely used in characterising the dispersed solid or liquid particles over the last two decades. However, there is still a lack of availability of devices capable of characterising multiphase flow applications such as when a mixture of droplets and solid particles are dispersed in air or gas. This type of flow exists in applications like

chimney in power plants, exhaust emissions from internal combustion engines and pollution control devices such as venturi scrubbers [3]. In addition, the device that implements the DI technique has some limitations in characterising liquid or solid particles. This is the motivation behind this study of particle characterisation on dispersion medium. This work is also focused on the improvement of the particle sizing techniques and investigating the parameters that contribute to the errors in their measurement.

1.3 Objective

A new improved device or technique is required to overcome the limitations that have been described in Section 1.2. The objective of this work is therefore to develop a device that can simultaneously measure the particle size, size distribution, size concentration and its shape. Furthermore, these properties are to be measured when the particles in moving conditions.

The work involves combining existing knowledge and techniques as well as developing novel ideas to deliver a new device capable of solid/liquid particles measurement. This new device utilises a digital imaging technique and laser sheet technology. It should be able to characterise both solid and liquid particles dispersed in fluid medium. The main measured outputs will be particle or droplet size (diameter of spherical particles or equivalent diameters of non-spherical particles), particle shape and particle concentration. It should be able to perform online particle sizing, which range from a few micrometers to a few millimetres. The device should also be portable, robust, user friendly and nonintrusive.

1.4 Methodology

The development of a new prototype device is the aim in this study. It is divided into two major components: hardware and software. The hardware system consists of the integration of several components including a camera, optical lens, laser, monitor and compact vision system (CVS). On the other hand, the software package is designed to perform image processing and analysis tasks required by the application.

This prototype device employs a combination of shadow and DI techniques. To fully investigate the accuracy and reliability of the prototype device, testing is carried out in different types of applications such liquid spray, dispersion of solid particles and particles suspended in water. The device is used to measure the known standard particle size to verify the accuracy of the measurement. The measurement of solid opaque particles dispersed in air and liquid are also performed. Transparent liquid particle sizes were obtained using shadow and DI techniques and a new improved shadow technique is produced to characterise a mixture of opaque and transparent particles dispersed in air. The sensitivity of light intensity, scattering angle and image magnification on particle size were investigated to evaluate the accuracy of the prototype device.

1.5 Thesis Layout

This thesis is divided into 6 chapters. A review of particle size measurement techniques and the representation of particle size are given in Chapter 2. Here, the intrusive and nonintrusive techniques are described and the advantages and limitations of each technique are listed. Chapter 3 gives a brief theoretical background on the imaging system and the fundamentals of image processing. Basic functions of image processing and types of filters are also described.

Chapter 4 is focused on the development of the dynamic image analysis software. The methods of processing the acquired images using shadow and direct illumination modules are explained in details. Chapter 5 provides various experimental results that have been obtained using the developed device. Measurements of solid and liquid particles dispersed in fluid medium are presented and discussed. Finally, Chapter 6 summarises and concludes the contribution and finding of this study and outlines further work.

Chapter 2

Literature Review

2.1 Introduction

Particulate matter can be either in the form of solid, liquid or gaseous or a mixture of them transported by a carrier fluid. Some of these particles are either natural or industrially processed (Table 2.1). The particles are widely used in industrial applications such as power generation, automotive, aerospace, turbo-machinery, food processing, agriculture, painting, mineral processing, pharmaceutical and biotechnology [3-6]. The particles which are involved in each application must lie in a certain size ranges in order to optimise the product performance. Figure 2.1 shows some particulate materials and their approximate size ranges that represent natural and industrial processed particles.

Table 2.1: Examples of particulate material (adapted from [2]).

Type of particles	Applications
Dry particles	Coal, sugar, flour, sand, powder.
Liquid mixtures	Emulsion (L/L) + suspension (S/L), milk, butter, paint.
Solid mixtures	Rocks, sediments, pharmaceuticals.
Aerosols (L/G + S/G)	Sprays, mist, fog, which may consist of dust, salt, coal, sand.
- where 'L' stands for liquid, 'S' for solid and 'G' for gas.	

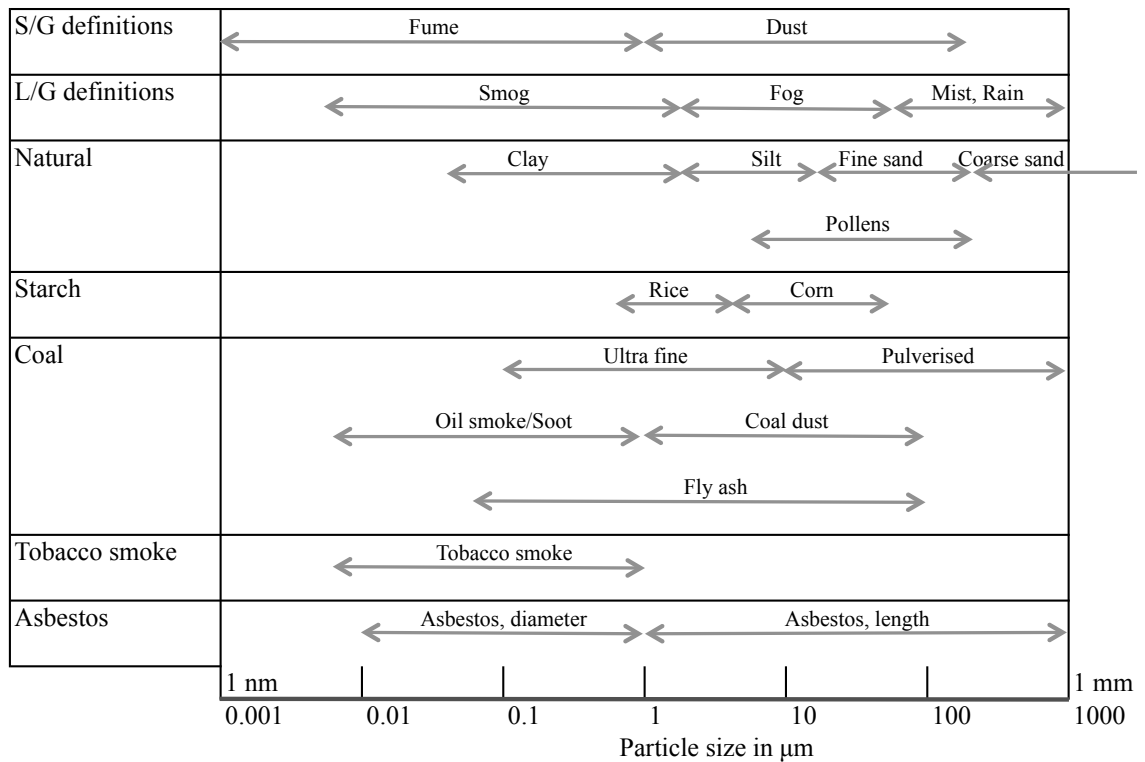


Figure 2.1: Particle size range of some particulate material [2].

It is important to characterise the particles in order to assess the quality of the product. The most common parameter is the size. This study is concerned with particle sizes which are in the range of a few micrometres to a hundreds of micrometres. Also, the particles can be the form of solid and liquid; i.e., in the dispersion phase.

Generally, the requirement to produce particles with the desired size distribution and concentration is very important in the quest to optimise the product performance in specific applications. The size distribution is always monitored to give the user an understanding about the performance of the measured particles. These measurements can be performed using particle size measurement instruments, which are usually based on various techniques. The following sections will discuss the most common techniques employed in measuring the size of solid and liquid particles. The advantages and

limitations of the techniques will also be summarised. Then, the representation of particle size in term of its distribution and statistical values will be explained.

2.2 Review of Particle Size Measurement Techniques

Important particle characterisation parameters include particle size, shape and concentration. The sizes are commonly presented in the form of mean values and size distribution plots. This information is useful for the users in order to monitor and examine the quality of their products and also to assess the performance of the processes.

In order to measure the size of a particle, a specific device or instrument is required. There are many devices available for the characterisation of particles in multiphase flows. Each device is purposely designed using a single technique or sometimes combination with other techniques. Some techniques may only be suitable for measuring solid particles while some of them are designed specifically to size liquid particles. In addition, certain devices are used to characterise static particles [7, 8] and other devices to be used to measure the size of the particles that are in moving or dynamic conditions [9-12].

Generally, the techniques of particle characterisation can be divided into two main categories: intrusive and non-intrusive (Figure 2.2). Here, the intrusive category is briefly reviewed, but more emphasis is placed on the optical or non-intrusive that employs light scattering and imaging techniques.

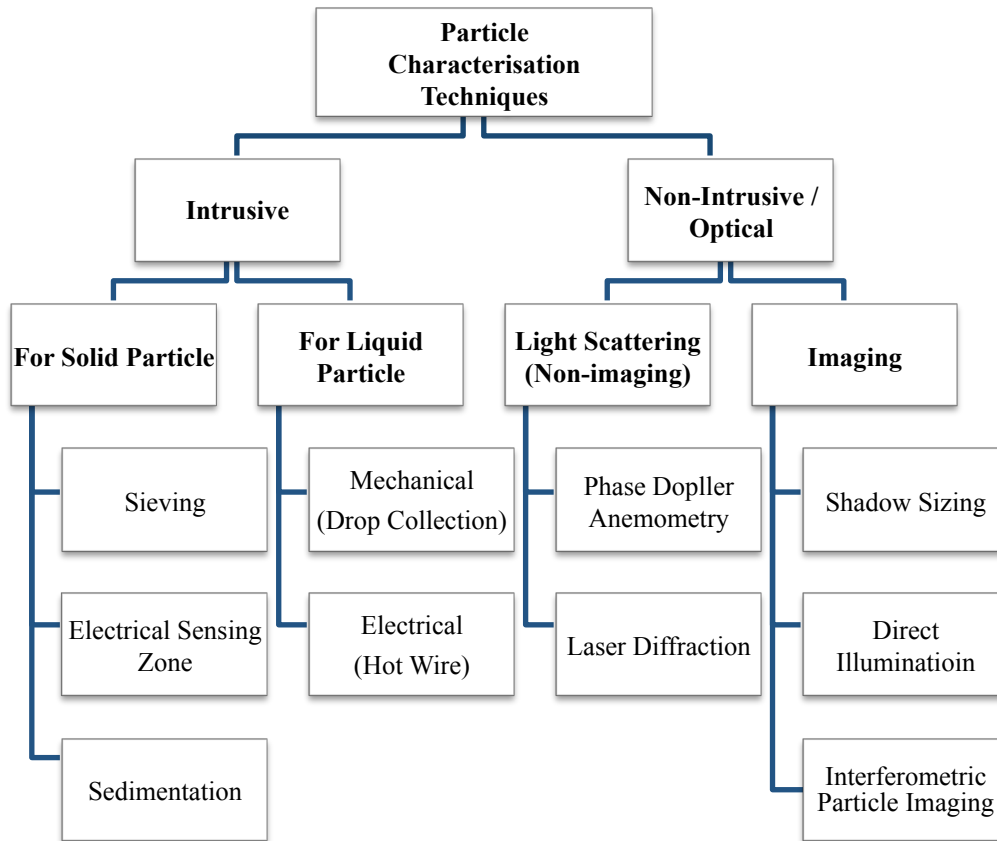


Figure 2.2: Particle characterisation techniques.

2.2.1 Intrusive - Solid Particles

Intrusive, also called sampling techniques, are defined when probes or other instruments applied to collect samples of solid or liquid particles from the flow. As given in Figure 2.2, several intrusive techniques are categorised for the characterisation of solid and liquid particles applications. The most common intrusive techniques in characterising solid particles include sieving, electrical sensing zone and sedimentation.

Sieving is the simplest and oldest method and is widely used in classifying the particles. It can be performed in a wide range of mesh sizes from around 5 μm to 125 mm [3]. The size classification is based on sieve openings or mesh sizes that allow particles to

pass through them [5]. Sieving produces a mass size distribution and the size is known as the sieving diameter. Some of the advantages of this technique are: (i) it has cheaper equipment to run, (ii) the principle is easy to understand and (iii) it allows relatively large samples for analysis. However, the technique requires significant manual operation, where the skills of the operator are essential [2]. Some automatic operations are possible, but require expensive equipment.

Electrical sensing zone, also known as coulter principle, is a method of measuring the size distribution and the number of particles. The particles are suspended in a diluted electrolyte (with a voltage applied across it) and forced to pass through a small orifice, where a voltage pulse of each particle is recorded [6]. The amplitude of the pulse is related to the volume of the particle that passes through the orifice. The range of particle sizes that can be resolved by this method is between 0.6 to 1200 μm [5]. The principle of the technique employs a conductive liquid, therefore limits its ability to perform direct measurement of dry particles or droplets that are dispersed in air.

Sedimentation is a method based on recording the sedimentation of particles dispersed in a liquid in a sedimentation column. The particle size distribution is obtained by measuring the rate of change of particle density or concentration at a given location in the column [3]. Andreason pipette is a common device that employs sedimentation method and is capable of measuring particles in the range from 2 to 100 μm [6]. The technique is not suitable for measuring liquid or solid particles that are dispersed in air.

2.2.2 *Intrusive - Liquid Particles*

Over the past decades, various techniques have been developed to measure liquid particle or droplet sizes. Conventional methods, which are intrusive, are widely used to characterise liquid particles or spray droplets in terms of their size (Figure 2.2). However, in certain conditions, these intrusiveness may disturb the flow field and affect the flow behaviour and can cause significant measurement errors [13]. To characterise droplets with intrusive techniques, two broad methods are commonly used: mechanical and electrical.

Mechanical methods employ a collection of drops on a solid slide or in a cell containing a special liquid. The collected drops are then examined through observation, or photography with the aid of a microscope [1]. This method has many variations, which include the collection of drops on slides, collection of drops in cells, molten wax techniques, drop freezing techniques and cascade impactors.

On the other hand, electrical methods are based on the detection of electronic pulses produced by drops when they hit a wire. The electronic pulses are then analysed for size distribution calculations. Common variation of this method includes a charged wire technique and hot wire technique [14, 15].

Many of the disadvantages of these conventional methods have been described by previous researchers [1, 14-18]. The problems that contribute to the error of drop collection methods are drop evaporation process and drop collection efficiency. According to Kim et al [17], a small water drop has a very short lifetime. A drop with 10 μm diameter may evaporate in about 1 second at 90% relative humidity atmosphere.

Therefore, the evaporation process significantly affects the measurement of smaller drops. Also, small drops collection is less efficient compared to large drops. This is due to the fact that large drops have enough inertia to hit the collected surface, while the small drops tend to follow the streamlines [1]. Another problem with drop collection on slide is that the diameter of flattened drop does not represent the actual spherical size. Thus, a proper correction factor has to be applied to determine the actual drop size. The main disadvantage of electrical based method is the accuracy of size distribution which can be reduced due to the position of drops impingement to the wire. Both mechanical and electrical techniques are limited to sizing the liquid particles only and are impossible to be applied to solid particles. Also, most of these conventional techniques have to be run manually, thus making them computationally intensive.

2.2.3 *Non-intrusive/Optical*

Nowadays, due to the rapid development of modern technology such as powerful computers, lasers, cameras and automation systems, the methods involved in particle characterisation have changed significantly. These conventional methods have gradually been replaced by non-intrusive methods which are based on light-matter interaction.

Non-intrusive or optical techniques are widely used in fluid mechanic applications to visualise and determine the properties of flow particle such as the sizes, shape, velocity and concentrations. These methods do not interfere with the flow and as such are iso-kinetic samplers. The fact that the flow is not disturbed, allows the application of these methods in high speed flows. As shown in Figure 2.2, non-intrusive methods can be classified into two categories: light scattering and imaging. The latter consists of shadow sizing, direct illumination (DI) and interferometric particle imaging (IPI)

techniques while the phase Doppler anemometry (PDA) and laser diffraction techniques can be categorised as laser diffraction method.

2.3 Light Scattering Techniques

The light scattering techniques are the most common methods used in monitoring and characterising particles in both industrial and laboratory applications. The other name of the techniques is also known as non-imaging. These techniques have faster processing time and a greater flexibility when performing an on-line measurement. Generally, the techniques are based on the production of wide range of light beam angles by the interaction of incident beam with solid or liquid particles. When the size of a particle is larger than the wavelength of the incident light, it scatters the light in proportion to the their diameter squared [13]. The particles that are illuminated by the light beam will scatter the light in three different modes which are diffraction, reflection and refraction [19, 20]. Diffraction and reflection occur for all particles, however refraction only occurs for transparent particles. Based on these modes of light scattering, the techniques of particle sizing can be categorised as laser diffraction (LD) and PDA.

2.3.1 Laser Diffraction

Currently, the standard name of this method is laser diffraction. Other names also known as static light scattering (SLS), forward light scattering (FLS), low-angle laser light scattering (LALLS) and Fraunhofer diffraction [2]. The working principle is based on the simultaneous collection of scattered light from hundreds of particles inside a laser beam. This scattering pattern is measured by several detector elements positioned at different angles, mostly in the forward direction. Then, the signals from detectors are converted to a particle size distribution (PSD) by applying a model-based matrix. This

matrix contains calculated signals at all detectors per unit volume of spherical particles for each of a defined set of size classes.

LD measures the particles and reports the size distribution on the volume basis. It does not know the number of particle it detects, therefore it is not suitable for particle counting. A representative particle size distribution of the complete diameter is obtained, and because scattering in the forward direction is measured (up to about 10 degree scattering angle), the scattering mode of diffraction is dominating [4].

The advantage of the LD method is that it can be employed to size the particles that are involved in either dry or wet dispersion. Dry dispersion is where the particles are dispersed in air, while wet dispersion is where the particles are dispersed in a liquid medium. Tinke [21] has developed a dry dispersion method for LD to perform particle characterisation in pharmaceutical industry applications. Hewitt [22] has applied LD to measure droplet size from a range of spray nozzles for the aerial spray application.

Traditionally, the equivalent circular area diameter is used to represent the non-spherical particles measured by LD. Recently, Tinke [23] reported method to characterise rectangular particles by introducing spherical diameters that are equal to the breadth and length of the rectangle shape.

For good operation of this LD technique, it requires a low to medium particle concentration during the measurement. If the concentration is too low, the produced scattered light signals are too weak. This causes low signal-to-noise ratio and poor

repeatability. Also, if the concentration is high, multi-scattering effects from the particles may reduce the accuracy of the size measurement [24].

2.3.2 *Phase Doppler Anemometry*

It is a method that is widely used in the spray applications [25-27]. This method applies two identical laser beams that crossed together to form a pattern of fringes [28]. The fringes are in light and dark illumination shape. These fringes dimensions contain a region that define the measurement volume and they can be controlled by the optical arrangement. The measurement volume has to be small enough so that only one drop is allowed to flow into it at any given time. Thus, the PDA is actually based on a single particle counting technique and has a capability to accept drops that arrive at measurement volume of up to 250 kHz [4].

Generally, two or more photo-detectors are used to measure the scattered light signal and they are processed in order to obtain drop diameter and also velocity component at right angles to the fringes. The determination of the drop size is obtained from the phase differences of the signals of the different photo-detectors [4]. The PDA has an ability to size accurately fine particle which is $<10\ \mu\text{m}$ [29] and up to a few millimetres.

However, the PDA technique has some limitations. The measured particles or drops must be spherical between close limits. The optical properties such as refractive index of the particles or drops must be known and used as an input to the instrument [30]. The effect of refractive index on particle size may degrade the accuracy of the measurement [31]. The location of the detectors have to be properly set so that either reflection or refraction modes of the light scattering dominate [4].

2.4 Imaging Techniques

This technique is based on a digital image that is acquired, processed and analysed using several steps in order to determine the particle sizes. The techniques have been widely used in application such as agriculture [32] , spray droplets [33, 34], combustion studies [35, 36], pharmaceutical and industrial applications. As shown in Figure 2.3, the working principle of the imaging techniques start with the sample preparation process. It is a method to present the particles to a measuring device. The sample which is made from solid or liquid particles can be presented as a static or a dynamic dispersion in a fluid medium.

Image capturing operations employ an optical system such as a digital camera and its lens to capture a magnified image of the stationary or moving particles. Light source is required to illuminate the particle during the image capturing step. Image processing operations modify one image into another image by applying some refinement such as image smoothing, edge detection and image enhancement processes (details in Section 3.5). Image analysis operations are frequently used to quantify some aspect of image such as area of single particle and number of particle in an image.

The captured image is then processed by specific software to extract useful information such as the number of pixel that compose a single particle. Then the data is analysed to produce results in terms of size distribution, the number of detected particles and its mean. The advantages of this technique over light scattering are the ability to produce quantitative data on drop sizes and qualitative results in understanding the spray structure such as the droplet breakup and impact [4].

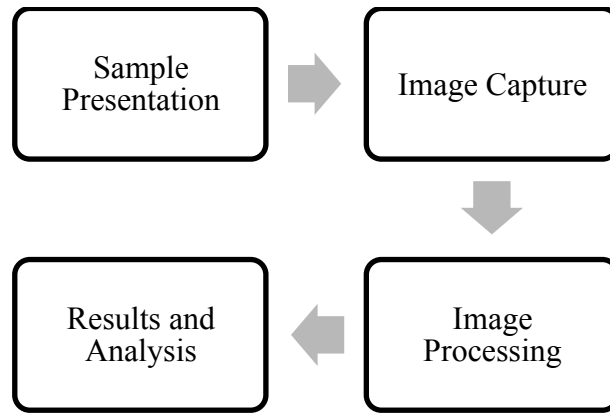


Figure 2.3: Working principle of imaging technique.

Usually, illumination of the particles in the imaging systems applies a laser light source. A common method of illumination is backlighting where a shadow image of particles is produced. Direct illumination of particles is also commonly used to highlight the particles so that clearer image can be recorded. The back-lighted or shadow sizing is the most popular imaging techniques in characterising the particles. Other techniques include direct illumination and interferometric particle imaging.

2.4.1 *Shadow Sizing*

It is a technique that captures shadow images of particles and processes them to extract useful information such as particle size and number of particle [33, 37, 38]. The setup of this technique is illustrated in Figure 2.4. The technique consists of a light source (usually a laser or strobe light), a digital camera and a computer. The light is used to back-light the particles so that they appear as shadow, then the camera is used to record the shadow image of particles. Following that, the image is processed and analysed in the computer by employing some image processing techniques. As a result, the particles are then sized and separated into different classes to indicate its size distribution. The

measurement range of these techniques is 1 μm to a few μm with the system optics determining the range [39].

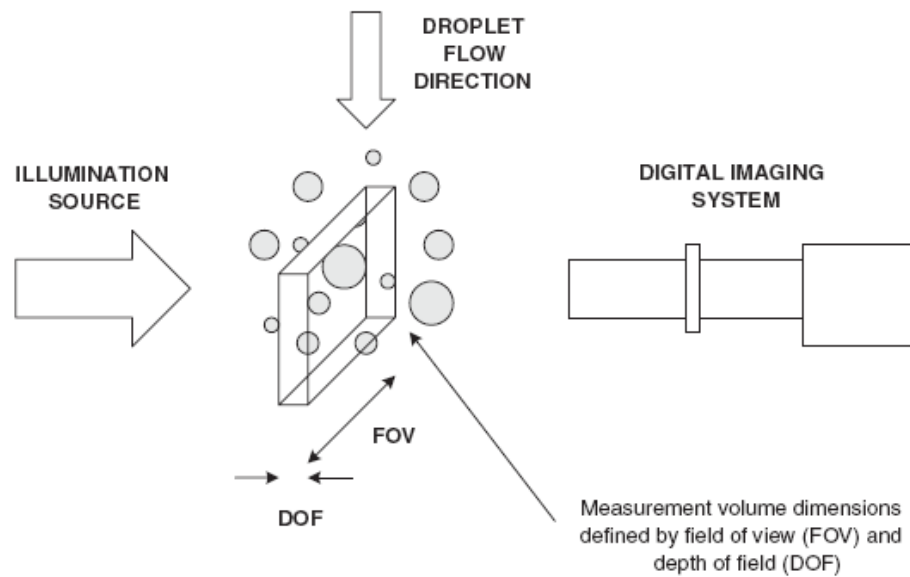


Figure 2.4: Schematic representation of the experimental setup for the shadow sizing technique [40].

There have been a number of studies that implement the shadow technique principle in characterising the particles of multiphase flow. Butler et al. [37] has investigated the performance of air induction nozzles spray by obtaining a volume median diameter of droplets having a size in the range of 40 to 1500 μm . Measurements of high density spray with minimum detected size of 5 μm were carried out and the comparison were made to the PDA system [33, 41].

A light distribution of the captured image background of multiphase flow was appeared to be rarely uniform [42]. An image enhancement process needs to be applied to normalise the background. A grey level gradient method is applied to the image to identify the in focus particle from the background [33, 43]. High measurement accuracy and robustness of shadow technique has been reported by Kashdan [41, 43], where the

effect of image depth of field (DOF) variation and the sensitivity of threshold level on the particle size has been identified. It was found that the wavelength of the illumination light does not significantly contribute to the accuracy of the size measurement [40]. Spray droplets were measured using two sources of laser light having 808 and 532 nm in wavelength, respectively, have shown a very good agreement [40].

The technique also enables the measurement of solid or liquid particles dispersed in a fluid medium. It has also an advantage of measuring non-spherical particle characterisation and is able to define the shape of each particle [33, 40, 44]. In order to obtain useful information from the captured images, they have to be processed and analysed using appropriate image processing techniques such as image enhancement, noise removal, thresholding and morphological functions. There are many possible methods that can be applied to process the image depending on requirement of the measurement. [42, 43, 45].

2.4.2 *Direct Illumination*

It is a method where the particles are illuminated by a direct light sheet and is also known as a direct imaging technique. The light scattered by the particles is imaged using a digital camera at a certain scattering angle (an angle between an incident light and the camera). The image is then processed and analysed to determine the size distribution of the particles.

Previous researcher has developed a novel imaging system for the on-line measurement of particle size distribution in particulate flows [36]. Image processing techniques were employed to analyse the captured images in real-time using a custom software tool.

Continuous wave laser was used to produce and feed laser sheet to the system and a camera was placed in similar axis as the particle flows in order to prevent a streak image of the particle. As shown in Figure 2.5(a), the scattered light of opaque particles is recorded at angles of 90° and at 135° . There might be an effect of the accuracy of particle size if the scattering angle is set to other degree due to the behaviour of particles in scattering the light [19]. Also, by varying the intensity of the laser light that hits the particles, it may be possible to record larger image of particles by the camera compared to their real size. However, these problems of studies have not extensively been explored yet.

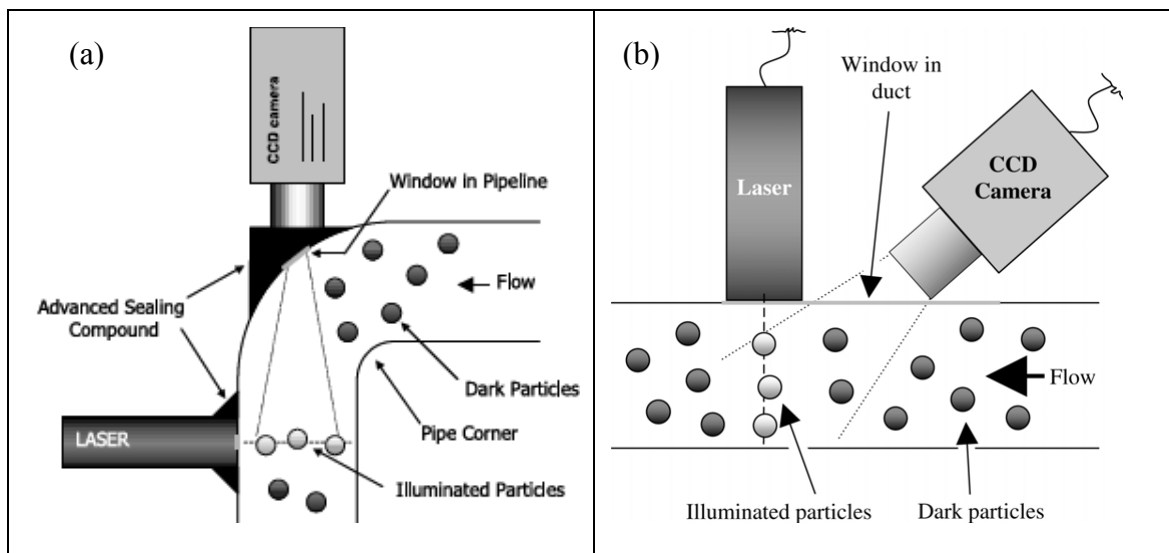


Figure 2.5: Two different setups produced by Carter et al. in sizing the particles by DI technique (a) Scattering angle at 90° [36], (b) Scattering angle at about 135° [46].

Carter et al. [36] has reported that the current system is only limited to the opaque particles. When it is applied to transparent particles such as glass beads or liquid droplets, it produces unreliable results due to the refraction effect. This problem has been addressed by measuring a separation of two glare points that appear in the image when a transparent particle is hit by the laser sheet at a certain scattering angle [47-49]. As shown in Figure 2.6, some rays of light are reflected by the droplet and others are

refracted through the droplet. This produces the glare points which represent the point of reflection and refraction of a spherical droplet [19]. It has been found that the refracted light is at least 40 times stronger than the reflected light for a range of refractive index between 1.3 to 1.6 and at scattering angle of 25 to 70 degree [36]. However, in this glare points method [47, 48], the refractive index of transparent particle and scattering angle must be known in order to obtain accurate sizes. Also, it is only suitable for transparent particle that has a spherical shape.

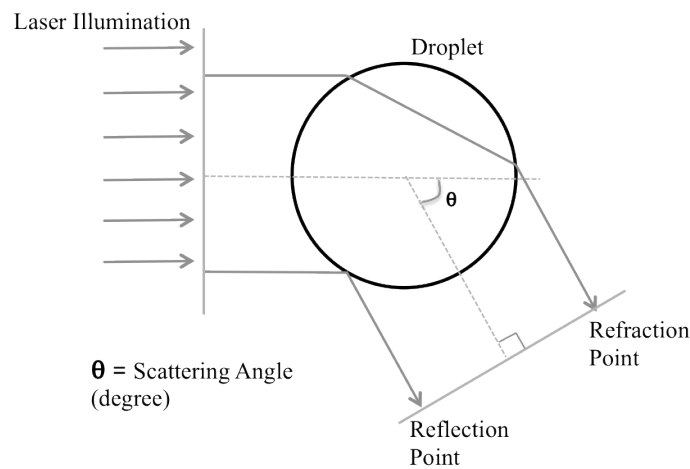


Figure 2.6: Schematic of the optical paths of reflection and refraction points through transparent spherical particle [50].

2.4.3 Interferometric Particle Imaging

This Interferometric Particle Imaging (IPI), also known as Interferometric Laser Imaging for Droplet Sizing (ILIDS) or Mie Scattering Imaging (MSI), was originally proposed as described in [51-53]. There are numerous papers published on this technique which is applied to a study of liquid particles dispersed in a fluid medium [54-58]. The technique is based on acquiring an out-of-focus image of the droplets which are present in laser sheet. It is reported by [51] that the corresponding defocused image of a droplet appears in the form of interference fringes (Figure 2.7). The number of fringes on a single droplet can be related to its diameter.

The restriction of older IPI technique leads to overlapping of the fringe patterns in the images and contribute to errors in determining the number of fringes on each droplet. The problem has been solved by Maeda et al. [50, 59], where they introduced a new optical compression method that acquires the interference image without overlapping the fringe patterns. However, the IPI technique is limited to measuring spherical transparent particles only. In addition, the refractive index (RI) of the particle must be known for the determination of the size. If the RI of the droplet is unknown or varies due to a heating process or chemical reactions, it has to be measured to achieve a better accuracy of particle size [60].

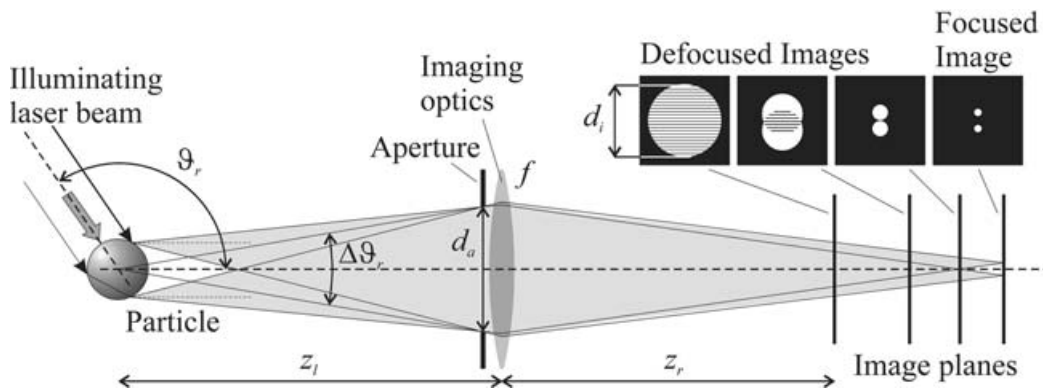


Figure 2.7: Focus and defocus images from a spherical particle [54].

2.5 Summary of Particle Size Measurement Techniques

When characterising multiphase flow such as solid or liquid particles that are dispersed in a fluid medium, non-intrusive or optical measurement techniques are preferred due to their principle that does not disturb the flow behaviour. At present, the intrusive techniques such as sieving and sedimentation are still very convenient and cheap to use in certain applications related to solid particles, while mechanical and electrical techniques for droplet sizing are not relevant anymore due to their limitations and also availability of other techniques.

For the laser scattering techniques, both LD and PDA are proven to be very good in performing size measurement for solid and liquid particles. They have the ability to perform on-line measurements. The size measurement can easily be performed for solid particles that are dispersed in a liquid or air, and also for droplets dispersed in an air medium. However, there is no technique available to characterise a mixture of solid and liquid particles that are dispersed in an air medium. A mixture of particles may occur in applications like venturi scrubber, solid-liquid separation in suspension atomization process, chimney and exhaust vehicle system [61-63].

In certain applications such as in high concentration of particles or dense spray of diesel injection, the light scattering technique may be difficult to be applied. As mentioned in Section 2.3, the LD will produce multiple scattering effects and thus degrade the accuracy of the measurement, while the PDA is found to be unreliable for non-spherical particles of dense spray application [33]. Due to these limitations, imaging techniques can be employed for their ability to describe the shape and quantify the size of the particles.

In the case of imaging techniques, the shadow, DI and IPI methods can be performed as an on-line measurement. For example, the shadow sizing method is able to determine the size of solid or liquid particles. However, IPI is restricted only to liquid droplets which have transparent particles and this is not suitable for opaque particles. On the other hand, DI has a difficulty in characterising transparent or opaque particles in the same instrument. Images may be captured at different scattering angles to enable the DI technique to measure opaque and transparent particles. At present, there is no such instrument that can size solid or liquid particles without varying the scattering angle.

Some problems have been reported regarding particles overlapping in an image captured using shadow and DI techniques [33, 42]. Nevertheless, this can be solved by applying overlapping algorithms as described in [64, 65]. However, the algorithms require extensive computational complexity to process the images. This can be seen as a drawback of such on-line measurement methods.

Therefore, the objective of this study is to develop a device that can perform on-line measurement of solid and liquid particles dispersed in a fluid medium. The scope of this research will be focused on imaging techniques, which may combine both the shadow and DI techniques. A new measurement technique will be proposed to characterise a mixture of opaque and transparent particles dispersed in air. DI technique will be improved so that it can obtain opaque or transparent particles at similar scattering angles. The sensitivity of the light intensity, the scattering angle and image magnification of the particle's size will be investigated to demonstrate the accuracy of the developed technique.

Ideal techniques for particle size measurement that can be used as a guideline when developing a new spray characterisation device which should have certain features [1]. These include non-intrusive methods, wide drop size ranges, capability of measuring both spatial and temporal distributions, and the ability to perform the means of sampling and counting. However, it is quite impossible for a single device to have all of these criteria. Often the application dictates the dominant features desired. Therefore, it is important to highlight the capabilities and limitations of the proposed techniques.

2.6 Representation of Particle Size

Particles exist in the form of regular and irregular shapes. The size of a regular shape such as spherical, can be accurately represented by a single parameter such as the diameter. Other shapes like cube and tetrahedral can also be defined with a single dimension. More parameters are required to describe the size of irregular shapes. Given a cone particle for an example, the base diameter and the height are required whilst for cuboids the shape requires three dimensions such as sugar and salt.

In many industrial application, a single parameter is required to represent the particle size. This is not a problem with the particles having spherical or cube shape. However, for a non-spherical shape, the equivalent spherical diameter is widely used to represent the particle size [5]. In image analysis, the particle sizes are measured by looking at the projection of the shape of the particles. Some common diameters used in image analysis include Martin's diameter, Feret's diameter, shear diameter and equivalent circle diameter [6].

According to British Standard [66], there is no single definition of a particle size that can be used. Different techniques used in sizing the particles are based on different physical properties. Particle size can be defined as the diameter of a sphere having the same physical properties, which is known as the equivalent spherical diameter. Some examples of equivalent diameters are given in Table 2.2.

Table 2.2: Types of equivalent spherical diameters [2].

Equivalent Diameters	Definitions
Equivalent Projected Area Diameter, d_A	Diameter of a circle having the same area as the particle's projection.
Equivalent Surface Area Diameter, d_S	Diameter of a sphere having the same surface area as the particle.
Equivalent Volume Diameter, d_V	Diameter of a sphere having the same volume as the particle.
Equivalent Sieve Diameter, d_{Si}	Diameter of particles that just pass through the apertures of a sieving medium.

2.6.1 *Size Distribution*

When characterising the particles, thousands of them are measured to obtain better statistical results. These measured particles can be described by a size distribution plot. To obtain this distribution, the measured size of many particles are categorised based on their size interval, ΔD . This interval has to be large enough to contain many particles and small enough to determine sufficient detail. The representative size of each interval is defined by a mid-point of the interval, D_i . Then, the number of particles in each size class are counted and divided by its size class and the total number of particles detected. The results are usually expressed in the form of histogram or density plot and also cumulative plots.

Generally, the density and cumulative distribution plots can be categorised into two classes: linear abscissa (Figure 2.8) and logarithmic abscissa (Figure 2.9). The former is preferable for narrow size distribution while the latter is useful for wide size ranges [5]. The methods to plot these distributions can be found in [66].

The size distribution plot indicates the dominant size detected in the distribution and gives the deviation of the measured particles to indicate whether the distribution is narrow or wide. There are different types of distributions, which are dependent on the methods of each instrument applied. The standard symbols that represent the size distribution of particles are given in Table 2.3.

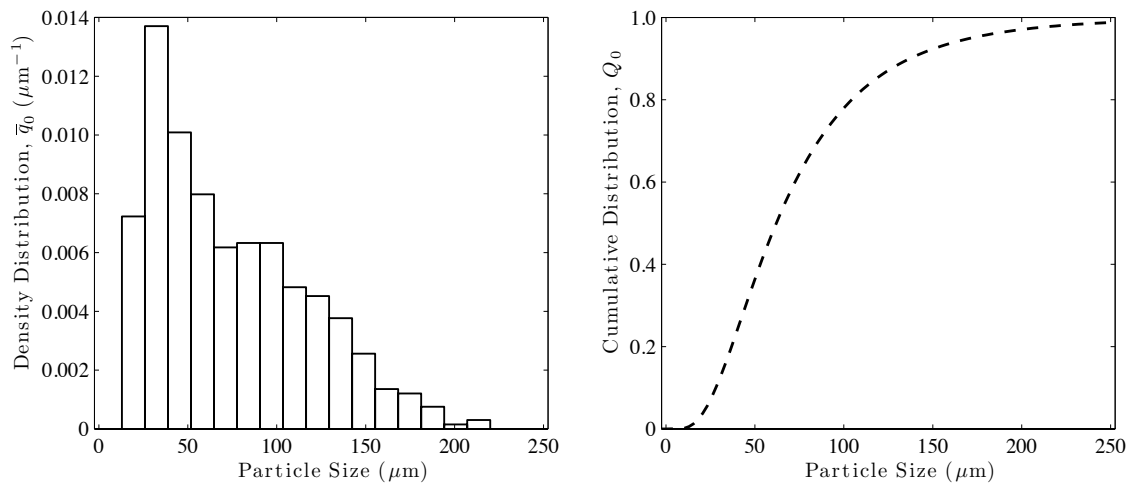


Figure 2.8: Number size distribution of particles based on linear abscissa.

The common types of size distribution used are the number and volume distributions. A number distribution can be determined using microscopy, imaging techniques and sieving, while a volume distribution can be obtained by laser diffraction and PDA techniques [6]. A number distribution can provide the exact quantities of specific types of particles such as how many particles have spherical shapes or what is the ratio between solid and liquid particles detected in an image. The imaging techniques that

generate the number distributions may convert the measured distribution into volume by employing conversion algorithms as described in [67].

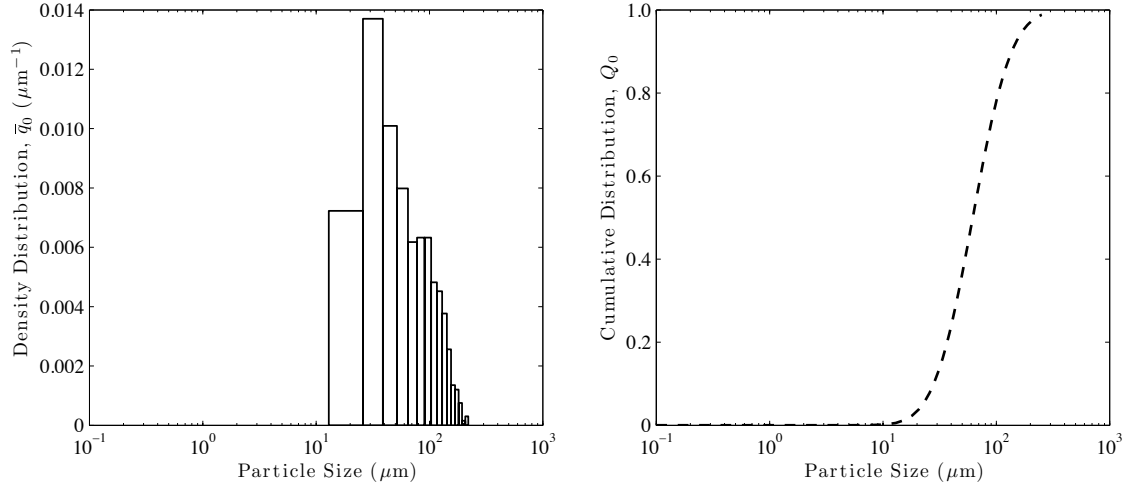


Figure 2.9: Number size distribution of particles based on logarithmic abscissa.

Table 2.3: Symbols that represent size distribution [66].

Distribution Type	Density Distribution	Cumulative Distribution
General symbol	$q_r(d)$	$Q_r(d)$
Number	$q_0(d)$	$Q_0(d)$
Length	$q_1(d)$	$Q_1(d)$
Area	$q_2(d)$	$Q_2(d)$
Volume or Mass	$q_3(d)$	$Q_3(d)$

Volume distribution is very useful for obtaining mass distributions. It is important in many industries where they can determine how much material they required. Here, the

exact number of particles is not important. Conversions from volume to number distributions are subjected to errors [6].

The relationship between the number and volume distributions can be explained by Figure 2.10. In a spherical volume, 1 million of 1 μm particles are similar to 1 single of 100 μm particles. An instrument plots the volume distribution with 50:50, but by number it is not significant because only 1 single particle of 100 μm is detected.

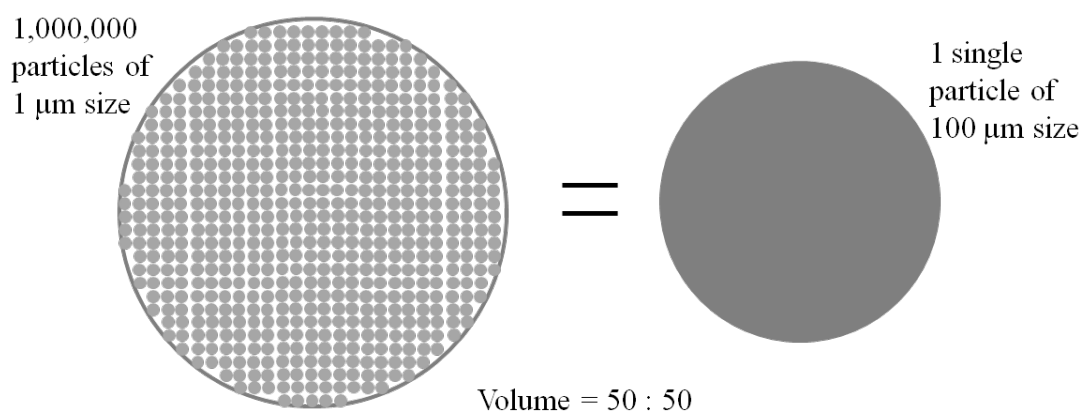


Figure 2.10: Relation between number and volume distribution.

For a given population of particles, the distribution of the number and volume can be significantly different [6]. This can be described by measuring the same samples and plot both the distributions in one graph. Figure 2.11 shows the comparison of the number and volume distribution obtained from the similar samples. Both distributions indicate a large different in terms of the mean particle sizes. It is found that by number distribution, a lot of smaller particles are detected compared to larger size. This is a good illustration how the results can differ.

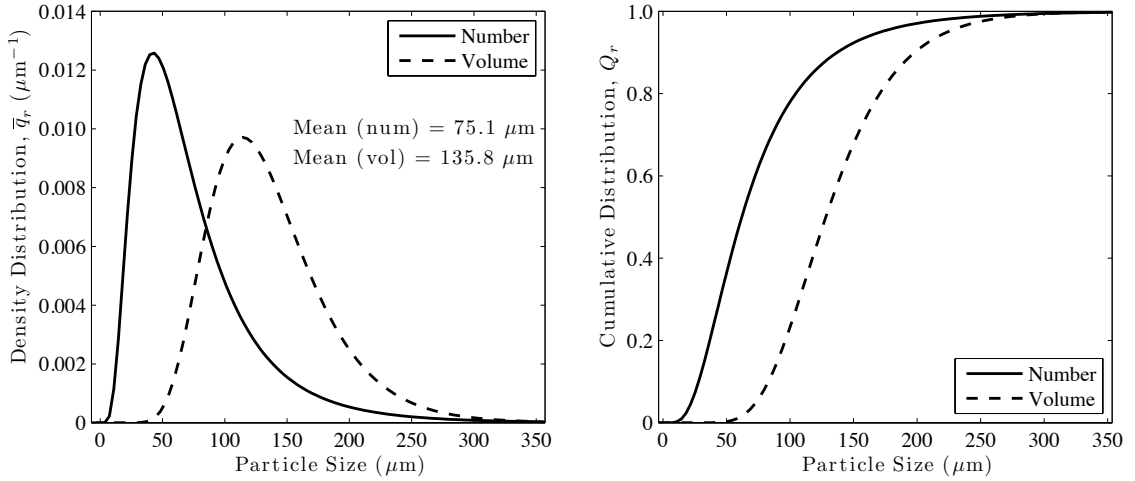


Figure 2.11: Comparison between number and volume size distribution.

2.6.2 Frequently Used Size Distribution Functions

Generally, in many areas of statistical analysis, the experimental data tends to follow the Normal or Gaussian distribution function [5]. In the case of a particle size, the distribution is more common to follow the Log-normal distribution function [1, 3, 6]. Other distribution functions that frequently used is the Rosin-Rammler, where it is applied to represent droplet size distributions in spray applications [1, 3]. The mathematical representations for each function are given in Equations 2.1 to 2.3.

$$\text{Normal (Gaussian)} \quad q(D) = \frac{1}{\sigma\sqrt{2\pi}} \exp\left[-\frac{1}{2}\left(\frac{D - \mu}{\sigma}\right)^2\right] \quad 2.1$$

$$\text{Log-normal} \quad q(\ln D) = \frac{1}{\sigma_g D \sqrt{2\pi}} \exp\left[-\frac{1}{2}\left(\frac{\ln D - \mu_g}{\sigma_g}\right)^2\right] \quad 2.2$$

$$\text{Rosin-Rammler} \quad Q_3(D) = 1 - \exp\left[-\left(\frac{D}{D_e}\right)^m\right] \quad 2.3$$

where:

$q(D)$	density function of particle diameter
D	particle diameter
μ	population mean diameter
σ	population standard deviation
$q(\ln D)$	density function of $\ln D$
μ_g	population geometric mean diameter
σ_g	population geometric standard deviation
$Q_3(D)$	cumulative undersize volume (mass) distribution
D_e	reference size constant
m	Distribution constant (slope in a linear graph)

A well known distribution, which is Normal or also called Gaussian is based on the occurrence of given particle sizes. It is simple to use but the application is limited to processes that are random in nature [1]. Usually, if a large number of measurements are performed and the results are plotted as a frequency distribution, the Gaussian bell shaped will be obtained. A plot of this distribution function is depicted in Figure 2.12(a). It produces symmetrical distribution around the mode and the standard deviation represents the distribution width.

The log-normal distribution is commonly used to present the population of measured particle sizes. This distribution produces symmetrical around geometric mean on a logarithmic size scale and often be used for wider particle size distribution as shown in

Figure 2.12(b). The distribution width of a log-normal process is defined by the geometric standard deviation.

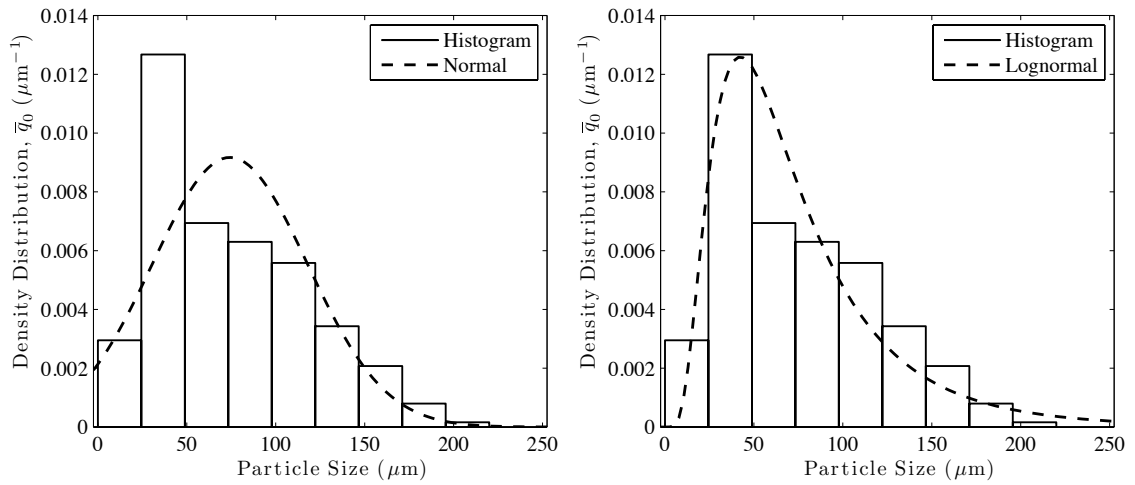


Figure 2.12: Number based distribution of (a) Normal and (b) Log-normal distributions.

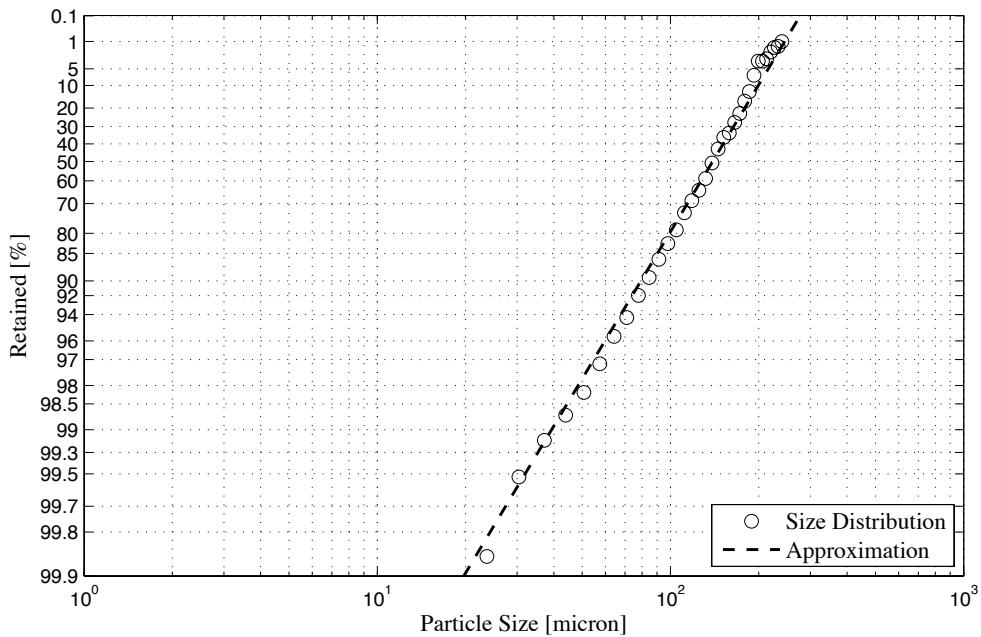


Figure 2.13: Rosin-Rammler distribution.

The Rosin-Rammler (RR) distribution or also known as Weibull distribution was derived originally to present the size distribution of crushed coal. It has also been

widely applied to describe the size distribution of many other particles including solid particles and droplets [68]. This RR distribution is often applicable to a broader size range of particles. Figure 2.13 illustrates that the RR generates a straight line to present the size distribution in the log of percentage weight retained against the log of particle sizes.

2.6.3 Statistical Parameters

There are several parameters that are usually applied to quantify particle size distributions. The most important and frequently used include mean, median, Sauter Mean Diameter (SMD) and the standard deviation. The mean diameter is a single value that represent an average of many individual values in the histogram or density distribution plot [69]. The median diameter is a value of particle size that corresponds to the 50% of the cumulative distribution. The SMD is defined as the ratio of the particle volume to surface area of the distribution. The standard deviation indicates the spread of the distribution, where the large value corresponds to the wide distribution. These parameters can be calculated using Equation 2.4 to 2.6.

$$d_{mean} = \sum_{i=1}^N D_i (\bar{q}_r \Delta D) \quad 2.4$$

$$\sigma = \sqrt{\sum_{i=1}^N (D_i - d_{mean})^2 (\bar{q}_r \Delta D)} \quad 2.5$$

$$d_{32} = \frac{\sum_{i=1}^N D_i^3 (\bar{q}_r \Delta D)}{\sum_{i=1}^N D_i^2 (\bar{q}_r \Delta D)} \quad 2.6$$

where;

d_{mean}	Mean particle size
ΔD	Size interval
D_i	Mid-point of size interval
\bar{q}_r	Density distribution on each interval
N	Number of particles
σ	Standard deviation
d_{32}	SMD

In addition to the mean and the median diameter, there are many possible terms to represent the particle sizes. The definition of each term is summarised in Table 2.4 and the corresponding locations on the distribution plot are illustrated in Figure 2.14.

Table 2.4: Definition of the term that represents particle sizes [1].

Term of sizes	Definition
$d_{0.1}$	The size indicates that 10% of total particle are below its size.
$d_{0.5}$	The size indicates that 50% of total particle are below its size. It also represents the median particle size.
$d_{0.9}$	The size indicates that 90% of total particle are below its size.
d_{peak}	The size indicates the peak of the histogram or density distribution.

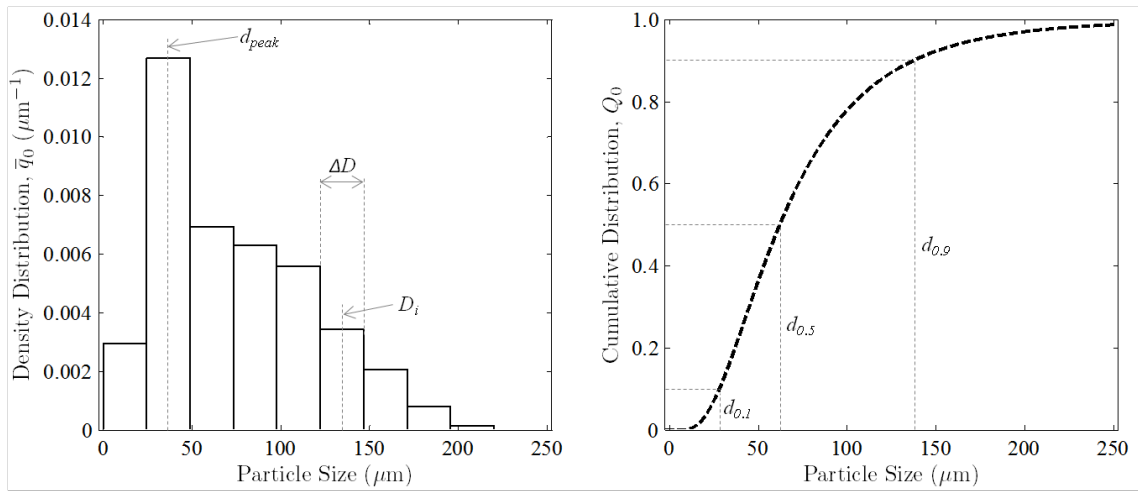


Figure 2.14: Locations of representative particle size.

Chapter 3

Fundamental of Image Processing

3.1 Introduction

In order to acquire a good quality image, and appropriate setup of the imaging systems is essential. Before an image is captured, some basic parameters have to be understood. The definition of each parameter is described in this chapter. Once an image is captured, it is processed and analysed using some image processing techniques. Therefore, the fundamental of image processing techniques is described in the following sections.

3.2 Parameters of an Imaging System

An imaging system should produce sufficient image quality in order to extract the desired information from an image. Good image quality can be acquired through a correct setup of the appropriate imaging system such as the one depicted in figure 3.1. Understanding the terms used in the imaging system will help the description of the setup process. Thus, some basic parameters of the imaging systems are described.

- *Field of View* - The area of the object that occupies the captured image by a camera is called the field of view (FOV). It indicates the physical dimensions of the frame of the image; namely the horizontal and vertical lengths. Figure 3.1 shows the illustration of the FOV.
- *Working Distance* - It is the distance from the front of the camera lens to the object under inspection.

- *Depth of Field (DOF)* - It is the maximum depth of the image that a lens keeps the object in focus.

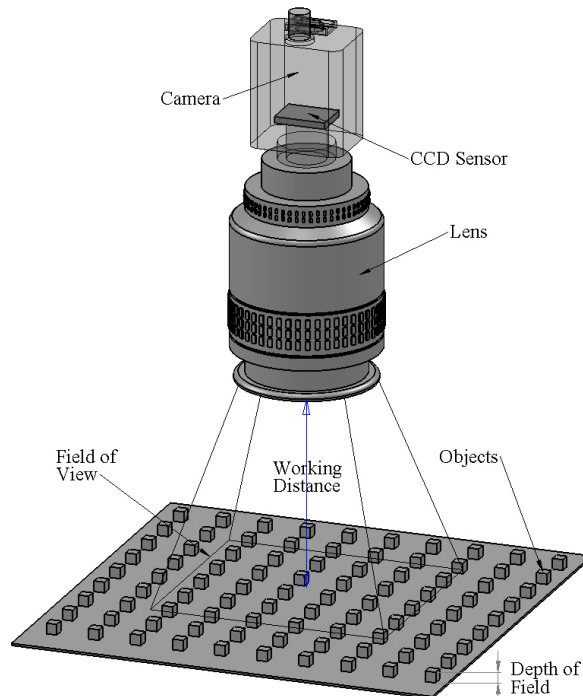


Figure 3.1: Fundamental parameters of an imaging system.

- *Sensor Size* - The size is important in determining the FOV. The size of a sensor's active area is defined by the sensor's horizontal length.
- *Image Magnification Factor (IMF)* - It is also known as primary magnification factor which is an important parameter in determining the proper lens magnification required to obtain a desired FOV. It is defined as a ratio between the sensor size and the FOV as given in Equation 3.1. High magnification lens has to be used to determine small FOV's, which means the value of IMF is more than 1.0 as illustrated in Figure 3.2.

$$IMF = \frac{\text{Sensor Size (mm)}}{\text{FOV (mm)}} \quad 3.1$$

- *Resolution* - It represents the amount of detail that an imaging system can produce. Images with low resolution lack detail and usually appear blurry. Several factors contribute to the resolution of imaging systems, which include FOV, camera sensor size and the number of pixels in the sensor.

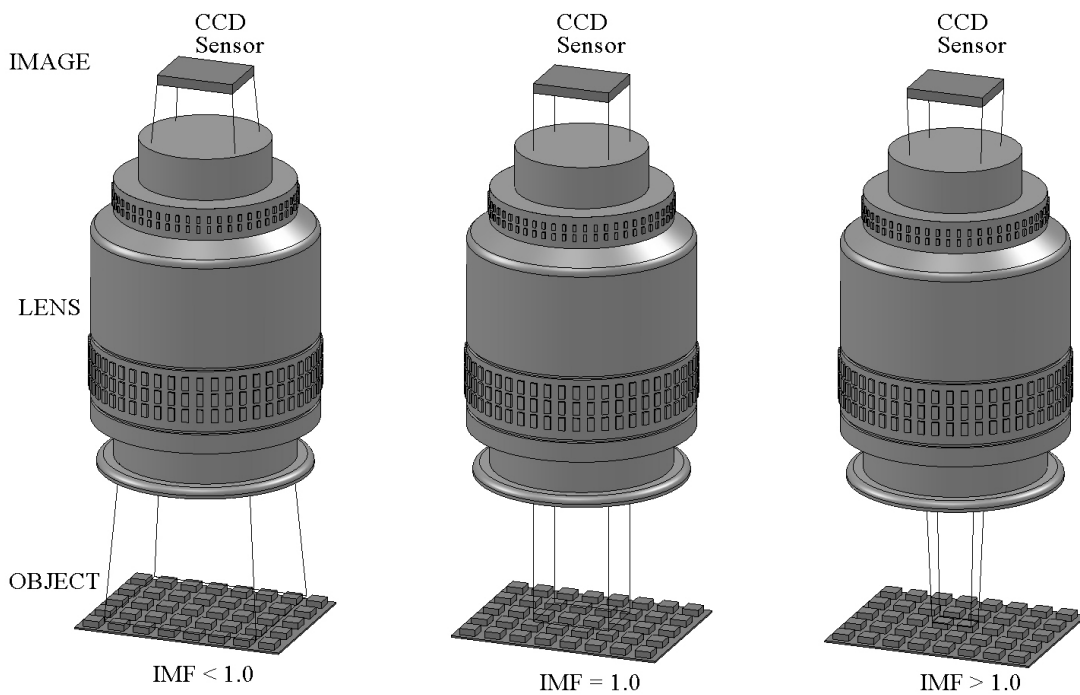


Figure 3.2: Illustration of the ratio between CCD sensor size with FOV.

- *Contrast* – The resolution and contrast are closely related factors that contribute to the image quality. The contrast defines the differences in intensity values between the object under inspection and the background. The imaging system should have enough contrast to distinguish objects from the background. Proper lighting techniques can be applied to enhance the contrast of the imaging system.

3.3 Electronic Imaging

A camera which consists of a sensor and other electronic components plays an important role in the performance of imaging systems. An optimum system performance can be achieved by a proper integration of all components including camera, capture board, software and cables. Several terms that apply to the components have to be understood in the selection of the camera.

3.3.1 Charge Coupled Device

The most common camera sensors used in machine vision applications are the charge coupled device (CCD). A CCD camera contains a silicon chip which consists of a matrix of light sensitive photosites called pixels. When light falls on this chip, it is collected by a matrix of pixels. The image is divided into these small discrete pixels. The information from these pixels is collected, organised and transferred to a monitor to be displayed.

3.3.2 Charge Coupled Device Size

The size of the sensor active area is important in determining the dimension of FOV. Larger sensor sizes offer greater FOV when a fixed IMF is applied. There are several standard CCD sensor sizes which are available in the market as given in Figure 3.3. They are known as 1/4", 1/3", 1/2", 2/3" and 1".

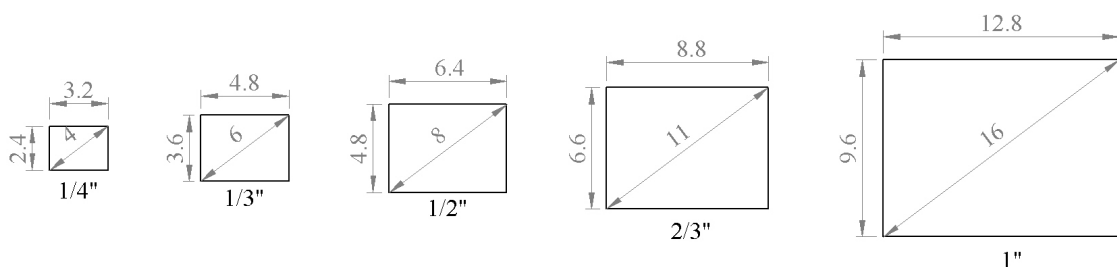


Figure 3.3: Illustration of the dimensions in (mm) of CCD standard sizes camera.

3.3.3 *Monochrome CCD Camera*

Monochrome camera produces only greyscale image. This greyscale image or also known as 8-bit image is produced when the CCD chip detects the minimum amount of contrast which is 256 shades of grey.

3.3.4 *Interlaced and Progressive Scan*

Conventional CCD cameras employ an interlaced scanning across the chip. The chip is divided into two fields which is odd (rows 1, 3, 5,...) and even (rows 2, 4, 6,...). Both fields are then integrated to produce a full frame of image. Each field is scanned one after the other. For most applications, this scanning method will not cause a problem. But some problems may arise in high speed applications because by the time the second group is scanned, the object has already moved. This causes a blurring or a ghosting effect in the final image. This problem can be solved by applying a progressive scan CCD camera. This method scans the lines across the chip sequentially (rows 1, 2, 3, 4,...). It only scans as single field, so it produces a full frame faster than interlaced scan.

3.3.5 *Frame Rate and Shutter Speed*

The frame rate is defined as the number of images acquired in a second. A faster frame rate is required for high speed applications where the camera captures more images of the object as it moves.

The shutter speed refers to the exposure time of the CCD chip. The exposure time controls the amount of light incident to the chip. Lowering the shutter speed will increase the exposure time and allows more light to the chip and this is suitable for low

light environment applications. Increasing the shutter speed reduces the exposure time and limits the amount of light to the chip. It also helps in producing snap shots of a fast moving object.

3.4 Illumination

An important aspect in an imaging system is illumination. A correct illumination is critical to an image system and an improper illumination can cause a variety of image problems. Poor illumination can also result in low signal-to-noise ratio. Non-uniform lighting can harm signal-to-noise ratio and make tasks such as thresholding more difficult.

3.4.1 White Light

Light is electromagnetic radiation that is visible to the human eye. Electromagnetic radiation includes all forms of radio waves, microwaves, infrared radiation, visible light, ultraviolet radiation, x-rays and gamma rays (Figure 3.4). The visible light spectrum covers the wavelength range from about 380 nm to about 770 nm [70]. White light is dispersed by a prism into the colours of the visible light spectrum. Each colour can be represented in the range of wavelengths as given in Figure 3.4.

In imaging systems, every component affects the amount of light incident on the camera sensor and therefore affects the image quality. The imaging lens aperture ($f/\#$) controls the amount of light incident on the camera. Illumination should be increased as the lens aperture is closed (i.e. higher $f/\#$). High power lenses usually require more illuminations, as smaller areas viewed reflect less light back into the lens. These are related to the particle sizing application, where the small FOV is needed to record

particles images. Therefore, high intensities of light source are very useful in this kind of application.

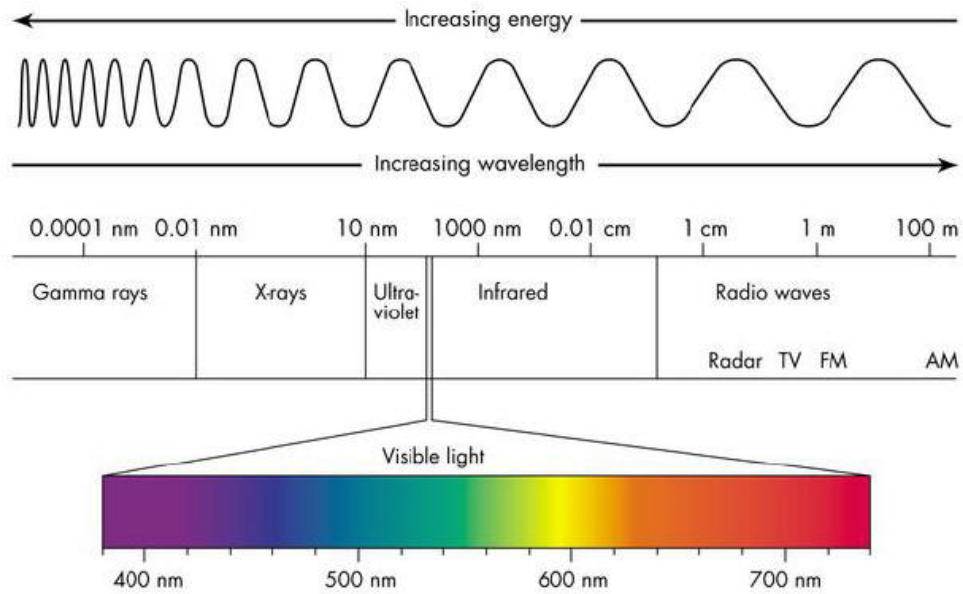


Figure 3.4: Electromagnetic spectrum [71].

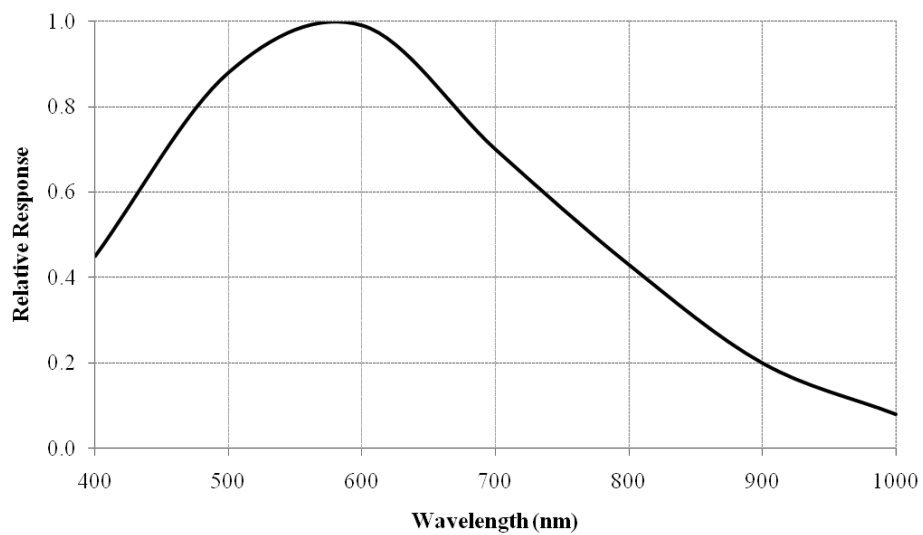


Figure 3.5: Spectral sensitivity of the XCD-SX90 SONY camera [72].

The sensitivity of the camera is also important in determining the type of illumination required in the system. Figure 3.5 depicts the sensitivity or relative response of the camera on the wavelength of incident light. It shows that the peak of the camera sensitivity is around 600 nm. It is noted that above 0.9 of the camera sensitivity, the light with wavelength between 500 to 650 nm is also suitable for this imaging system. Therefore, white light is inappropriate for this application due to its wide range of wavelength, which covers the entire visible light spectrum as given in Figure 3.4.

3.4.2 *Laser*

A laser is a device that produces light, which is an electromagnetic radiation, through a process of optical amplification based on the stimulated emission of photons. It has three special properties that contribute to its usefulness in many applications: coherence, monochromatic and collimation (Figure 3.6).

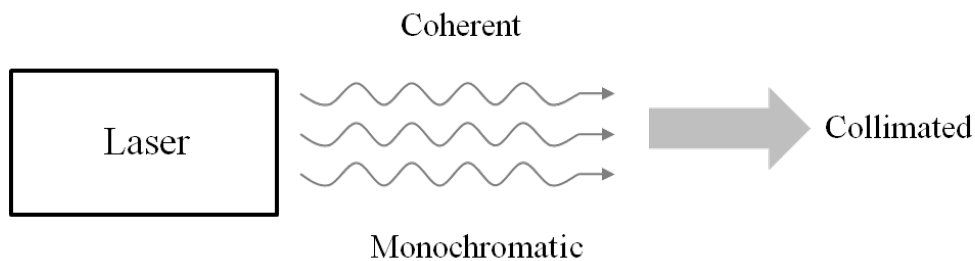


Figure 3.6: Properties of laser light [73].

Coherence is the property of light where all waves that are emitted from a laser source are at exactly the same phase. In order to maintain in similar phase, all the emitted waves have to be in the same wavelength. The laser has an ability to produce light at a single wavelength, which is defined as monochromatic light. This property is very important in determining the suitability of the light in terms of the camera sensitivity as given in Figure 3.5. Collimation is the term used to define the property of laser light that

allow it to stay as a tight, parallel rays and confined beam for large distances. In other words, the light does not dispersed or dispersed minimally with increasing distances.

A critical property of lasers is their ability to produce high intensity light. This is helpful for applications where high illumination is required such as in acquiring images of small FOV by high power lenses. Also, the laser has an ability to produce very short pulses of light within nanoseconds or picoseconds. This pulsed light can be applied to fast moving object applications. The pulsed laser stroboscopically freezes the object movement and the camera captures clear image without object streak.

3.5 Image Processing Fundamentals

3.5.1 Digital Image Representation

A digital image is a two-dimensional array of numbers showing values of the physical image at a rectangular matrix form. Each image corresponds to a small region of the physical image called a picture element or pixel. As illustrated in Figure 3.7(a), each pixel is addressed by an intensity function $I(x, y)$, where x and y denote the spatial coordinates of the pixel. Image resolution is represented by its number of pixels where M columns and N rows in the image has a resolution of $M \times N$. For a monochrome or greyscale image, a typical bit depth of 8 bits are employed so that 256 possible grey levels ranging from 0 (black) to 255 (white) are used as pixel values (Figure 3.7(b)).

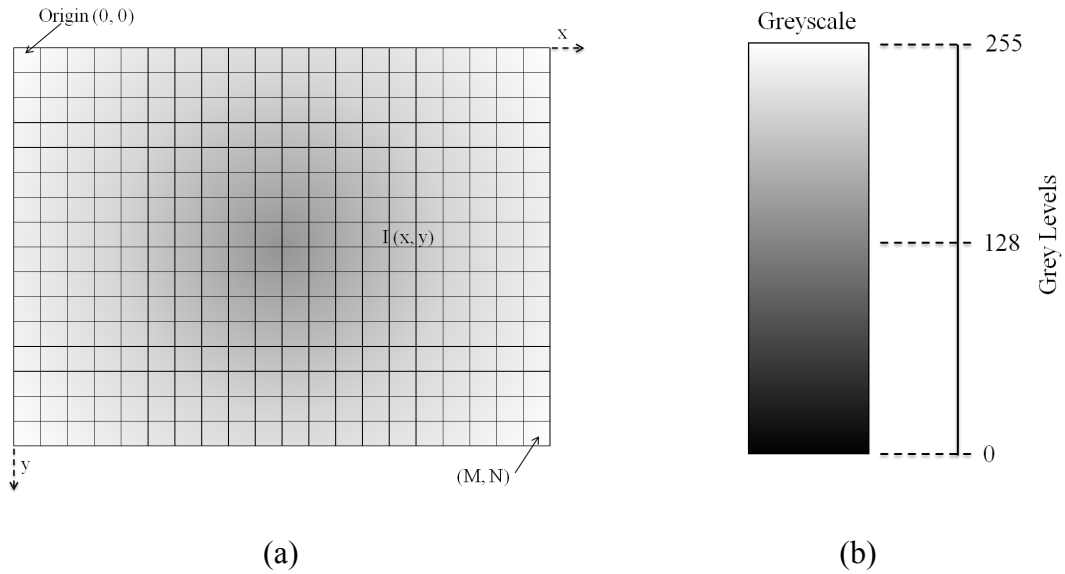


Figure 3.7: (a) Greyscale image representation. (b) Grey levels for 8-bit image.

3.5.2 Grey Level Histogram

A histogram provides a general description of the pixel distribution intensities in an image. It is usually presented as a plot of the number of occurrences of a greyscale value in relation to the intensity of that value. Generally, the histogram is applied to determine the overall quality of the image to establish its suitability for any measurement task. Figure 3.8 shows a sample of particles image with its associated grey level histogram. The histogram contains a large number of pixels with very high grey level values, which are depicted by a peak at the upper end of the histogram. The horizontal axis of the histogram represents the grey scale ranging from 0 (black) to 255 (white) and the vertical axis the number frequency of pixels at each grey level.

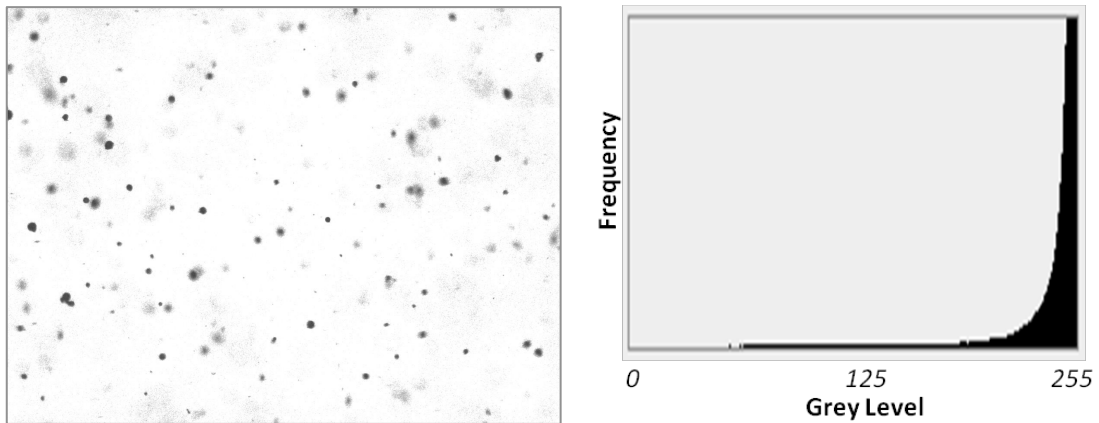


Figure 3.8: Sample of particles image with its associated grey level histogram.

3.5.3 *Lookup Tables*

This is the basic functions of image processing that highlight details in areas containing significant information. The lookup table (LUT) functions are generally used to improve the contrast and brightness of an image by adjusting the dynamic intensity of regions with poor contrast. These functions include histogram equalisation, gamma corrections, logarithmic corrections and exponential corrections. Details of these functions can be found in reference [74].

3.5.4 *Convolution Kernels*

Generally, the convolution kernel is employed to filter a greyscale image. The purpose of image filtering is to improve the image quality so that it fulfils the requirements of the application. Improvements of an image include image smoothing, remove image noise, enhance the edge information and many more.

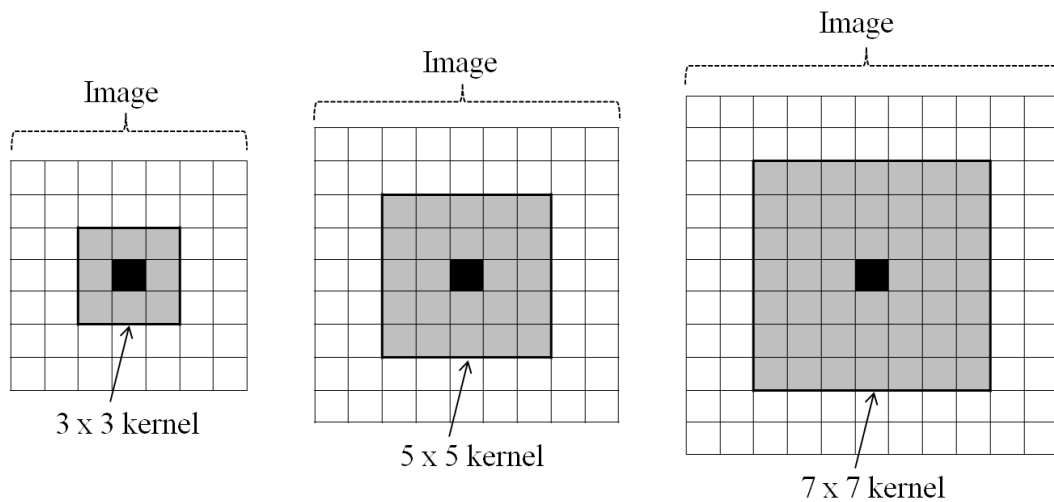


Figure 3.9: Examples of kernels.

A convolution kernel defines how a filter alters the pixel values in a greyscale image. The convolution is an operation in which the final pixel is the weighted sum of the neighbouring pixels. This convolution operation is based on a matrix which gives some weight to each one of the neighbour pixels. This matrix is called convolution kernel. The common convolution kernel is a square 3×3 , 5×5 or 7×7 dimension matrix. The kernel size determines the number of neighbouring pixels whose values are considered during the filtering process.

In the case of a 3×3 kernel, illustrated in Figure 3.9, the value of the central pixel (shown in black) is derived from the values of its eight surrounding neighbours (shown in grey). A 5×5 kernel specifies 24 neighbours and a 7×7 kernel specifies 48 neighbours.

A filtering operation on an image involves moving the kernel from the leftmost and topmost pixel in the image to the rightmost and bottommost point in the image. At each pixel in the image, the new value is computed using the values that lie under the kernel, as shown in Figure 3.10.

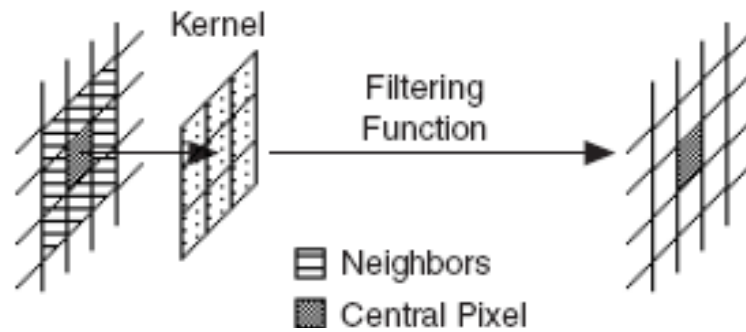


Figure 3.10: Mechanics of filtering [74] .

3.5.5 Spatial Filtering

Image enhancement procedures consist of a collection of techniques that are applied to improve the visual appearance of an image. They are used to emphasize certain image features such as to improve the edges boundaries or contrast of the image. The common method in performing image enhancement is using spatial filters. The filters serve a variety of purposes such as detecting edges, contouring patterns, reducing noise and detail outlining or smoothing. By applying the filters, an image can be made smooth, sharp and can be transformed or can have noise removed so that the required information can be extracted.

Spatial filters alter pixels values with respect to variations in light intensity in their neighbourhood. The neighbourhood of a pixel is defined by the size of a matrix or mask centred on the pixel itself. These filters can be sensitive to the presence or absence of light intensity variations. Filters are divided into two types, which are linear (also called convolution) and nonlinear.

Table 3.1: Types of spatial filters.

	Low-pass	High-pass
Linear	Gaussian Smoothing	Gradient Laplacian
Nonlinear	Low-pass Median Nth Order	Differentiation Gradient Prewitt Roberts Sobel

As shown in Table 3.1, linear and nonlinear filters are categorised into high-pass and low-pass filters. The low-pass filters attenuate variations of the light intensity. They help emphasize gradually varying patterns such as objects and the background. They have the tendency to smooth images by eliminating details and blurring edges. High-pass filters emphasize significant variations of the light intensity usually found at the boundary of objects. They help isolate abruptly varying pattern that correspond to sharp edges, details and image noise. Details explanations of each filter are described by reference [74].

3.5.6 *Segmentation and Thresholding*

Segmentation extracts the outlines of different regions in the image such as to divide the image into regions which are made up of pixels. In this case, threshold is applied to image to separate the objects from the background. A binary image is produced after the threshold process is applied. The binary image is an image that contains object regions with pixel values of '1' and a background region with pixels values of '0'. Threshold process defines which values (from 0 to 255) belong to the object and which values

(from 0 to 255) belong to the background in the image. The upper limit and lower limit of pixel intensity values in the image are specified so that the pixels inside the bounds of the limits are set to '1' and the outside the bounds of the limits are set to '0'. Once the binary image is produced, image processing functions such as a binary morphology and a particle analysis can be applied.

There are two types of thresholding, which are global and local thresholding. Global thresholding is more suitable when the images of the object have uniform lighting both within each image and across multiple images. It categorizes a pixel as part of a particle or the background based on a single threshold value derived from the intensity statistics of the entire image.

Second type of thresholding is the local thresholding. It is also called as locally adaptive thresholding. It categorises a pixel based on the intensity statistics of its neighbourhood pixels. This type of thresholding works best on the images that exhibit non-uniform lighting changes [41]. Non-uniform lighting changes, such as those resulting from a strong illumination gradient on the image, often make global thresholding ineffective.

3.5.7 Morphological Functions

It is an image processing functions that can be applied to improve the binary image. Binary image produced by threshold process may contain unwanted information such as noise particles, particles touching the image border and particles touching each other. These unwanted information can be removed by applying morphological functions and at the same time refining the information in the binary image.

Binary Morphological functions extract and alter the structure of particles in a binary image. The functions include erosion, dilation, opening, closing and contour extractions. These functions can separate particles, remove either small or large particles, fill holes and create the outline of particles.

3.6 Summary

This chapter has explained the basic parameters of imaging systems. Understanding the definition of each parameter is necessary to obtain the proper setup of imaging systems. Illumination is another aspect that has been discussed in this chapter. Better image quality can be achieved by improving the illumination of imaging systems. Illumination from the laser light source is more suitable for the fast moving objects and smaller FOV applications. An acquired image has to be processed to extract the required information from the image. Here, fundamentals of image processing are described. Understanding the definition and the purpose of image processing functions are important so that the proper steps in extracting the information from the acquired image can be designed.

Chapter 4

Development of the Dynamic Image Analysis Software

4.1 Introduction

In this work, a dynamic image analysis (DIA) technique is developed for the automated determination of the properties of particles such as size, shape and concentration. It requires 8-bit digital images of the multiphase-phase flow under investigation. The analysis of the images is performed through an automated processing algorithm.

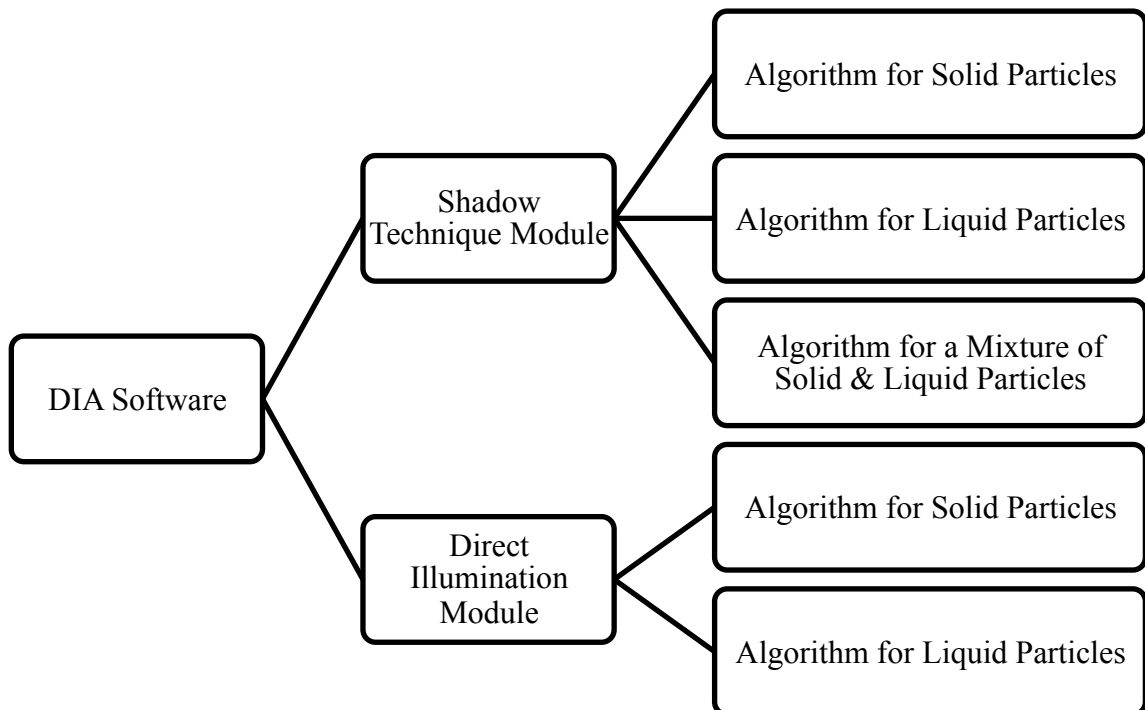


Figure 4.1: A schematic diagram of the DIA software.

To develop DIA software, rigorous LABVIEW codes have been manipulated to perform all the image processing and analysis tasks. A number of image processing functions are applied to extract the required information from an image. There are two different modules that have been developed for the DIA software (Figure 4.1). The first module is for shadow technique and second one is for Direct Illumination (DI) technique. These modules are designed separately to cater the different images of particles that are produced by shadow and DI techniques. The following sections explain both modules and describe the algorithms used to analyse solid and liquid particles images.

4.2 Shadow Module

The shadow technique is applied to perform measurements of moving particles that are dispersed in a fluid medium. The principle and setup of this technique is based on the shadow image of the particle that is described in detail in Section 5.4. An image processing module is developed to acquire, process and analyse images that are captured using this technique.

Figure 4.2 shows the flowchart of this module which was designed using LABVIEW platform. The module starts with a continuous acquisition by a camera where each acquired image is copied from an acquisition buffer into a processing buffer and displayed on a monitor. The image is processed and analysed to extract useful information such as particle size. These processes required different types of algorithms as images of solid and liquid particles captured by this technique produce different patterns as discussed in Section 5.4. An image may contain only solid particles or liquid particles or sometimes a mixture of both depending on the application. Therefore, two

sets of algorithms are developed to analyse each particle type as will be explained in Sections 4.2.1 and 4.2.2. Then, both algorithms are combined to enable the DIA software to distinguish between solid and liquid particles as described in Section 4.2.3.

The image acquisition is run continuously and every image in the processing buffer is processed and analysed until the acquisition is stopped. Then, the acquisition session is closed and the images are disposed of to clear the memory.

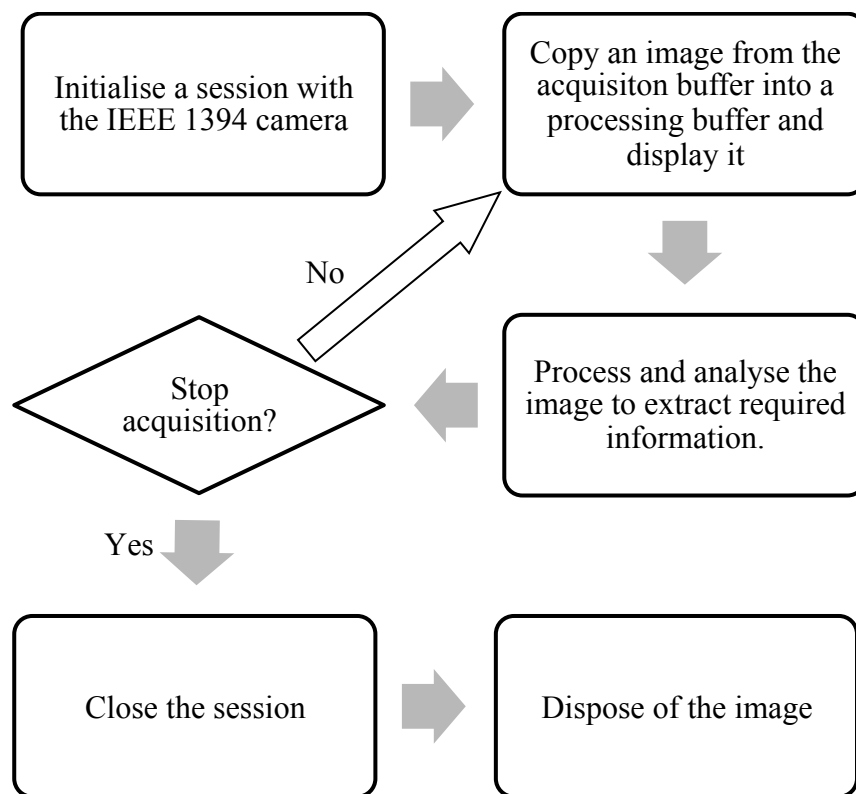


Figure 4.2: The flowchart of the DIA software for the shadow technique module.

4.2.1 Algorithm for Solid Particles

In the shadow module, a camera is used to acquire a raw image of particles. Once the image is captured, a sequence of steps as shown in Figure 4.3 are employed to extract the required information. The acquired image is enhanced so that it looks subjectively

better [75]. A lookup table (LUT) with a square function is applied to improve the contrast and brightness of the image by modifying the dynamic intensity of regions with poor contrast. The image is then subjected to a low-pass linear filter to reduce image noise and smooth the overall shape of objects. Non-linear high-pass Sober function with a 3 x 3 kernel is applied to the image to extract the outer particle region or particle edge. It highlights significant variations of the light intensity along the vertical and horizontal axes to produce a particle edge [74]. Images on each step are depicted in Figure 4.4.

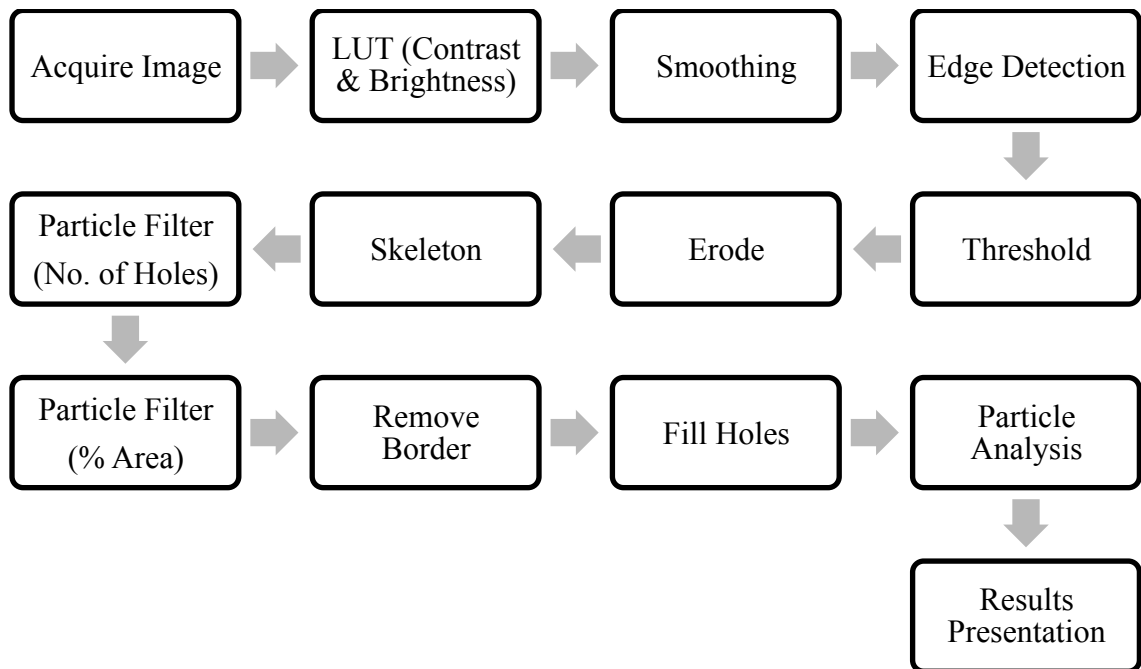
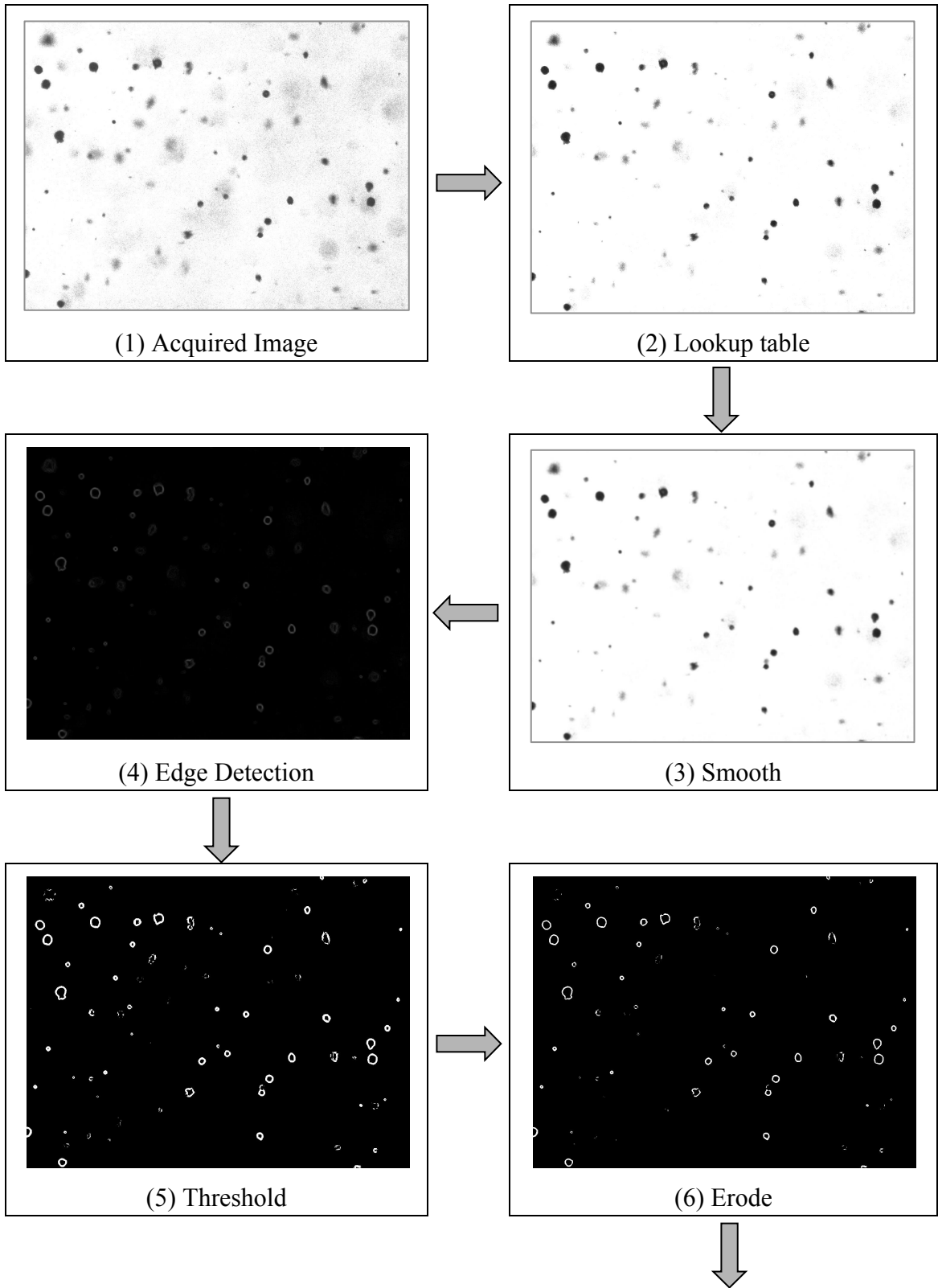
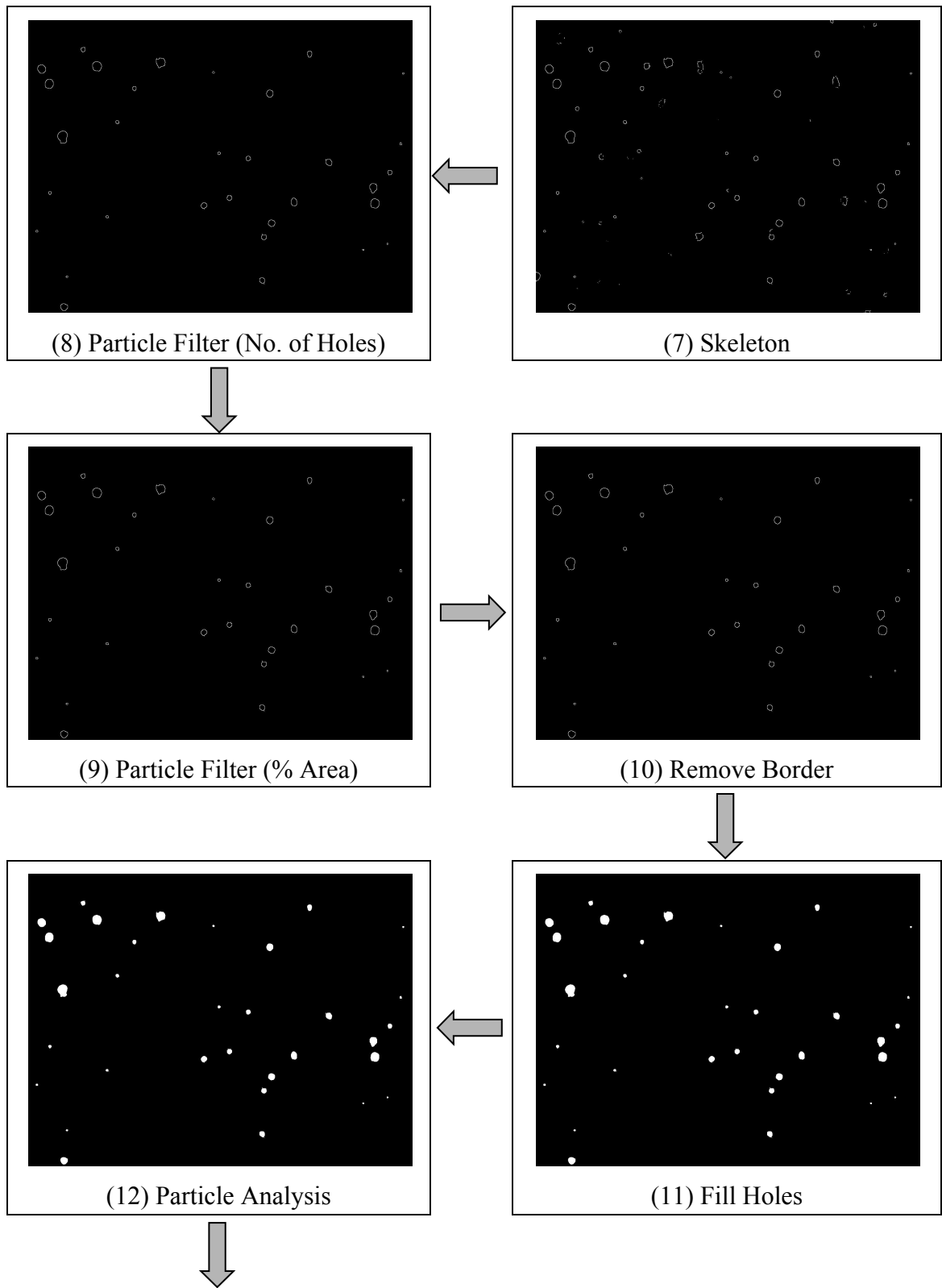


Figure 4.3: Sequence of solid particles image analysis in shadow module.

After the edge of the particle is detected, it is extracted from the image background by performing a thresholding process. This process converts the image to a binary image by defining the particle edge (black) to pixel value of '1' and background (white) to pixel value of '0' as described in Section 3.5. In this algorithm, local adaptive threshold is used to isolate the particle edge image. This type of thresholding is suitable for an image that has uneven light illumination [41].





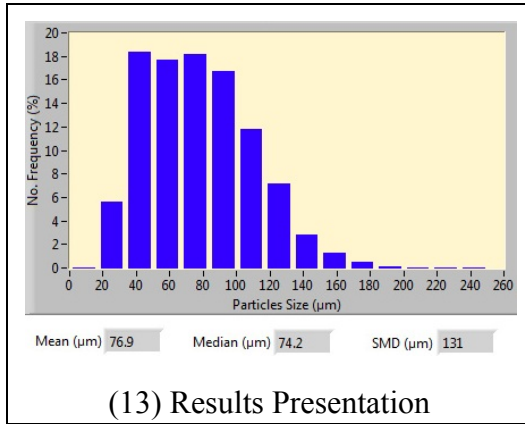


Figure 4.4: Images of the sequence of solid particle image analysis by the shadow module.

It is noticed that the binary image of the particle edge looks bigger compared to the greyscale image on edge detection as illustrated in Figure 4.4. Therefore, morphological functions are applied to the binary image to remove any unwanted information caused by the thresholding process. The erosion function with 3 x 3 element size is used to remove pixels isolated in the background and erode the contour of the particle edge. Then, another morphological function called skeleton is applied to produce thin particle edge where the width of each pixel is one.

The particle filter is employed to remove or keep particles in an image as specified by the filter criteria. First, the filter is applied to keep the particles that have only one number of holes. This eliminates all the unclosed particle edges, which belong to the out-of-focus particles. A second filter is applied to differentiate between the solid (opaque) particles with the liquid (transparent) particles. This is achieved by defining a percentage of the particle edge area in relation to its edge and hole area. This filter criterion can be explained through the Equation 4.1 and Figure 4.5.

$$\%Area = \left[\frac{A_E}{A_E + A_H} \right] 100 \quad 4.1$$

where A_E is the edge area and A_H is the hole area.

Figure 4.5 shows the representation of a single particle with its edge and hole area. The filter criteria which is %Area is set between 1 to 65% in order for a solid particle to be detected. This range of %Area will ignore any liquid particle which is explained in Section 4.2.2. The %Area values are determined through the experiment that will be explained in Section 5.5.4.

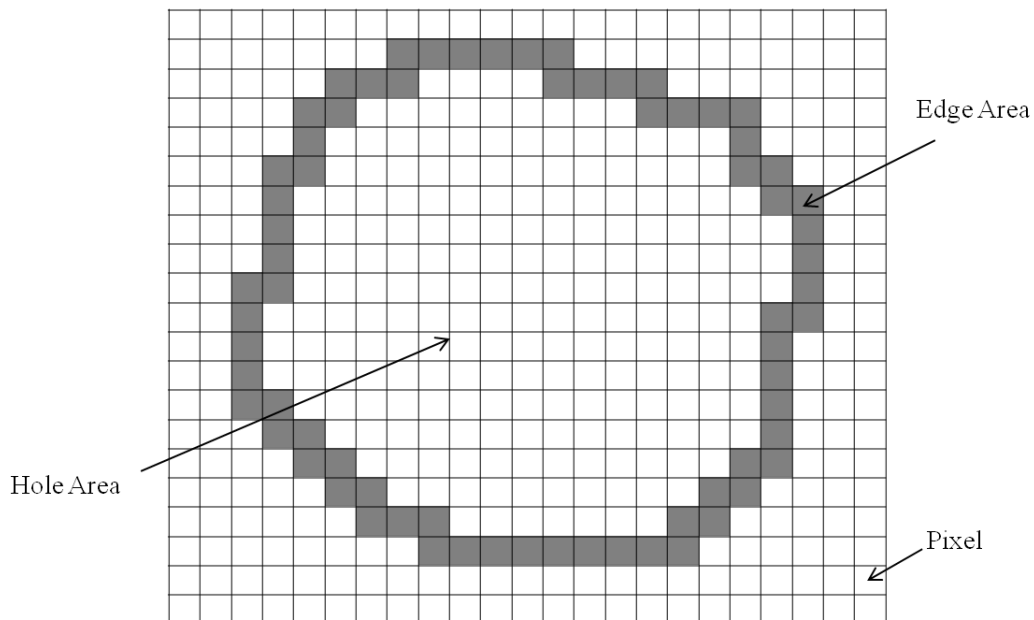


Figure 4.5: An edge and hole area of single solid particle image analysed by the shadow module.

Figure 4.6 illustrates the results obtained by performing image analysis of experimental work in Section 5.5.4. The numbers of pixels representing the edge and hole area are examined and the %Area is calculated using Equation 4.1. It is found that the %Area is lower at bigger particle sizes. This is due to the greater hole area of bigger particles compared to the smaller particles. At different IMF, the range of %Area is found from 8

to 64%. This box-plot shows the distribution of %Area on each IMF where a circle in the box represents the median. The edges of the box are the 25th and 75th percentiles and the dash-line extends to the most extreme data points.

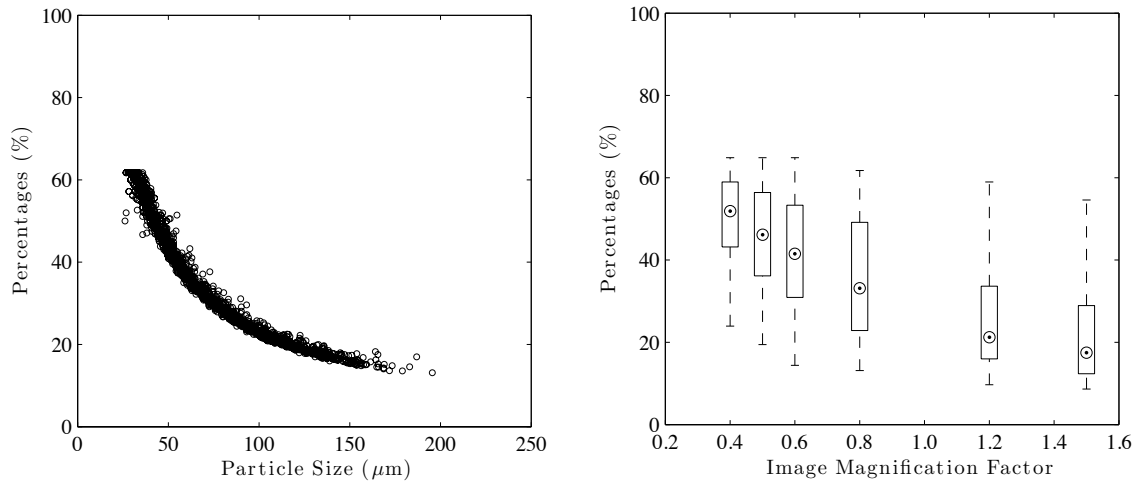


Figure 4.6: Detected %Area in relation to solid particle size and image magnification factor.

After the image is filtered by %Area criteria, a morphological operation called remove border filter is applied. This function removes particle edges that touch the border of the image. Another morphological operation called fill holes function is used to fill the holes within the remaining particle edges. At this stage, there is no more holes on particle images and all of them are filled with pixels.

Then, the particle analysis function is employed to initiate particle measurements in the binary image. This function is applied to measure the number of particles in the image, area of each particle and also its circularity factor. Finally, an algorithm is developed to manipulate the arrays of data extracted from the image. The results are used to plot the measurements such as particle size distribution, particle shape and concentration.

4.2.2 Algorithm for Liquid Particles

Once an image is acquired by a camera, a sequence of steps shown in Figure 4.7 is employed to process and analyse it. A similar lookup table, smoothing filter and thresholding function as described in Section 4.2.1 are used in this liquid particles image. As a result, an in-focus liquid particle produces a hole in the middle while out-of focus particles do not. This binary image is then applied subjected to a particle filter to keep the particles which have one hole number and removes the others.

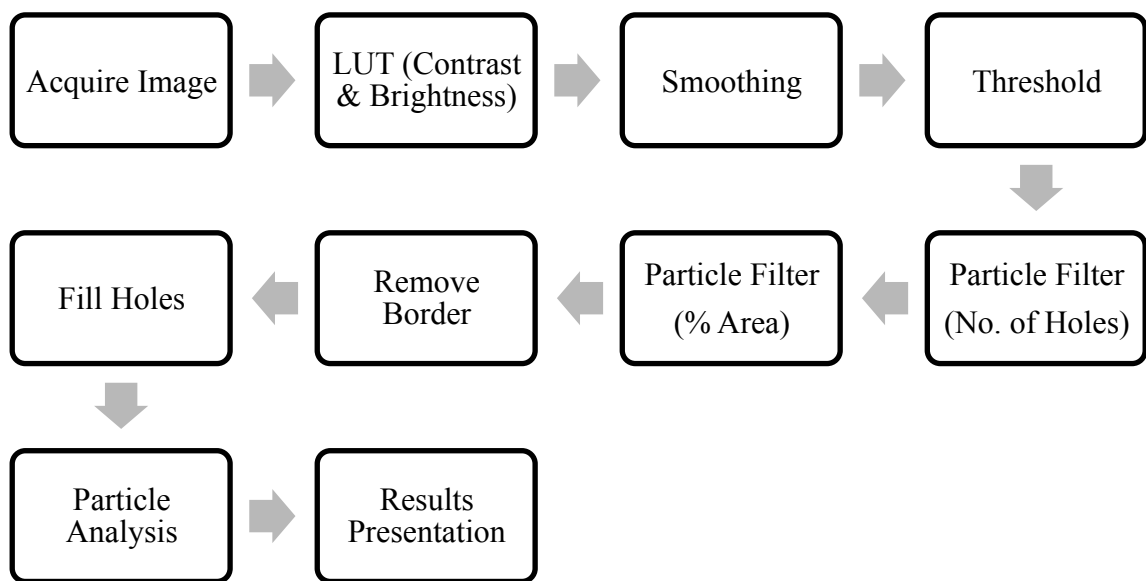
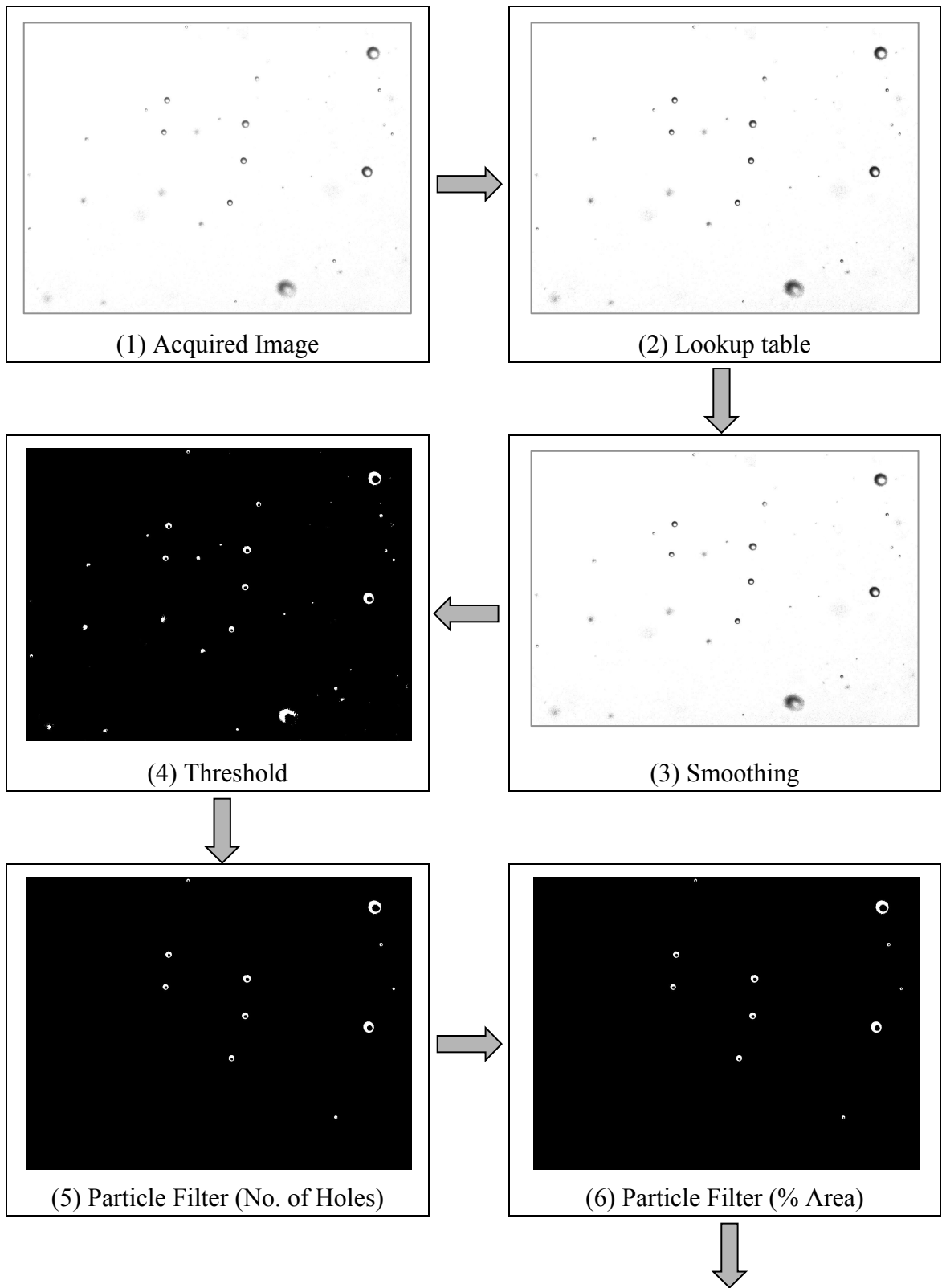


Figure 4.7: Sequence of liquid or transparent particles image analysis in the shadow module.

Then, the image is applied with another particle filter which keeps only the particles that have %Area from 65 to 95% to remain. These values will ignore solid particles if they exist in the image as described in Section 4.2.3. The values are obtained by defining a percentage of the particle edge area in relation to its edge and hole area. This filter criteria is explained through Equation 4.1 and Figure 4.9. The %Area of liquid or transparent particles was determined by performing experiments that will be explained in Section 5.5.2.



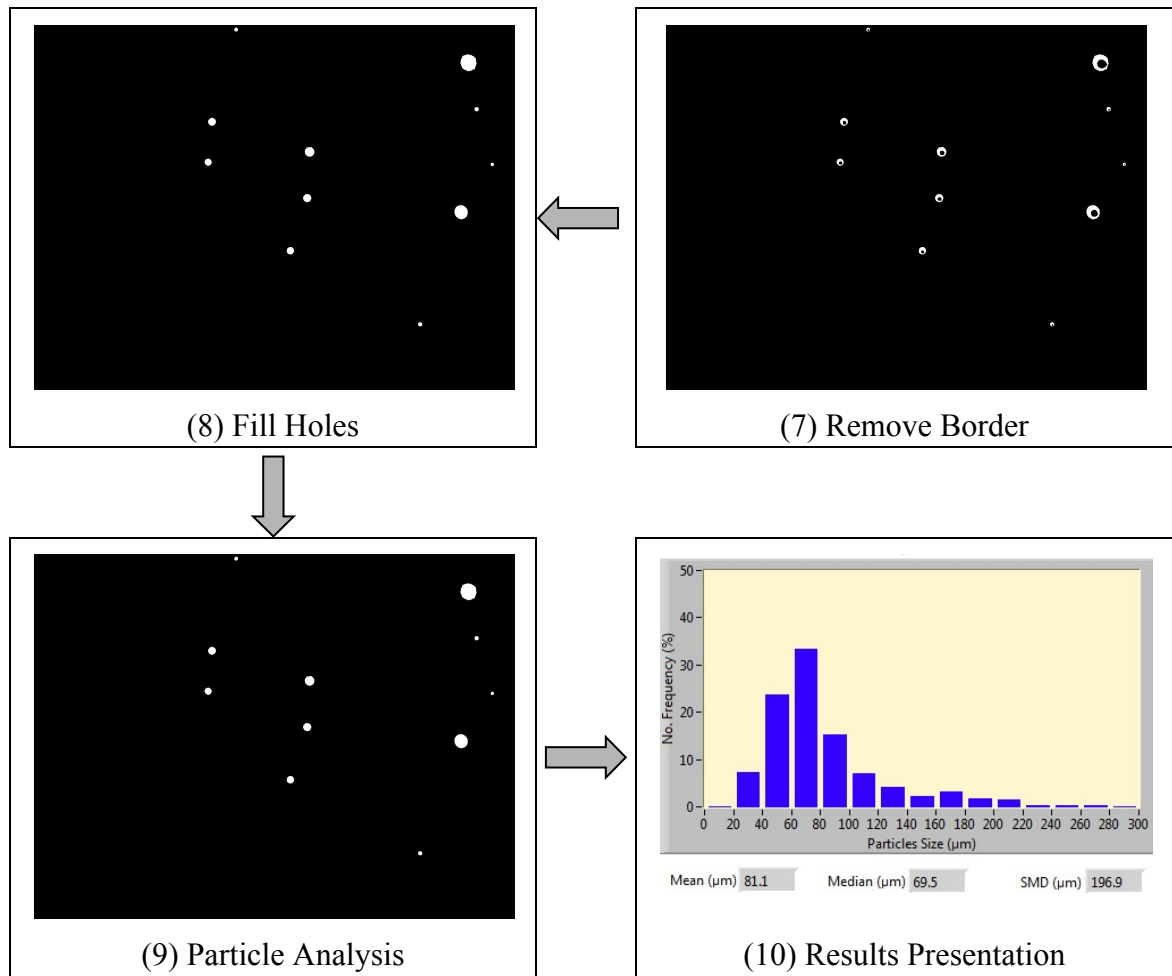


Figure 4.8: Images of the sequence of liquid particle analysis by the shadow module.

The relationship between %Area and particle size in Figure 4.10 is measured at IMF of 0.8. It shows that the %Area for liquid particles is more than 65% and this is confirmed with the plot of %Area at different IMF shown in same figure. It is found that the median of %Area at different IMF is about 80%.

After the particle image is filtered using the %Area criterion, the next steps will remove the borders, fill holes, compute the pixels and plot the results. These steps are similar to the sequences used in analysing the solid particles that are explained in Section 4.2.1.

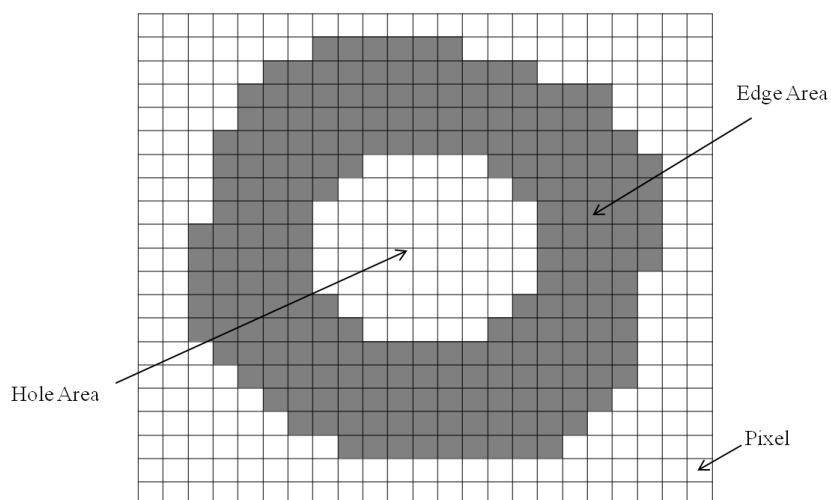


Figure 4.9: An edge and hole area of single liquid particle image.

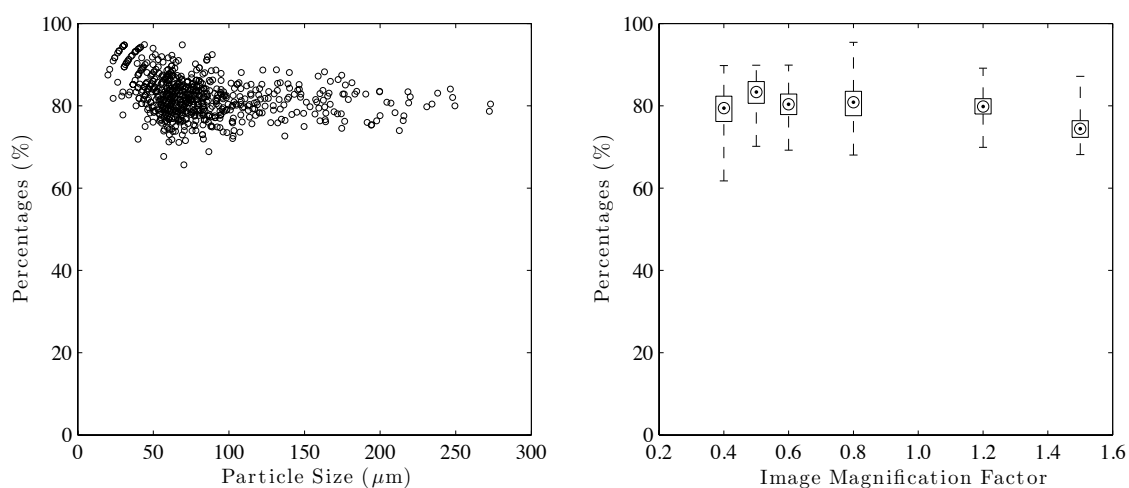


Figure 4.10: Detected %Area in relation to liquid particle size and IMF.

4.2.3 Algorithm for a Mixture of Solid and Liquid Particles

An acquired image may contain solid or liquid particles or a mixture of both depending on the application. This algorithm is developed to distinguish between solid and liquid particles and perform particles characterisation. It is applied in the DIA software and used in the Non-intrusive Particle Sizer (NPS) instrument. By developing this algorithm, the NPS can be used to perform automated on-line sizing either for solid or liquid particles or a mixture of both without changing any hardware or software parameters.

A novel method involving processing of shadow images to differentiate and recognise between solid and liquid particles is illustrated in Figure 4.11 and Figure 4.12. Essentially, once the particles image which contains both solid and liquid particles is captured by the camera, both algorithms for solid particle and for liquid particle as described in Section 4.2.1 and 4.2.2 are applied to the image. The acquired image is processed and analysed simultaneously by both algorithms. First, the algorithm is used to only recognise solid and reject liquid particles, and the second algorithm is applied to only detect liquid and reject solid particles.

A method used in characterising solid and liquid particles in an image is by applying two different algorithms. The complete algorithms described in Section 4.2.1 and 4.2.2 are used to obtain solid and liquid particle size. Figure 4.12 shows the produced images on each step for solid and liquid particles detections. After both algorithms performed the particle analysis steps, the extracted data from the images are manipulated to produce result presentations such as size distribution, particle shape and its concentration.

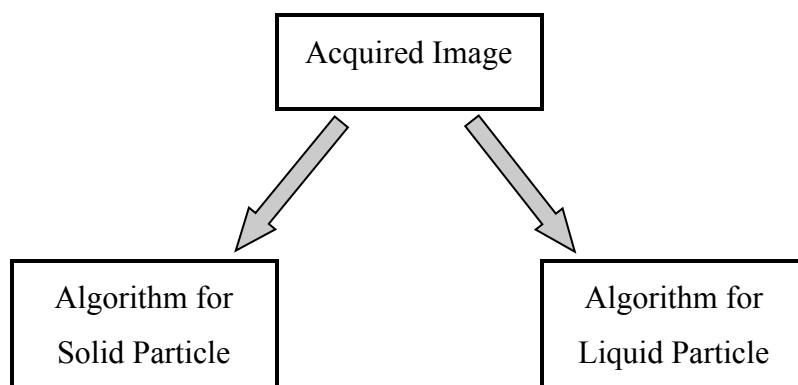
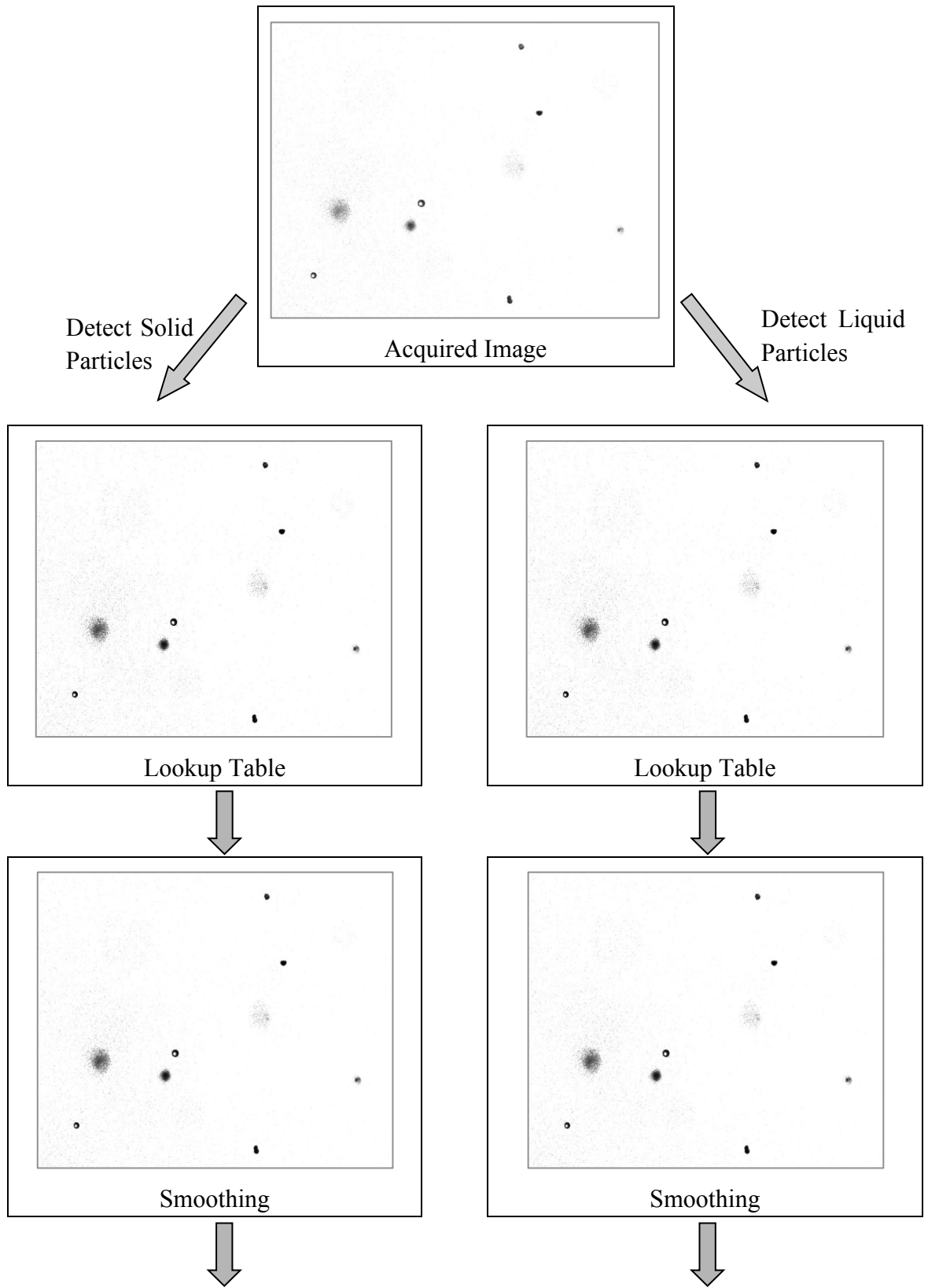
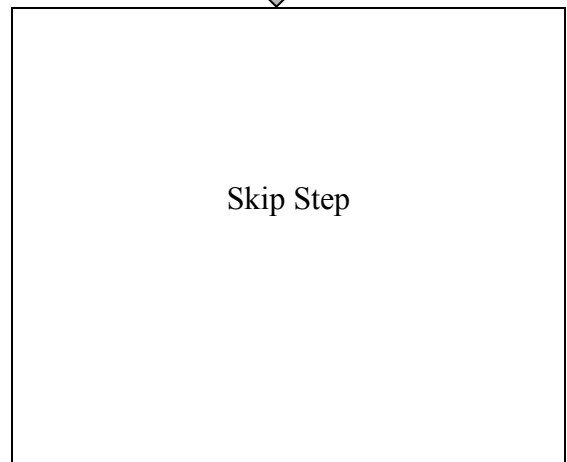
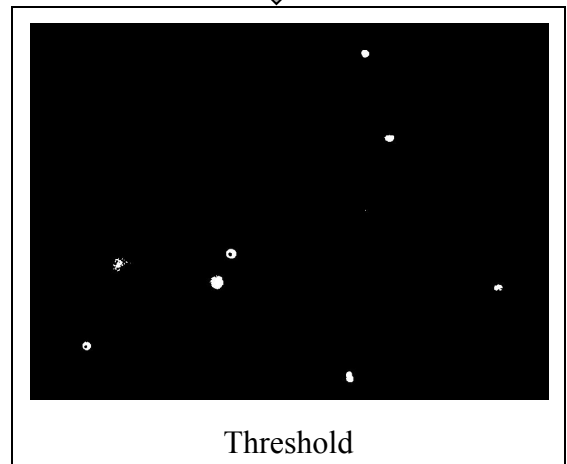
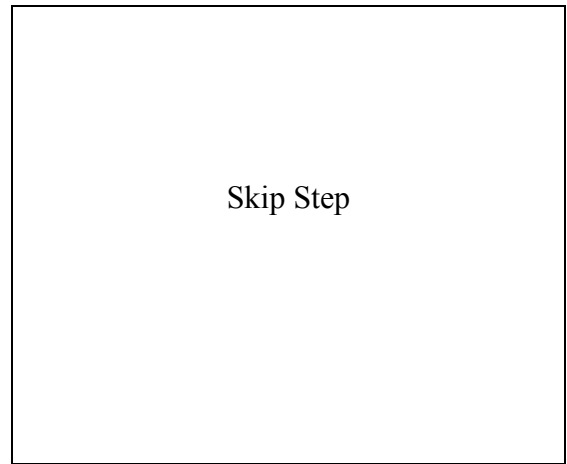
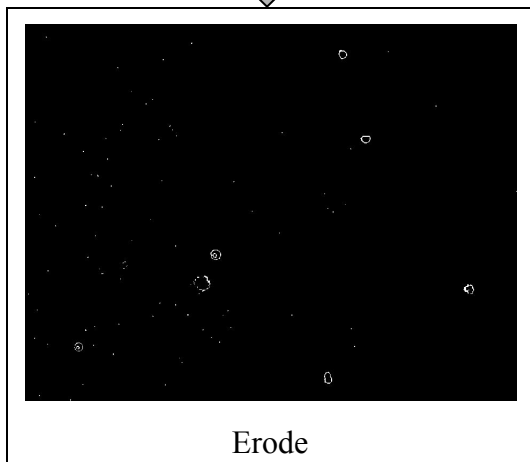
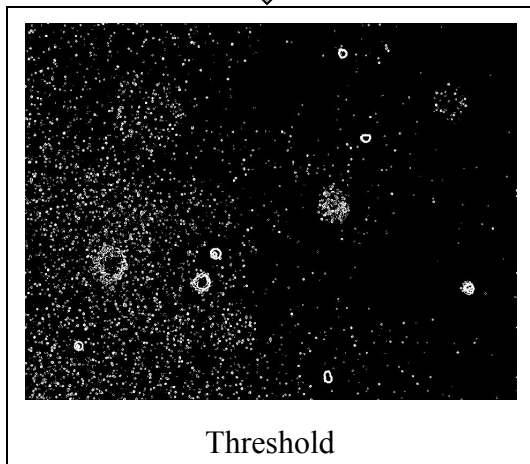
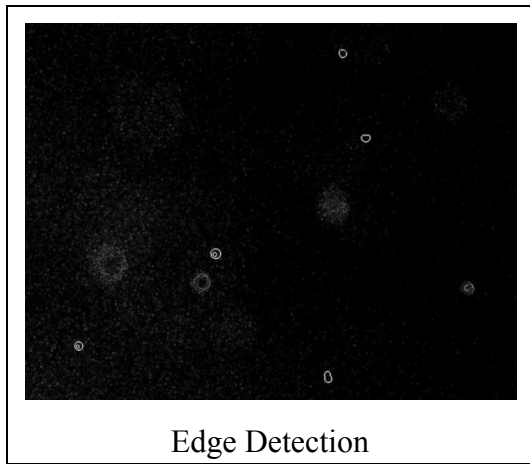
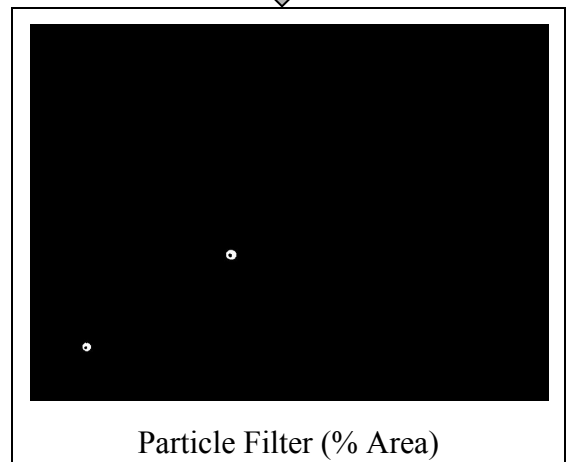
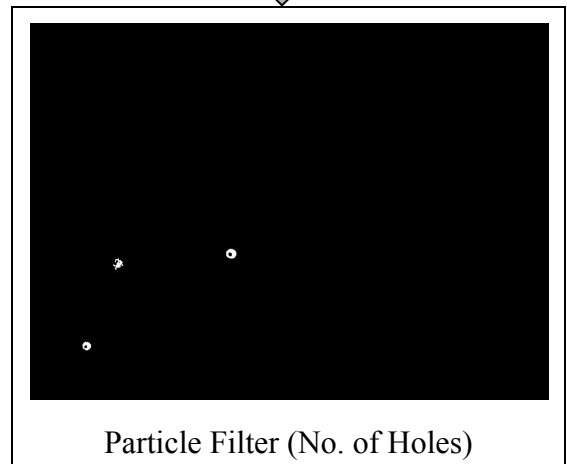
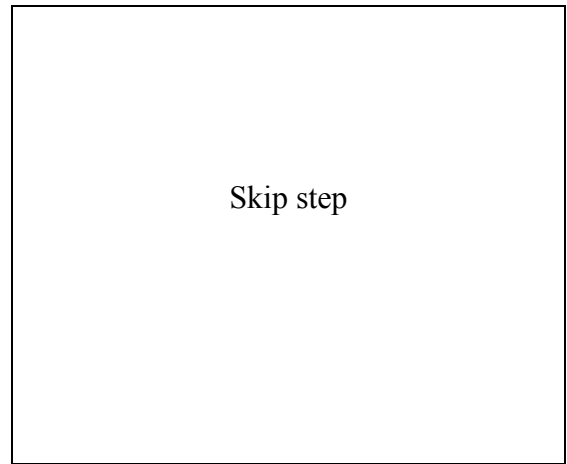
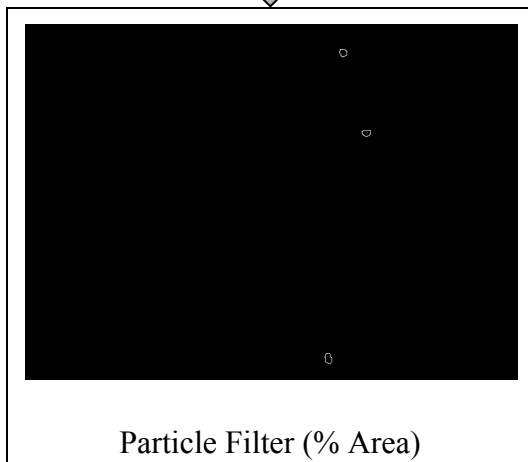
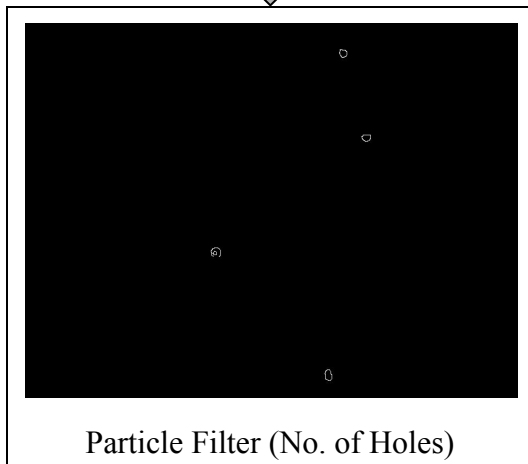
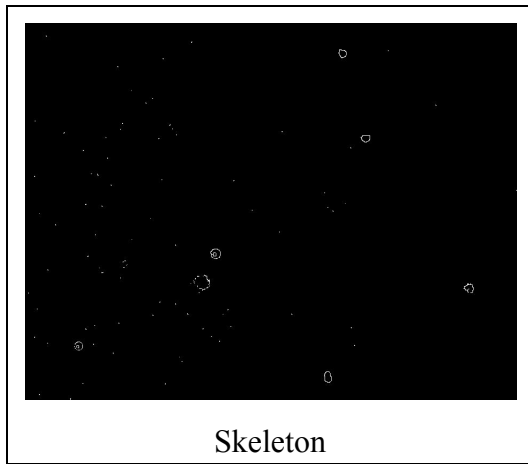


Figure 4.11: Method to differentiate between solid and liquid particles in the shadow module.







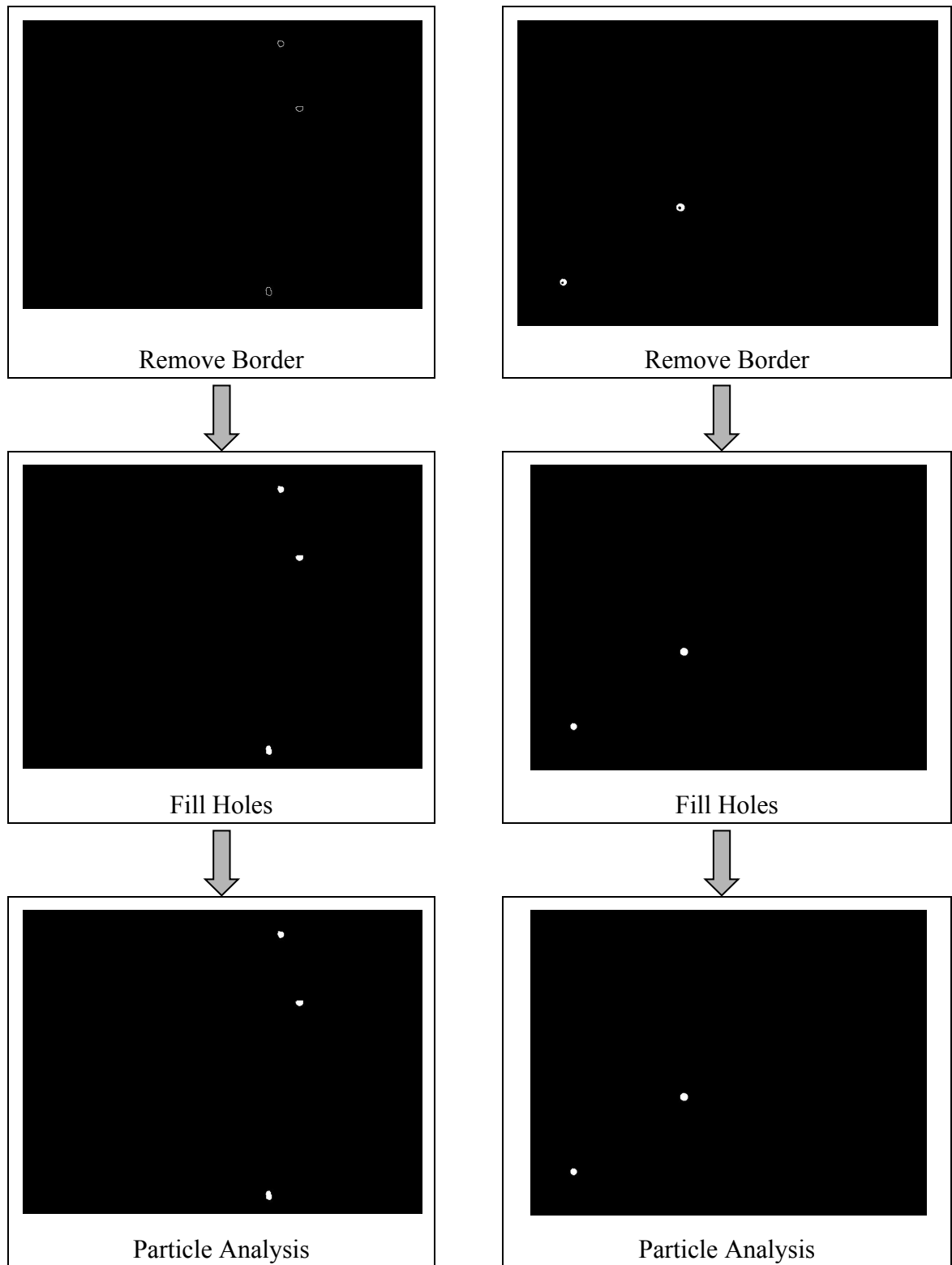


Figure 4.12: Image processing sequence for the solid and liquid particles recognition.

4.3 Direct Illumination Module

Direct illumination is an alternative technique used to characterise solid or liquid particles that are dispersed in a fluid. The principle and setup of this technique can be referred to Section 5.6. An image processing module is designed to acquire, process and analyse images captured using this technique. The flowchart of this module is fundamentally similar to the shadow module that is illustrated in Figure 4.2.

The image is processed and analysed to extract useful information such as particle size. The processes required different types of algorithms as images of solid and liquid particles captured by this technique produced different pattern as discussed in Section 5.6. An image may contain only solid particles or liquid particles depending on the applications. Therefore, two sets of algorithms are developed to analyse each type of particle and they are explained in Section 4.3.1 and 4.3.2.

4.3.1 *Algorithms for Solid Particles*

The sequence of steps illustrated in Figure 4.13 is employed to an image of solid particles acquired by DI technique. All steps in this algorithm are similar to those explained in Section 4.2.1. Every step and its sequence are designed to extract the required information such as the number of pixels occupied in a single particle and the total number of detected particles in the image. So, each step in the sequence produces less information from the image compared to the previous one. This is clearly shown in Figure 4.14 where the sequences are designed to only measure the in-focus particles and reject the out-of-focus particles.

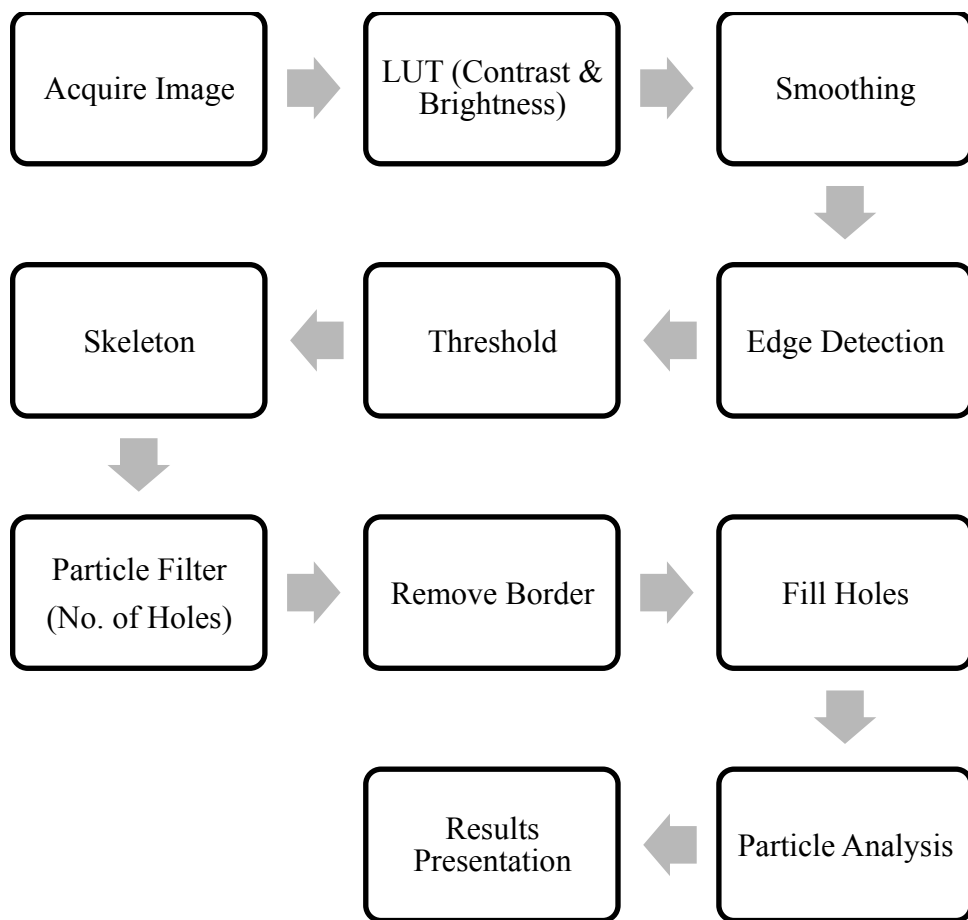
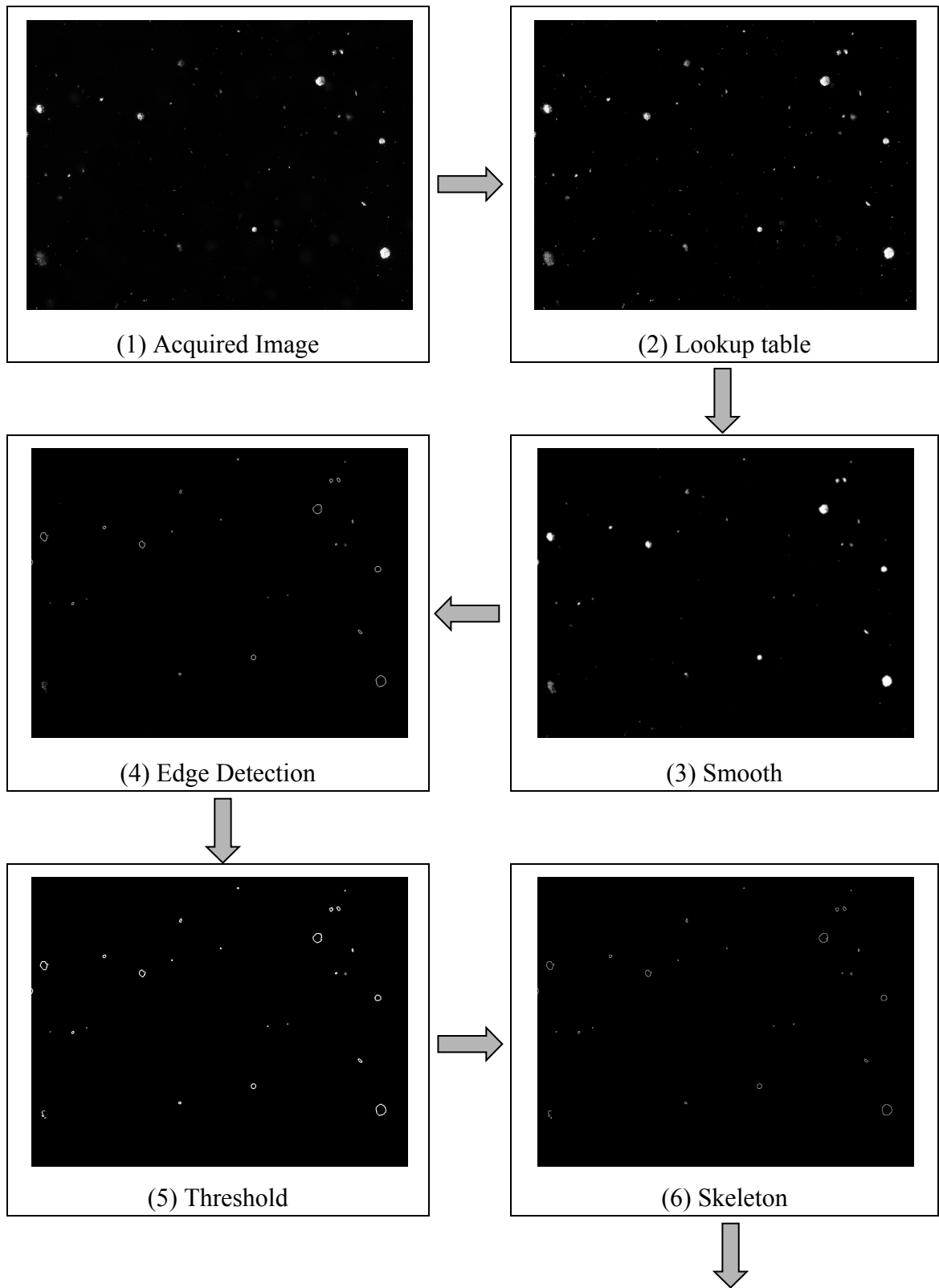


Figure 4.13: Sequence of steps used in analysing the solid particles images in DI module.



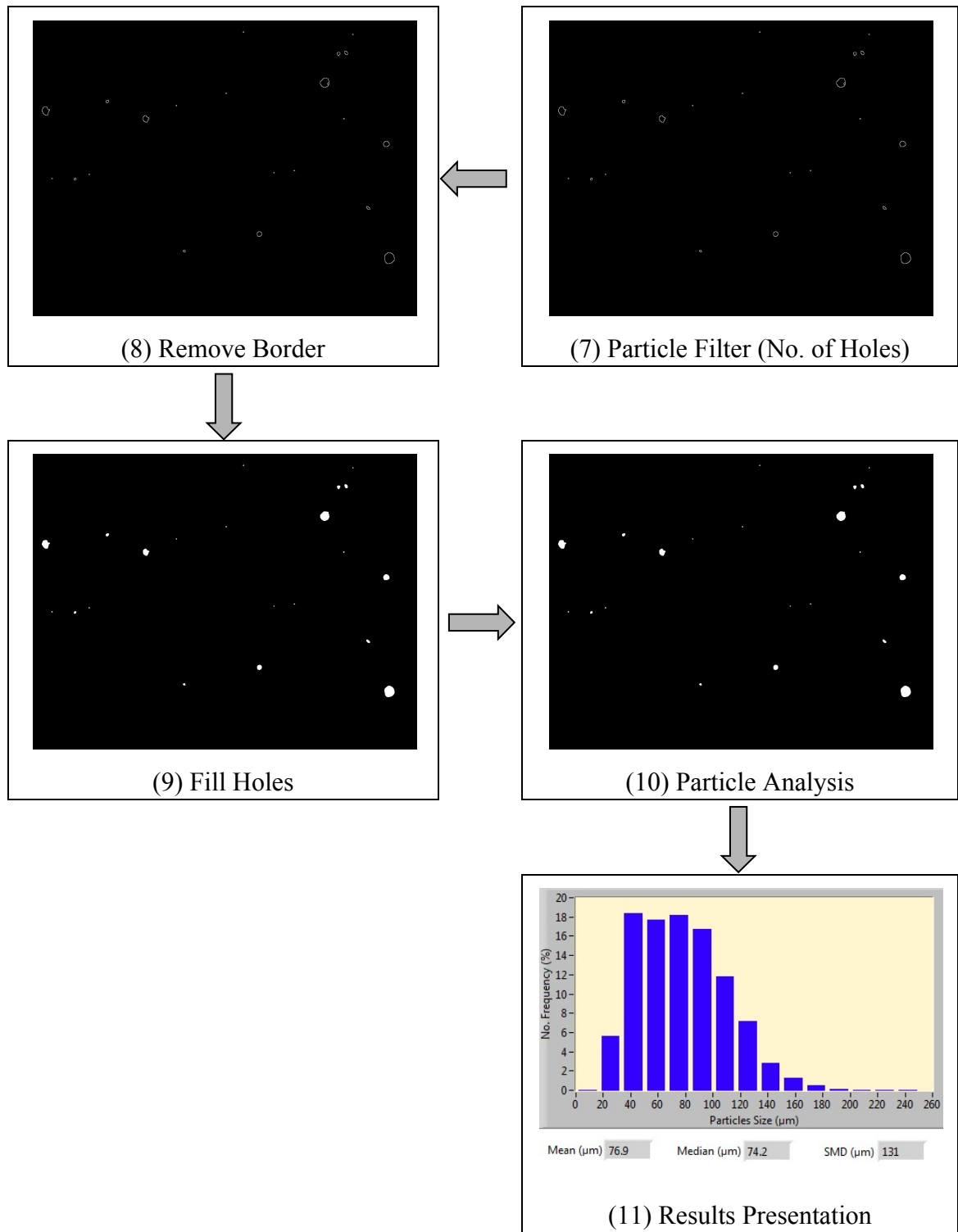


Figure 4.14: Image Processing Sequence for solid particles analysis by the DI module.

4.3.2 *Algorithm for Liquid Particles*

A liquid particle image captured by DI technique consists of two glare points with similar light intensities as is described in detail in Section 5.6. A specific algorithm has to be developed to extract these glare points from the image background and perform a method of particle size measurement. A sequence of steps as illustrated in Figure 4.15 is designed to achieve these objectives.

Once an image is acquired by the camera, the functions of LUT, smoothing, threshold and remove border are applied to the image. These functions are similar to those used in Section 4.2.1. The processed images of each function are given in Figure 4.16. Here, a morphological function (dilate an object) is introduced and employed to the image (Figure 4.15). This dilation function eliminates tiny holes isolated in particles (two glare points) and expands their contours so that both glare points attached together to become one particle.

Then, the particle analysis function measures the number of particles after the image is dilated. It also determines x and y coordinates of the leftmost and rightmost point in the particle. These coordinates represent a bounding rectangle of each particle. The number of particles and coordinates of the bounding rectangle are used for the extraction step in the loop process as depicted in Figure 4.15. The loop is applied to analyse the image of each particle in the bounding rectangle. The number of loops is equal to the number of particles detected by this particle analysis function.

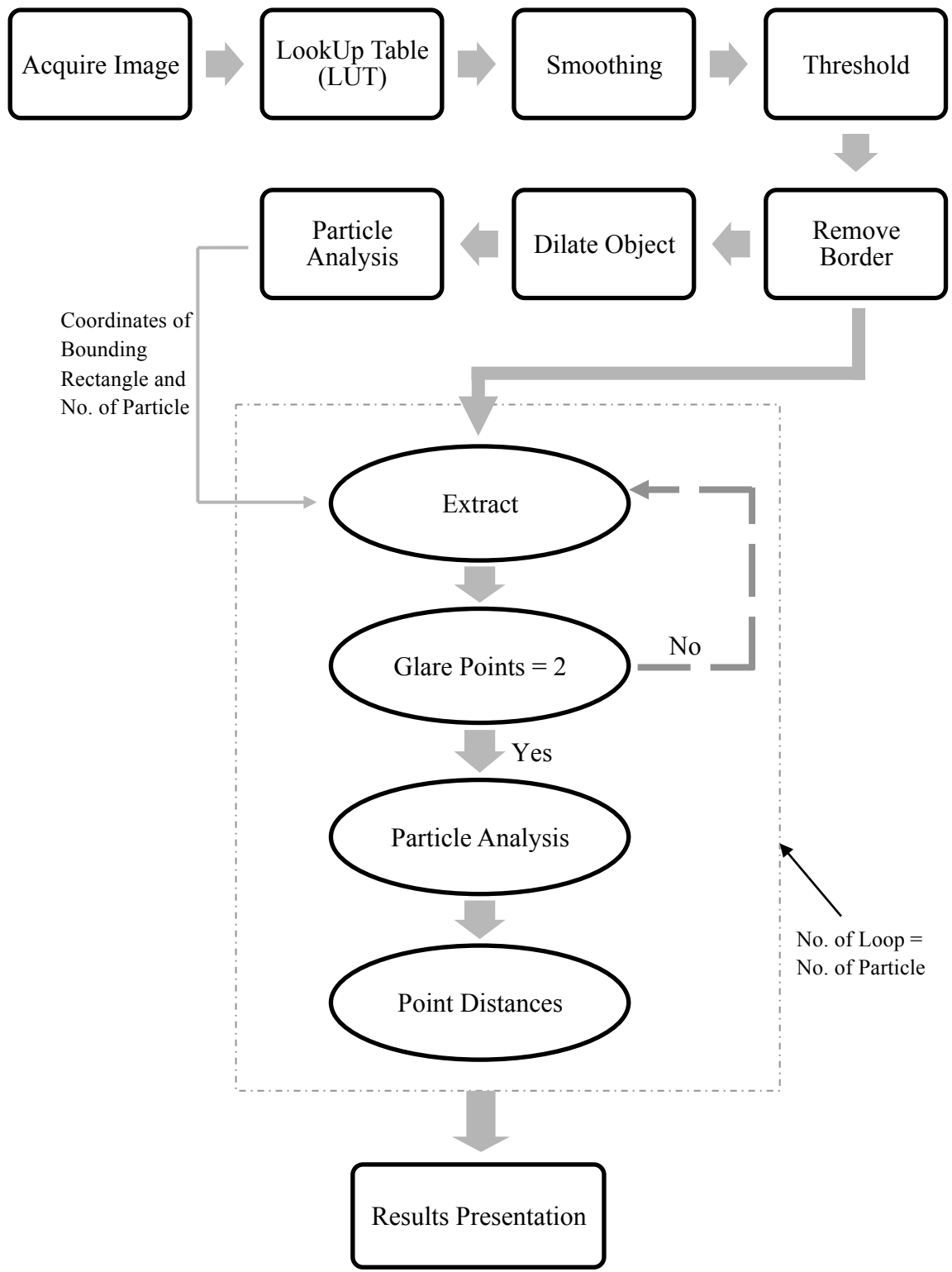
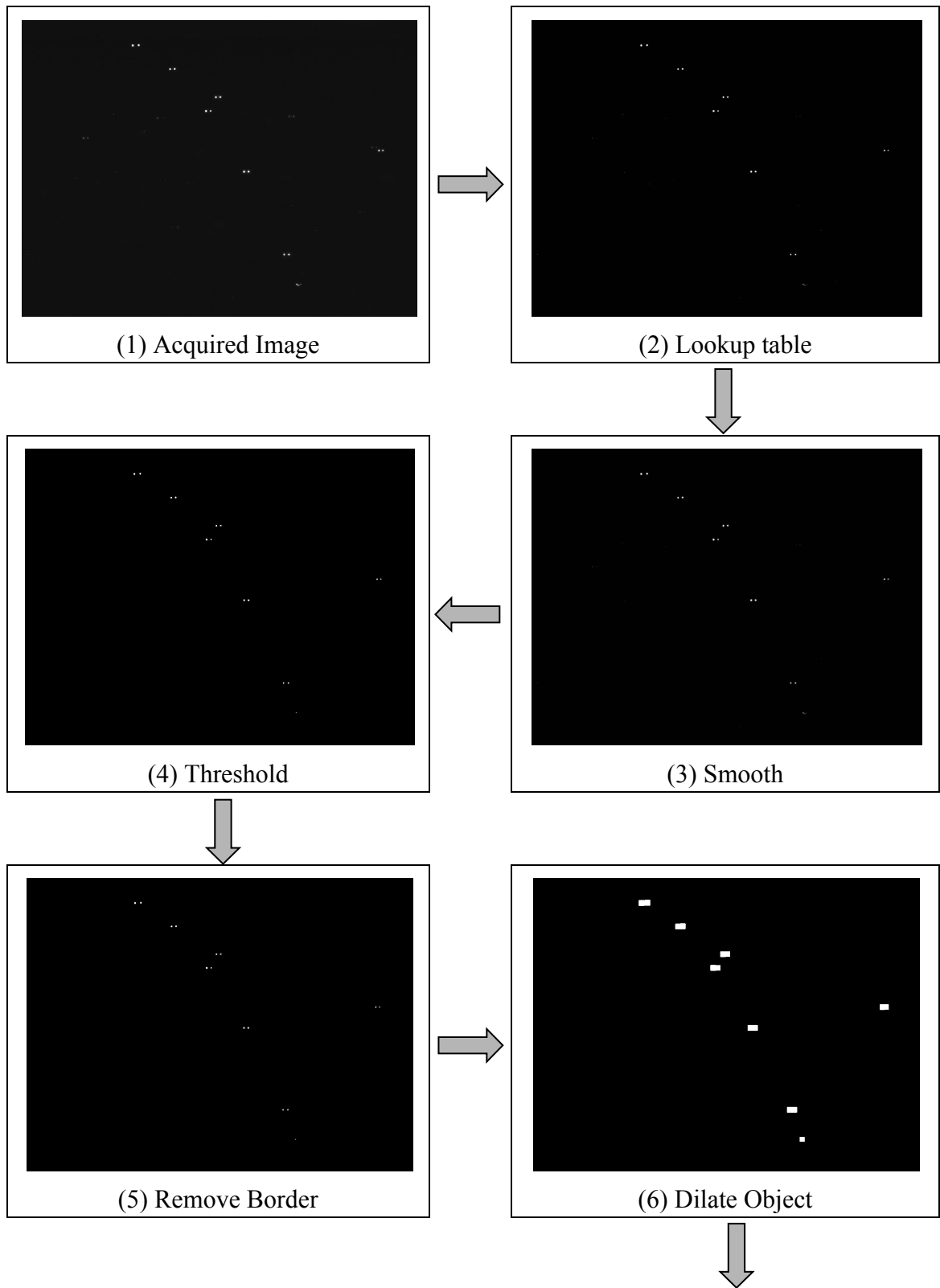


Figure 4.15: Sequence of steps used in the DI module to analyse the liquid particles images.



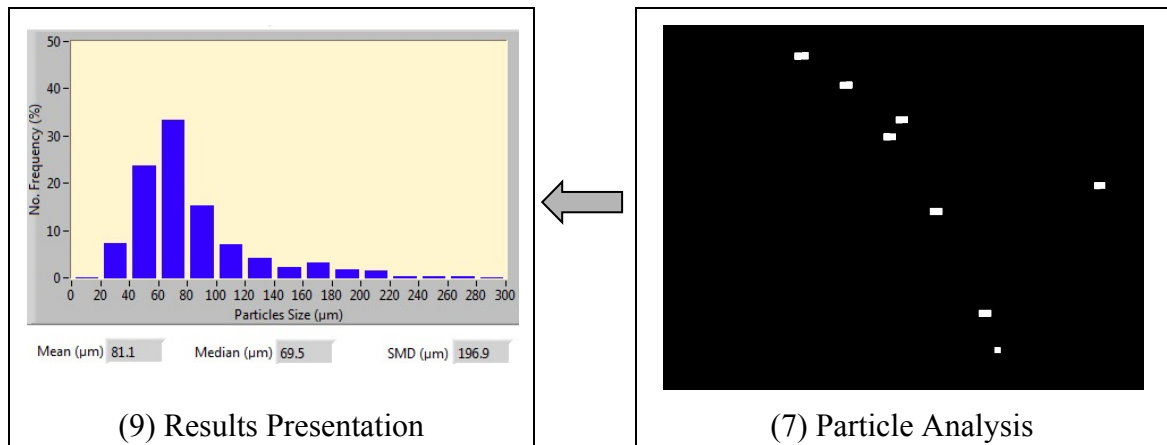


Figure 4.16: Processed images of each step of the liquid particles analysis by the DI module.

The first step employed in the loop process is the extraction function. It is used to extract parts of an image according to the coordinates of bounding rectangle supplied by the particle analysis function (Figure 4.15). For instance, this function extracts eight different particles from the image as shown in Figure 4.17. Each particle is then filtered to identify the number of glare points detected. If the glare points are not equal to two, the particle will be rejected and the sequence of step starts again with the extraction process for the next particle (Figure 4.15). If the particle has two glare points, a particle analysis function in the loop is employed to the image.

The particle analysis function in the loop process is applied to determine the centre of mass for both glare points and the number of pixels that occupied each region (Figure 4.18(a)). These data are used to obtain the particle size diameter as given in Figure 4.18(b). The data of centre of mass is used by point distance function to determine the distance between two glare points. The number of pixels occupied in each region represents the area of each glare point. This area is then used to calculate the diameter.

The relationship between particle diameter with area, distance and diameter of glare points are expressed in the equation below.

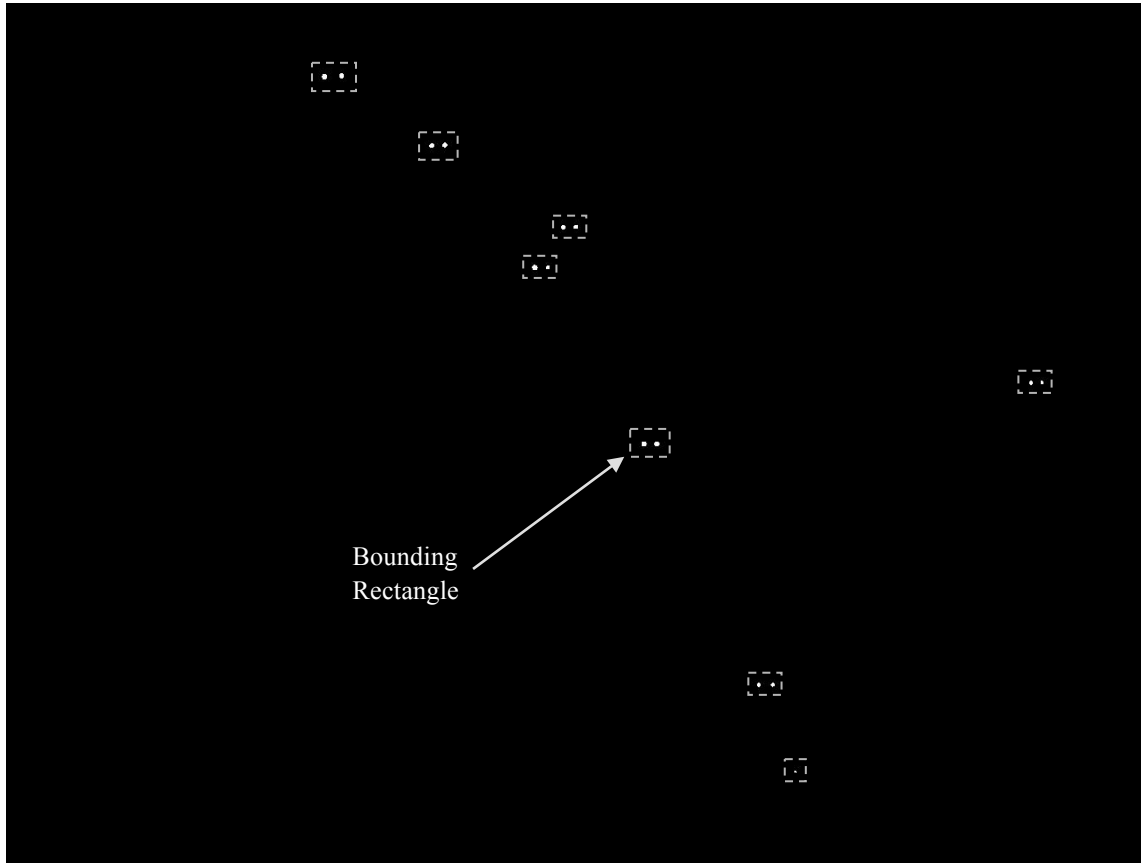


Figure 4.17: Extraction of liquid particles from the Removed Border image.

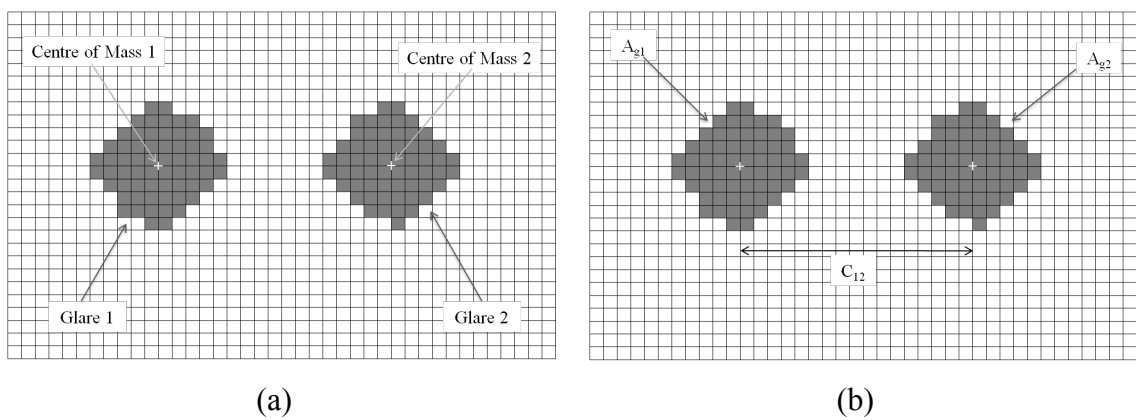


Figure 4.18: (a) Produced image after particle analysis function, (b) Method to determine single particle size from two glare points.

In Figure 4.18(b), the area of glare point 1, A_{g1} and glare point 2, A_{g2} can be expressed as

$$A_{g1} = \frac{\pi}{4} d_{g1}^2 \quad 4.2$$

$$A_{g2} = \frac{\pi}{4} d_{g2}^2 \quad 4.3$$

where d_{g1} and d_{g2} are the diameter of glare points 1 and 2, respectively. A liquid particle diameter which is based on glare points method, D_{gp} is determined by adding the distance between the two points, C_{12} to radius of each glare point.

$$D_{gp} = \frac{d_{g1}}{2} + \frac{d_{g2}}{2} + C_{12} \quad 4.4$$

Substituting Equations 4.2 and 4.3 into Equation 4.4 results in

$$D_{gp} = \frac{1}{\sqrt{\pi}} \left(\sqrt{A_{g1}} + \sqrt{A_{g2}} \right) + C_{12} \quad 4.5$$

Equation 4.5 can be used to determine the liquid particle or droplet size. This equation is only valid for the liquid particle image that is acquired using the Direct Illumination technique.

After all particle images have been analysed in the loop process, the particles that successfully meet the filter's criteria are plotted on the acquired image as depicted in Figure 4.19. It is clearly shown that only in-focus glare points are selected while the out-of-focus points are rejected. Also, it is noticed that only seven particles (Figure 4.19) are detected at the end of the image processing step compared to eight particles as given in Figure 4.17. The missing particle fails to meet the required conditions. This can be clearly seen at the bottom of the extraction image where the particle has only one glare point. Therefore, this particle is rejected.

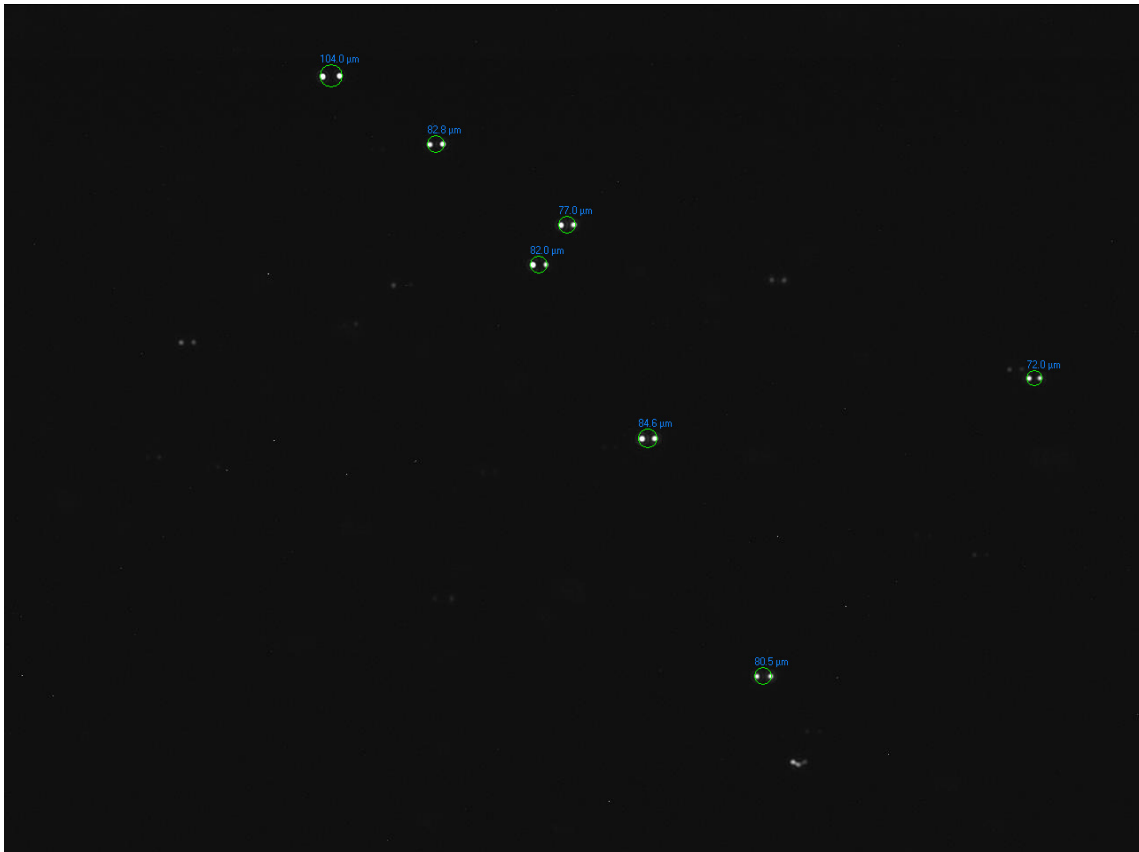


Figure 4.19: Successfully detected particles are plotted with their diameter size on the acquired image.

4.4 Measured Parameters from the Image

Image processing algorithms are employed to an image to extract required information. All data obtained from the image are expressed in pixels unit, which later are converted to real world unit by multiplying with the calibration value. Primary results extracted from the image include projected area of each particle, particle perimeter and number of particles in the image. Based on these results, the data is manipulated to produce other results such as particle size or diameter, particle shape and particle concentration.

4.4.1 Particle Size

In this study, the particle size is defined as the diameter of a sphere having the same projection area as the circular particle [66]; this is known as the equivalent spherical diameter d . This can be obtained from

$$d = 2 \sqrt{\frac{A_p}{\pi}} \quad 4.6$$

where A_p is the area of the particle in the image.

4.4.2 Particle Shape

Particle shape is used to identify either the particle is spherical or not. Here, the term applied to represent the particle shape is a circularity factor (CF). It is defined as the actual perimeter P_{act} divided by the perimeter of an equivalent spherical diameter P_{eq} as given in Equation 4.7. The closer the particle shape is to a spherical, the closer the CF to 1.

$$CF = \frac{P_{act}}{P_{eq}} \quad 4.7$$

where

$$P_{eq} = \pi d \quad 4.8$$

4.4.3 Particle Concentration

Particle concentration (PC) also called particulate loading is used to represent the concentration of particles in the image. It is defined as a summation of mass of detected particles divided by the measurement volume of the image. PC can be calculated using

$$PC = \sum_{i=1}^N m_i / (FOV)(DOF) \quad 4.9$$

where m_i is the mass of each particle, FOV is the field of view and DOF is the depth of field. Mass of each particle is defined as

$$m = V\rho \quad 4.10$$

where V is the particle volume and ρ is the particle density. The particle volume can be calculated using

$$V = \frac{\pi}{6} d^3 \quad 4.11$$

where d is the equivalent spherical diameter as stated in Equation 4.6.

4.5 Conclusions

This chapter has discussed the sequence of steps used in extracting particle size, shape and concentration from a digital image. The %Area of particle filter function in the shadow module is perhaps the most important finding in this study. %Area of 1 to 65% will classify the particles as solid and 65 to 95% as liquid. These definitions enable the characterisation of solid and liquid mixtures dispersed in air to be performed by combining the algorithms for solid and liquid particles.

The steps required in processing solid particles in the DI module are much simpler compared to the shadow module. The steps used are almost similar, except the %Area of particle filter function is not included due to lack of necessity to distinguish between solid and liquid particles in DI module. When processing a liquid particle image with the DI module, a dilation object function is successfully used in expanding the pixels of both glare points so that they attached together as single particle. A new method to

obtain liquid particles size automatically based on two glare points is determined. The area of each glare point and the distance between them are required in measuring the particle size as given in Equation 4.5.

Chapter 5

The Non-Intrusive Particle Sizer

5.1 Introduction

The development of the Non-Intrusive Particle Sizer (NPS) is based on a dynamic image analysis (DIA) method. The general principle of the DIA method has been described in details by British Standard [76]. In this method, the image of the moving particles is acquired using a camera, and a light source is required to illuminate the particles. The NPS has the capability to operate at two different types of particles illumination. The first type is shadow or back-lighted illumination and the second one is direct illumination (DI). Each type of illumination will produce its own technique of particle sizing. Details of the shadow and the DI techniques used in the development of NPS are described in this chapter.

The NPS system is designed to characterise moving particles dispersed in water or in air. It has the capability to characterise the particles which can be either solid, liquid or mixture of both. Here, the solid particles are assumed to be opaque, while the liquid are transparent. Techniques to characterise a mixture of both solid and liquid particles are explained in detail. This chapter also describes the working principle of the NPS instrument, the components involved including the parametric studies and performance of the NPS in characterising the particles.

5.2 Instrument Design

5.2.1 Requirement Specification

In the development of the NPS, five main components are required; a laser used to enhance the object under testing, a CCD camera to capture the image, a camera lens to magnify and to focus the objects, a Compact Vision System (CVS) for image acquisition, processing and analysing and finally a computer to control the inputs for the developed software and to display the output results.

It is very important to select the correct lighting (laser) in order to create a consistent and clean imaging environment. The proper lighting can increase the contrast and reduced the shadows and glares that may degrade the performance of image processing tools. The laser beam can be either continuous or pulsed. A pulsed beam is critical for fast moving particles and desirable even for slow moving fluids. For the NPS development, the air cooled Litron Nano 'O' was used to produce a maximum of 30 mJ pulsed beam with a wavelength of 532 nm.

The correct camera selection is vital to ensure that the particle sizer instrument operates successfully. There are many types of different camera technologies available in the market. They consist of high resolution cameras for precise measurement, high speed cameras for motion capture, line scan cameras for continuous web inspections, and infrared cameras for machine condition monitoring. The high resolution camera was selected for this study.

FireWire cameras offer plug-and-play connectivity and use standard FireWire port. One of the additional advantages that they can offer is they can be networked together and

give higher transfer rate. Therefore, a high resolution SONY XCD-SX90 FireWire camera was selected for the NPS development. It is equipped with IEEE1394-b connectors to allow high image transfer speeds. This monochrome camera has a resolution of up to 1280 x 960 pixels. It also has the ability to receive an external triggering signal for synchronization with the pulsed laser.

The camera is attached to a NIKON 200 mm micro-lens. The micro lens has longer working distance where it is necessary to protect the lens from the particles such as in particle spray applications. A spacer or bellow is also connected between the micro-lens and the camera. The bellow is used to increase the magnification factor of an acquired image so that a small particle will look bigger after it is magnified.

The CVS is a platform where the developed standalone application software was installed. The CVS uses FireWire technology to be connected to the camera. It contains a high performance processor which is used to process and analysed the acquired images.

All these components were integrated into the NPS system. Besides that, a software program was developed using LabView in order to perform automated image processing and analysis tasks. The description of the developed software was explained in Chapter 4.

5.2.2 Operating Principle

The main components involved in the development of the NPS are illustrated in Figure 5.1. When the NPS is switched-on, the developed standalone application software in the CVS is executed automatically. The software controls the pulsed laser by sending commands to produce a beam at a required intensity. This laser is used as a light source to illuminate the particles. Two types of illumination techniques can be applied in the NPS instrument. The techniques are explained in Section 5.4 and 5.6. The laser system produces a trigger signal which occurs at about $2 \mu s$ before the laser is pulsed. This trigger signal is used to synchronize the detection of the camera.

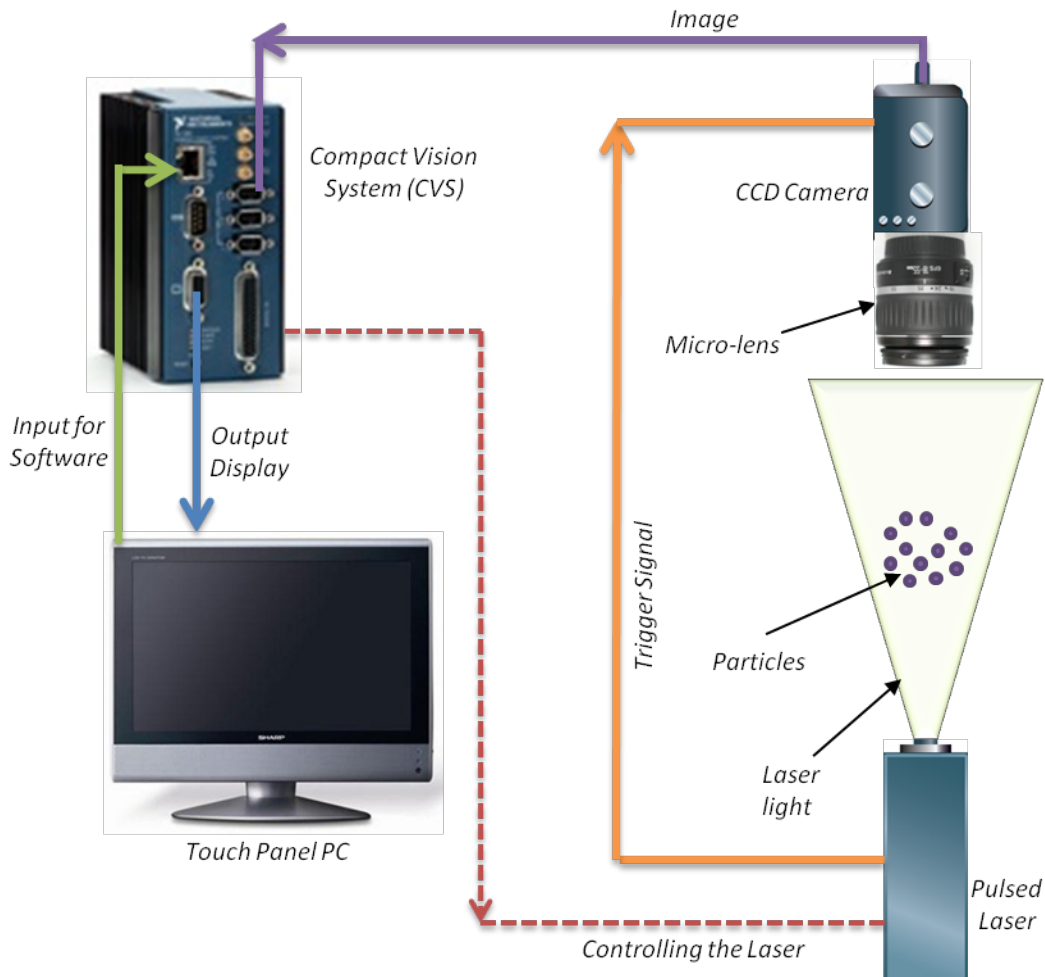


Figure 5.1: General diagram of the NPS

The camera acquires an image when it receives a trigger signal from the pulsed laser and the images of the particles are recorded by the camera as a sequence of frames. The acquired images are then directly transferred from the camera to a memory of the CVS. The developed software is used to perform an on-line image processing and particle characterisation analysis. The developed software is set as a standalone application. The Touch Panel computer is used to display the output from the software and is also used to control the inputs into the software.

5.3 Calibration of the NPS

In principle, the DIA method uses images to determine the particle size. Therefore, a calibration against known size or dimension is critical to the validity of the results. The calibration image is used to assess the absolute accuracy of the system. An image with known dimensions is applied to transform a pixel coordinate to real-world coordinate through scaling in the x and y (horizontal and vertical) directions.



Figure 5.2: The objective Micrometer Plate.

The calibration of the NPS is performed by measuring a known dimension of objective micrometer plate (Figure 5.2). The number on the plate shows that the minimum division distance is 0.01 mm or 10 μm . The camera is positioned in front of the micrometer to acquire the static image for the calibration purposes. Figure 5.3 illustrates the acquired image of the micrometer, where the visible minimum division is 0.05 mm (50 μm) instead of 0.01 mm. With current optical setup of the NPS, it is impossible to see clearly the 0.01 mm division, a higher magnification lens is required. The total length of the micrometer scale is 1 mm or 1000 μm . The image was then translated from pixels unit to real-world unit. Table 5.1 shows the results of the image calibrations of the NPS.

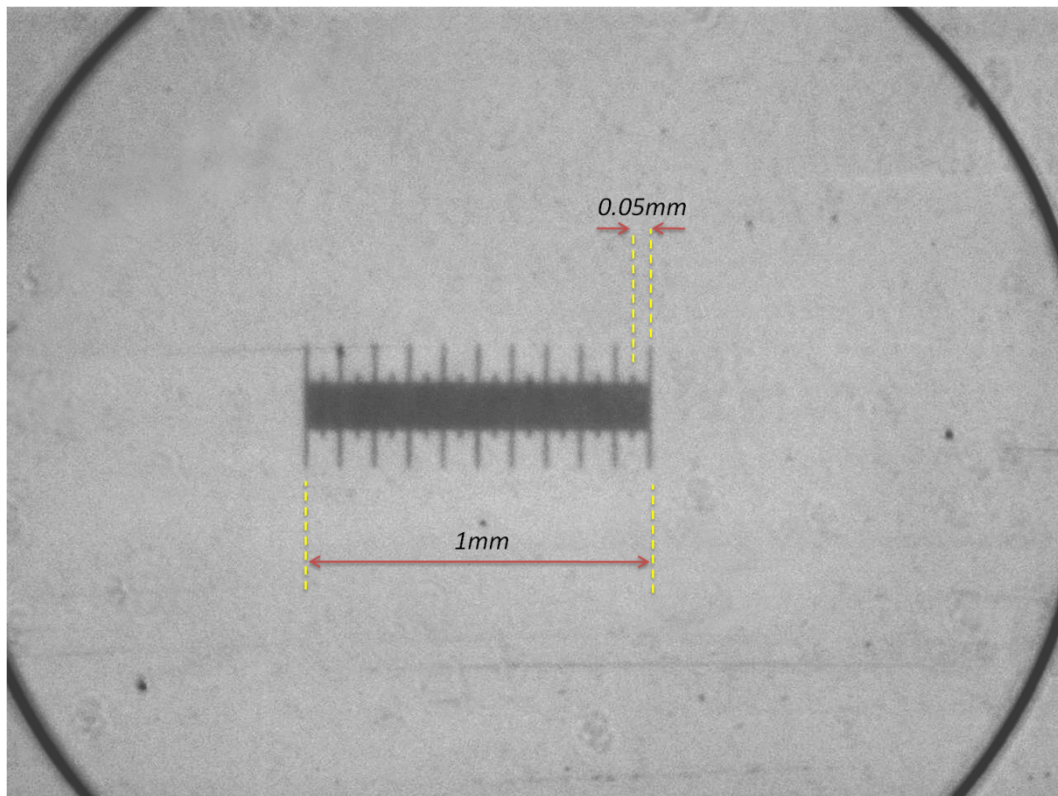


Figure 5.3: Calibrated image acquired from the objective micrometer plate.

Table 5.1: Static image calibration results

Image Properties	Descriptions
Real-world unit	1 mm or 1000 μm
Pixels unit	418 pixels
Pixels size	1 pixel = 0.0024mm or 2.4 μm
Image resolution	1280 x 960 pixels
Field of View (FOV)	3.06 x 2.29 mm

5.4 Particle Sizing by the Shadow Technique

As stated in Section 5.1, NPS can perform particle sizing using two different techniques. This section explains the details about the first technique, call the shadow or backlighting technique. The technique is based on a method on how to acquire shadow or silhouette images of particles and how to extract them to obtain useful information. The setup of the NPS that applied the shadow technique is shown in Figure 5.4.

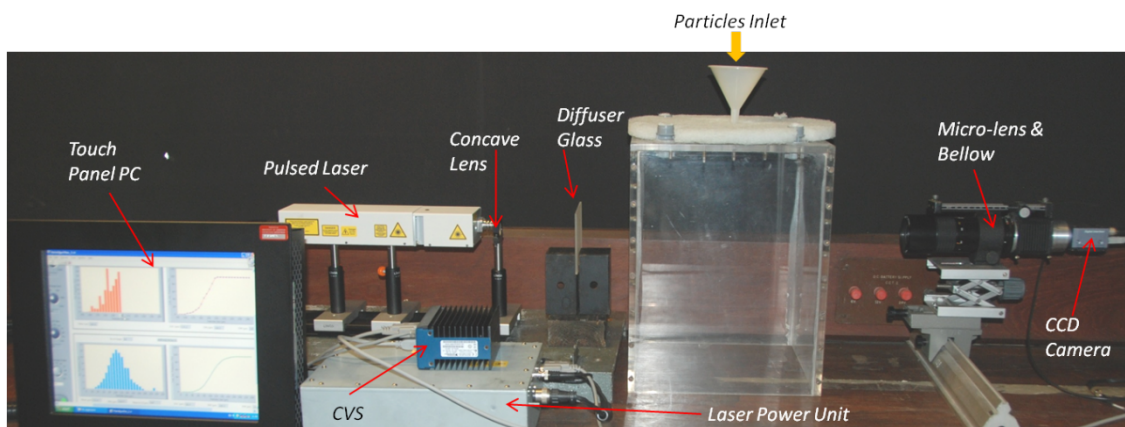


Figure 5.4: NPS setup for the shadow technique.

The digital camera is used to capture the shadow images of the dispersed particles which were back-lighted by a diffused light. The configurations of the camera and laser setup from the top view are shown in Figure 5.5. The pulsed laser beam is converted to a laser cone using a concave lens, and then it is diffused by a diffuser glass. The repetition rate and duration of this pulsed were about 0.5 Hz and 5 ns, respectively. The camera acquired the shadow image of the particles in a sequence of frames. Once an image of dispersed particles is acquired, it is processed and analysed by the software. The algorithms of the image processing software developed have been described in details in Chapter 4.

Figure 5.6 shows an example of raw images acquired by the NPS instrument. Figure 5.6(a) is a free-flow of solid particles (opaque) in the air while Figure 5.6(b) is of water droplets (transparent) dispersed in air produced by a spray atomiser. The acquired images by this technique produce bright background and dark images of solid particles, while for a liquid, it produces bright background and dark images with a bright spot in the middle of the liquid drop image. Both raw images are captured at a resolution of 1280 x 960 pixels with FOV of 3.06 x 2.29 mm.

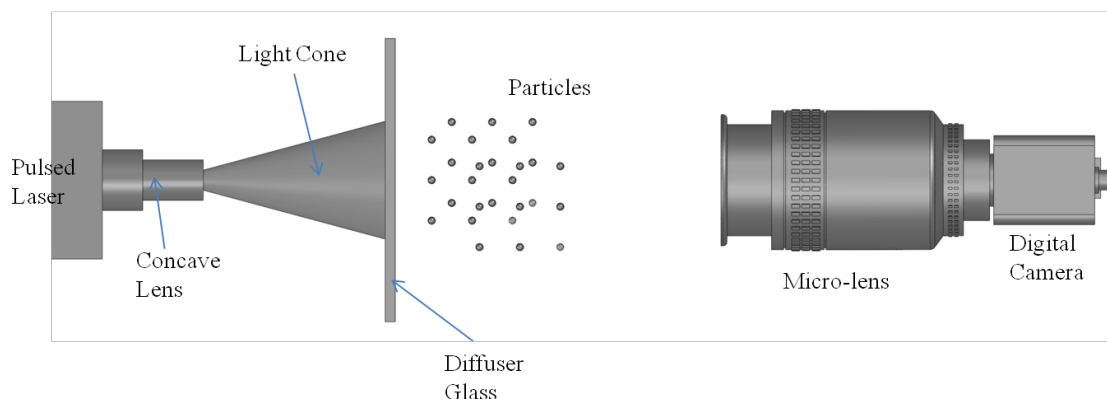


Figure 5.5: The geometrical configuration of the shadow imaging technique.

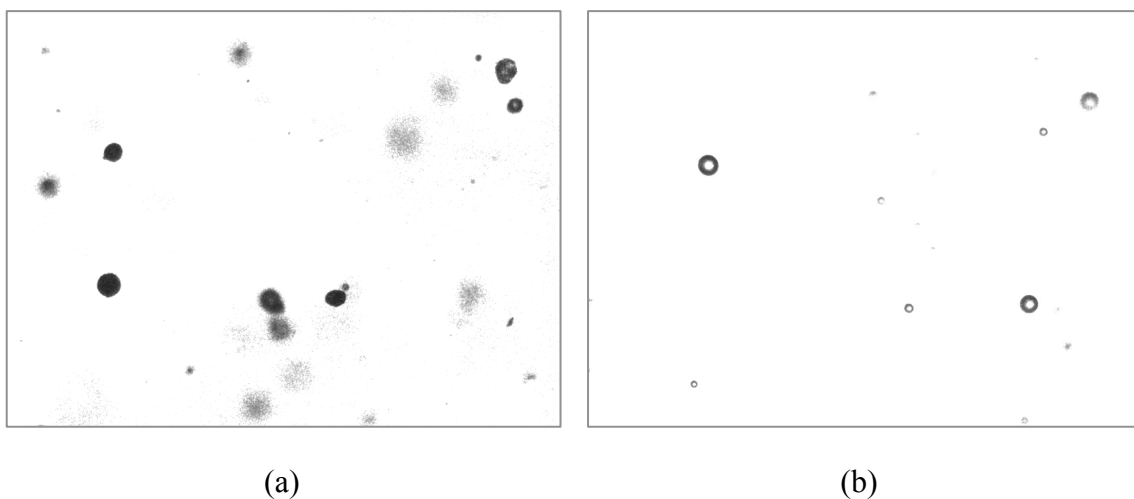


Figure 5.6: Examples of acquired raw images by NPS. (a) solid particles dispersed in air, (b) liquid particles dispersed in air.

5.4.1 *Measurement of the Certified Microsphere Particle Size Standard*

To validate the accuracy of the NPS, a set of measurements of monosized microsphere standards have been performed. The mean diameter of this product has been calibrated with Duke Scientific's NIST traceable microscopy methods while the size distribution and uniformity are measured by optical microscopy. The mean size and others properties of the certified particles are given by the manufacturer and listed in Table 5.2. Figure 5.7 shows that the certified microsphere particles are packaged as aqueous suspensions in 15 millilitre dropper-tipped bottles.

By applying the shadow technique of the NPS instrument, the certified particles are measured to determine the mean size, the standard deviation and the particle shape. The results are compared to the data provided by the manufacturer. In this experiment, the certified particles are suspended in water inside a transparent plastic container (Figure 5.8). The water is stirred constantly during the image acquisition process. This is to

ensure that all the particles are well dispersed in the water and to prevent them from overlapping between each other when the images are taken.



Figure 5.7: The Microsphere particles used for validation purposes.

Table 5.2: Properties of the certified particles

Product Attributes	
Particle Composition	Polystyrene
Particle Density	1.05 g/cm ³
Refraction Index (RI)	1.59 @ 589 nm (25 ⁰ C)
Certified Mean Diameter	72.3 µm ± 1.3 µm
Size Distribution (Standard Deviation)	0.9 µm
Coefficient of Variance (CV)	1.2 %
Solid Contents	2.0 %

Figure 5.9 shows an acquired and a processed image by the NPS instrument. It clearly shows that the particles are non-overlapped. Each particle produces a dark image with a bright spot in the middle of it when the particle is backlit. This is due to the transparency behaviour of the certified particle which allows a diffuse light to pass through it. This behaviour is similar to a liquid particle such as water droplet as depicted in Figure 5.6(b). The Refraction Index (RI) of the certified particle is 1.59 and the RI of water is 1.33.

In this experiment, four different tests are performed. About 100 images are taken for each test to get better a representation of the certified particles in the container. Each test measures different samples of particles. Here, the particles come from the same bottle which is illustrated in Figure 5.7. The water and samples of the particle in the container are replaced in every test. This is to examine the reliability and accuracy of the NPS in measuring the certified particles.

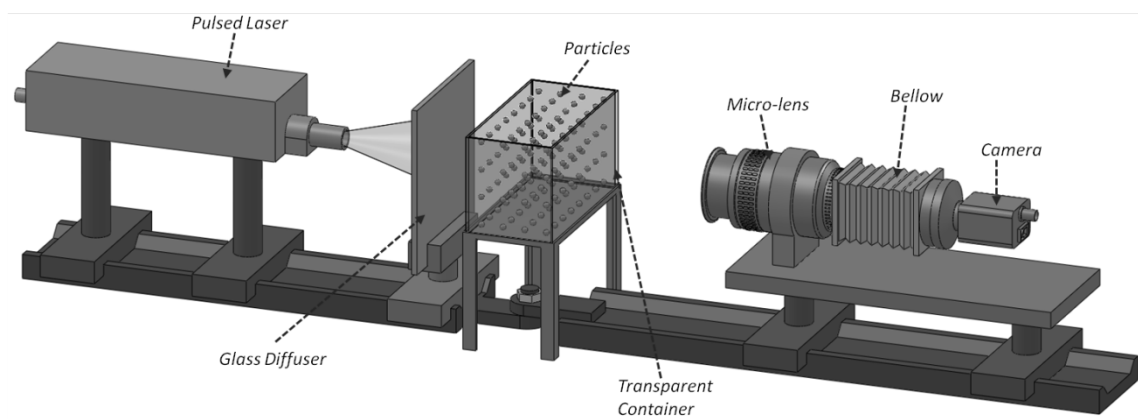


Figure 5.8: Experimental setup of size measurement for particles suspended in water using the shadow technique.

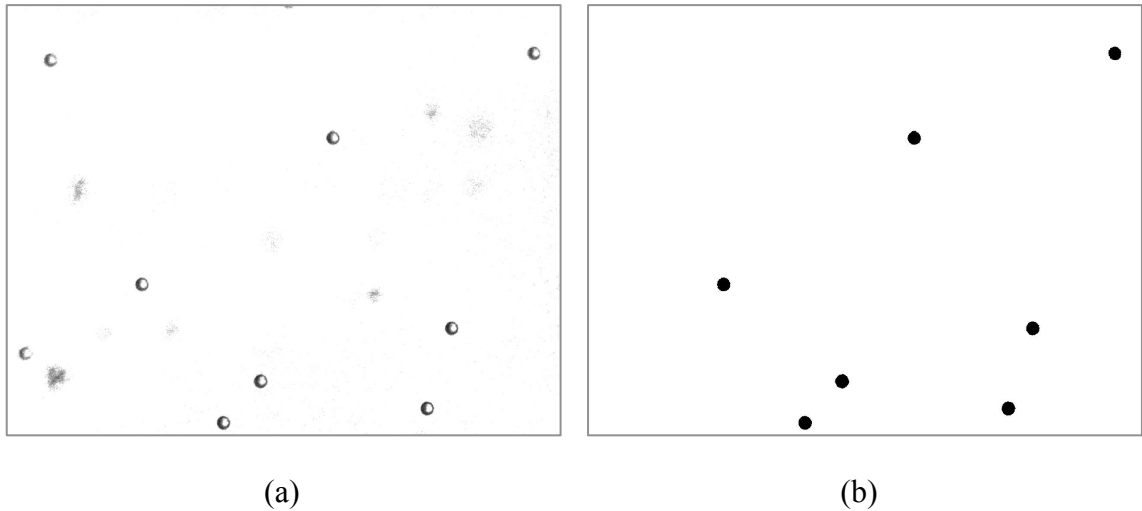


Figure 5.9: Image of certified particles dispersed in water by the NPS. (a) acquired raw image, (b) Processed image.

Figure 5.10 to Figure 5.12 show the certified particles results measured by the NPS using the shadow technique. The measurements are carried out with an image magnification factor (IMF) of 1.5 and a laser intensity of 95%. These two parameters have been determined by performing a parametric study as discussed in Section 5.5. Figure 5.10 depicts the density and cumulative size distribution for all four tests. All the tests in Figure 5.10(a) produce almost similar peak at the size around 72 μm . Figure 5.10(b) shows the size range of certified particle detected by the NPS is between 68 to 76 μm . Each size distribution produces a different mean size and standard deviation values as depicted in Figure 5.11. The error analysis of the mean and the standard deviation results are performed relative to the data in Table 5.2. It clearly shows that the measured results are in good agreement with the data provided by the manufacturer. Thus it can be concluded that the NPS instrument based on shadow technique is accurate and reliable in sizing the transparent particles.

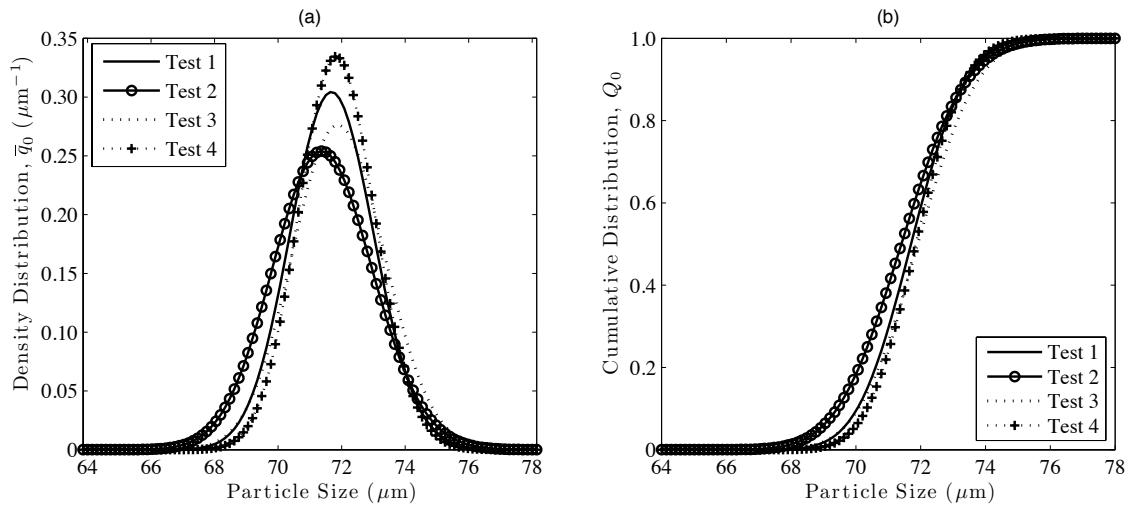


Figure 5.10: Number based size distribution of certified particles.

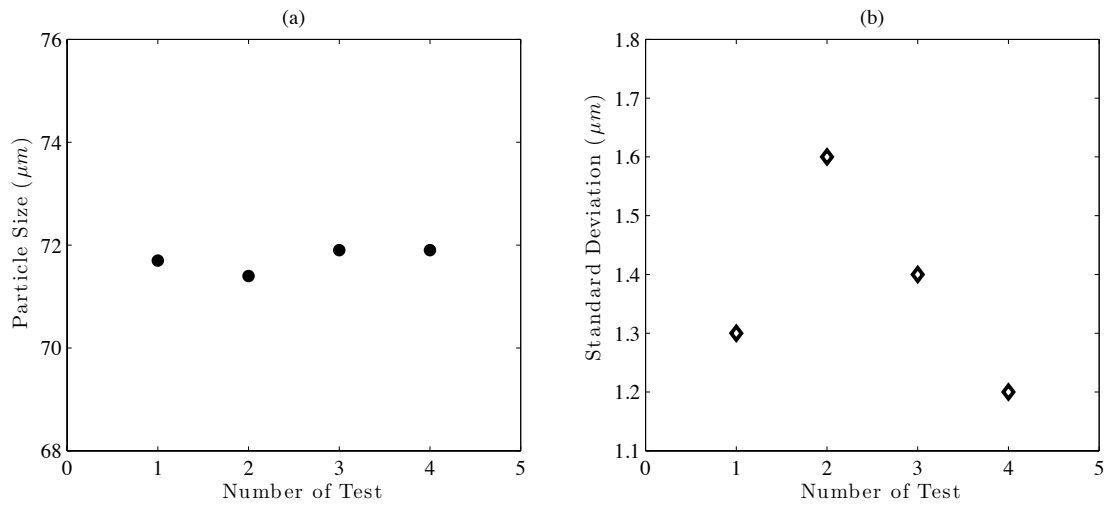


Figure 5.11: Mean size and standard deviation of certified particles.

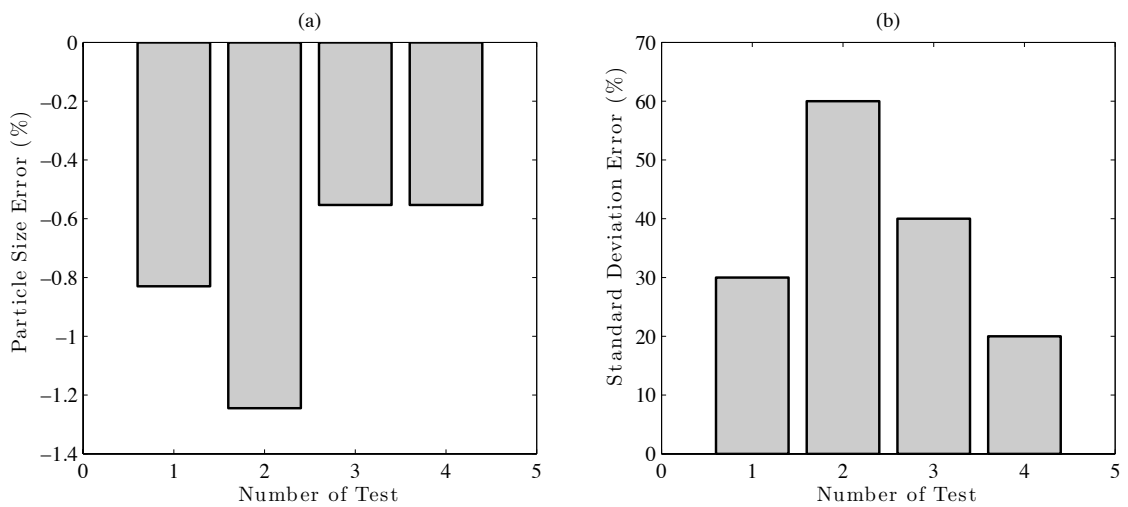


Figure 5.12: Mean size and standard deviation error of certified particles.

5.4.2 Measurement of Fillite particles

In this study, measurements of solid particles having opaque characteristics are also considered. In this case, the selected particles are Fillite Grade 160. According to the manufacturer, the particles are a glass hard, inert, hollow silicate sphere with having a grey colour. Table 5.3 shows the data of size distribution provided by the manufacturer.

Table 5.3: Data of Fillite size distribution provided by the manufacturer.

Item	Value (number based distribution)
Particle Size range (μm)	5 to 180
% Passing 300 μm	100
% Passing 180 μm	99.5 to 100
% Passing 106 μm	40 to 80
% Passing 50 μm	10 to 20

The measurements of particle size are performed to confirm the size distribution of the Fillite. This is done using a Scanning Electron Microscope (SEM). Figure 5.13 depicts an image of Fillite particles under the SEM. A total of 3540 particles are detected and sized. The arithmetic mean size and the standard deviation of the particle are recorded to be 75.5 μm and 39.3 μm , respectively. The particle size distribution is plotted based on the results obtained by the SEM method (Figure 5.14). It shows that 100%, 75% and 20% of a particle pass the 180, 106 and 50 μm , respectively. These results are in agreement with the data provided by the manufacturer as stated in Table 5.3. Different types of mean values are plotted in Figure 5.15 to show the distribution of Fillite

particles. These values will be set as references for Fillite size distribution and will be used for comparison purposes.

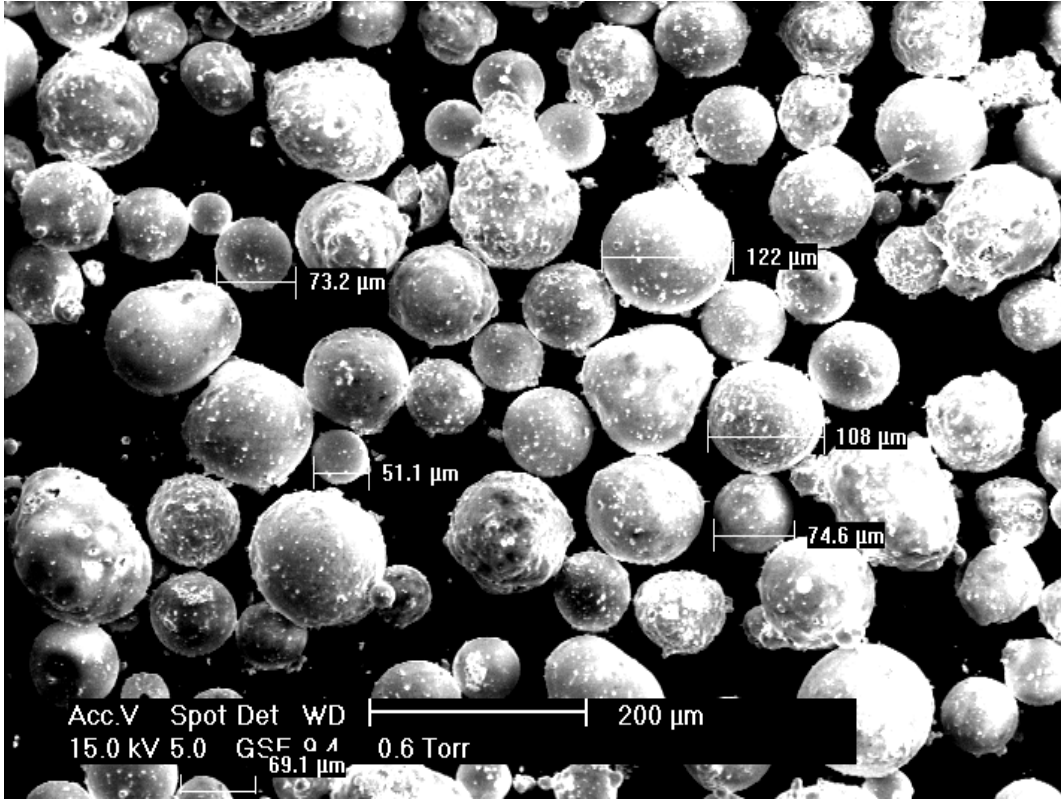


Figure 5.13: Image of Fillite particles measured by SEM.

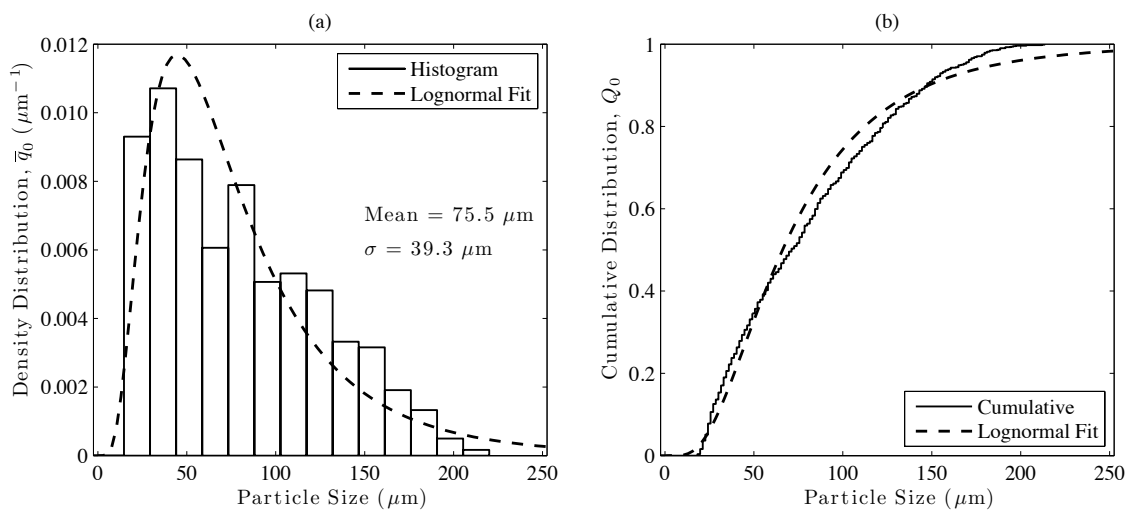


Figure 5.14: Number size distribution of Fillite particles measured by SEM.

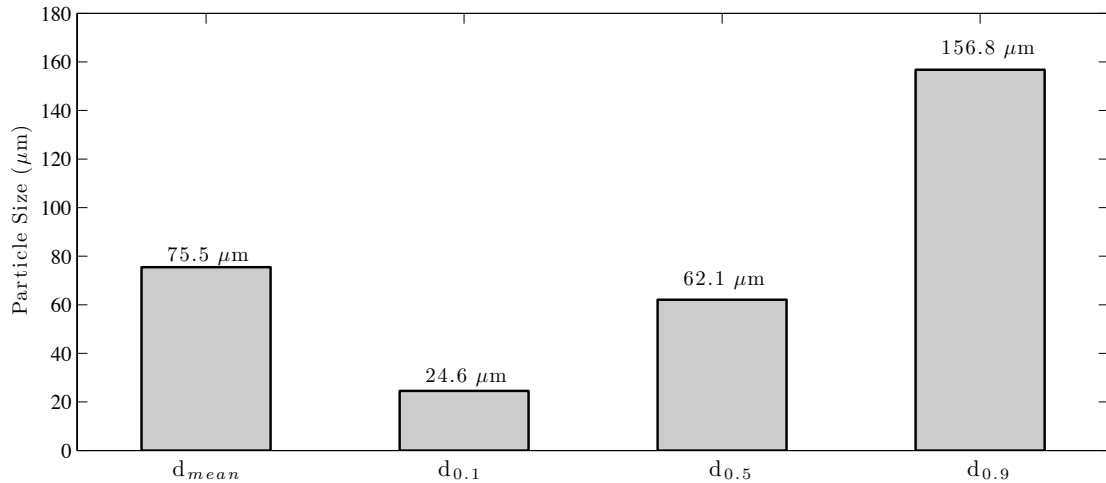


Figure 5.15: Different types of mean values measured by SEM that represent the Fillite particle size.

As discussed in Section 5.4.1, the NPS with the shadow technique has shown a good accuracy and reliability in sizing the particles. Therefore, the same NPS instrument with the same set up as of Figure 5.8 is used to characterise the Fillite particles. The method of the particle sizing is similar to the one described in Section 5.4.1. The only difference is that the particles inside the container are replaced with the Fillite.

Figure 5.16 shows an acquired and processed image of Fillite particles by the NPS instrument. Each particle produces a dark image with bright background when the particle is back-lighted. This is due to the opaque behaviour of the Fillite particle which prevent a diffuse light to pass through it. This behaviour is different from the certified particles as depicted in Figure 5.9.

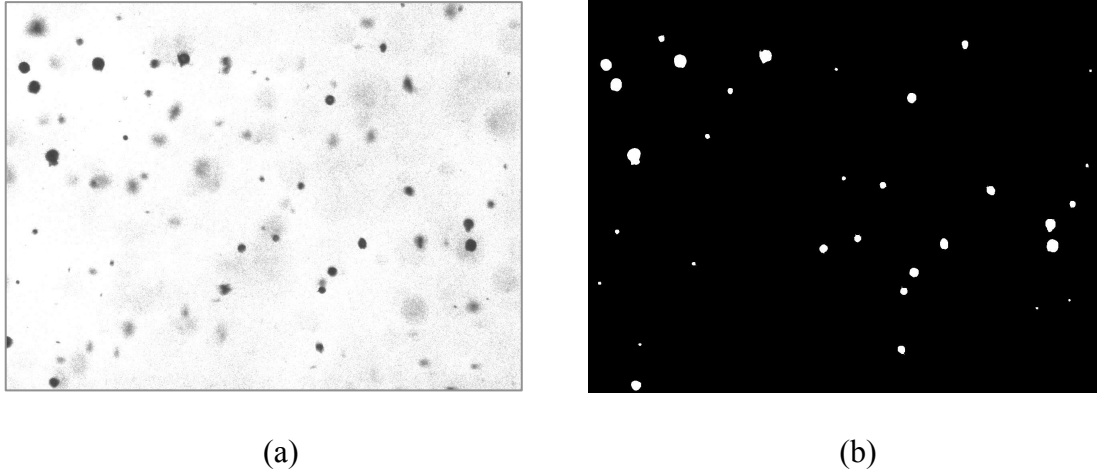


Figure 5.16: An image of Fillite particles dispersed in water. (a) acquired raw image, (b) Processed image.

In this experiment, four different tests are performed. About 100 images are taken in each test to get better representation of the Fillite particles in the container. Each test measures different samples of particles and the water and the samples of the particles in the container are replaced for every test. This is done to examine the reliability and accuracy of the NPS in measuring the Fillite particles.

Figure 5.17 to Figure 5.20 show the Fillite particles results measured by the NPS using the shadow technique. The measurements are carried out at an image magnification factor (IMF) of 1.5 and a laser intensity of 95%. Figure 5.17 depicts the density and cumulative size distribution for all of four tests and also the results by SEM. Both distribution plots by the NPS are in agreement with the results from the SEM machine. All the tests in Figure 5.17(a) produce almost similar peak at around 75 μm . Figure 5.17(b) shows the size range of Fillite particles detected by NPS is between 10 to 190

μm . Each size distribution produces different mean size and standard deviation values as shown in Figure 5.18.

The error analyses of the mean and the standard deviation results are performed relative to the results in Figure 5.15. All the tests show that the particle size errors are below 5% and the standard deviation error is below 18% compared to the SEM results (Figure 5.19). Figure 5.20(a) illustrates the particle size at 10, 50 and 90% of cumulative distribution, while Figure 5.20(b) shows their error compared to SEM results. A significant error is recorded at $d_{0.1}$ and this is believed due to the limitation of the NPS in detecting particle size lower than $15\ \mu\text{m}$, while the SEM machine has greater optical magnification and it is capable in measuring fines particle sizes.

It is clearly shown that the Fillite particles measured by the NPS are fairly accurate with the mean size error being lower than 5%. The results are not much different compared to the SEM results and the data provided by the manufacturer. Thus it can be concluded that the NPS instrument based on the shadow technique is accurate and reliable in sizing the opaque particles.

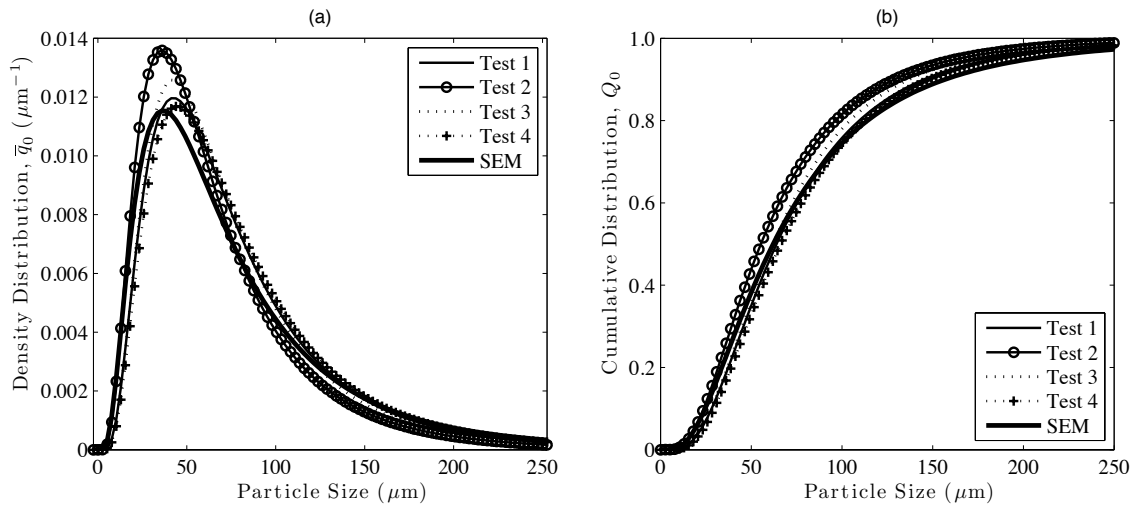


Figure 5.17: Number based size distribution of Fillite particles.

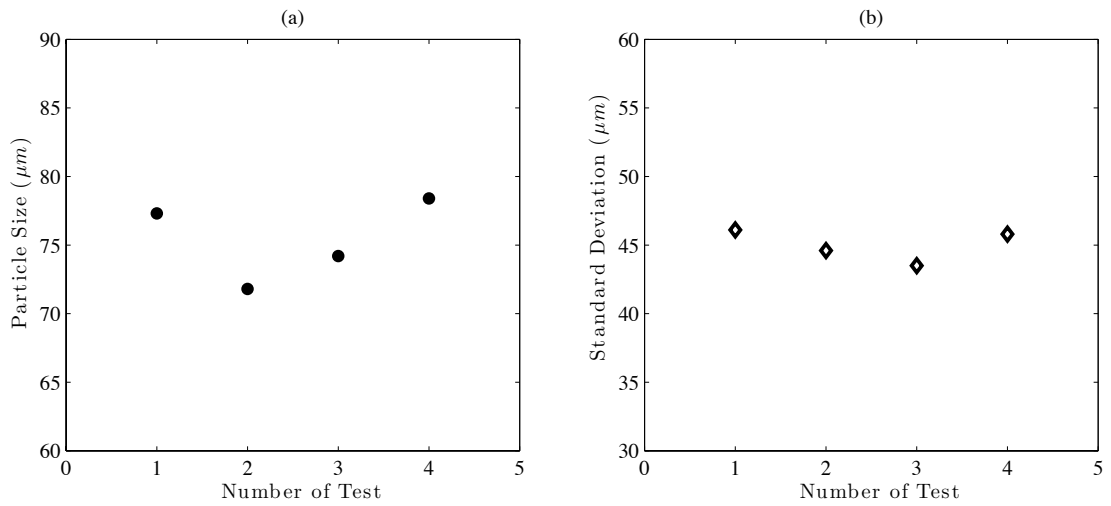


Figure 5.18: Mean size and standard deviation of Fillite particles.

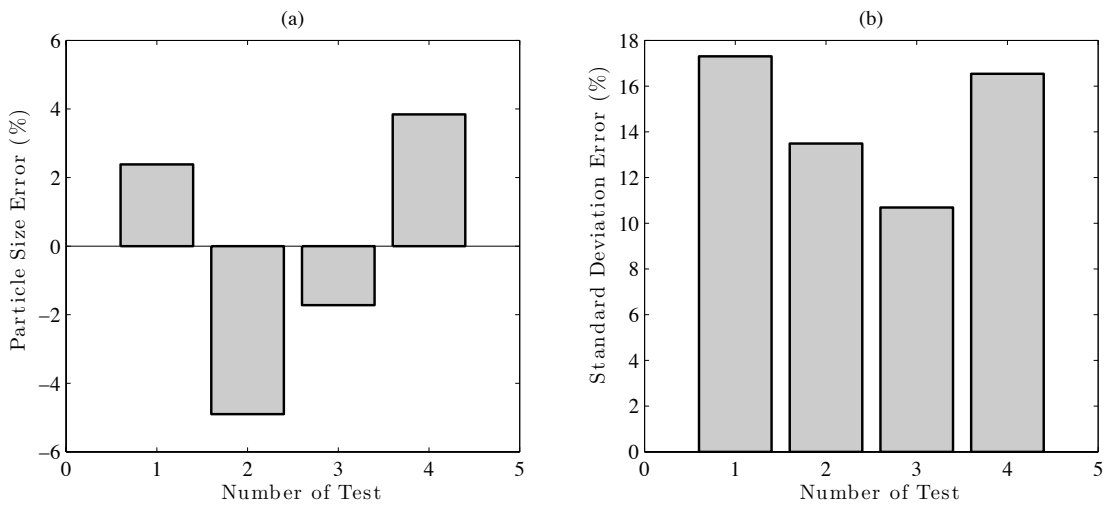


Figure 5.19: Mean size and standard deviation error of Fillite particles.

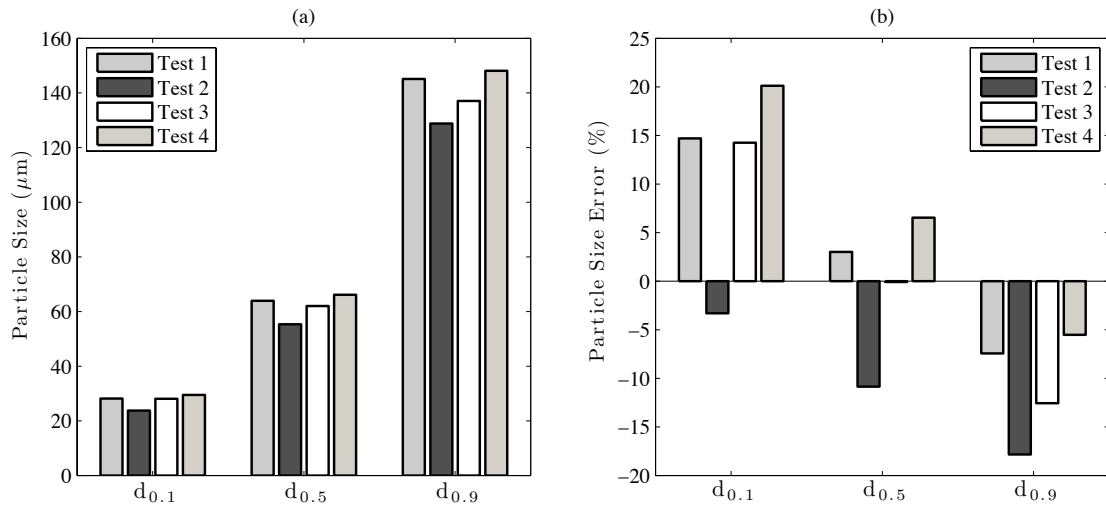


Figure 5.20: Particle size and its error at 10, 50 and 90% of cumulative distribution.

5.4.3 Evaluation of the Measurements of Liquid Particles

In this experiment, the shadow technique is applied to determine liquid particles (or droplets) size of a spray atomiser which is dispersed in air. The experimental setup of this experiment is similar to that of Figure 5.5. The acquired image illustrates bright background and a dark image with bright spot in the middle of a droplet (Figure 5.21(a)). This image is acquired at 90% of LI and 0.8 IMF. Figure 5.21(b) shows only in-focus droplets are selected for size distribution to ensure the accurate results.

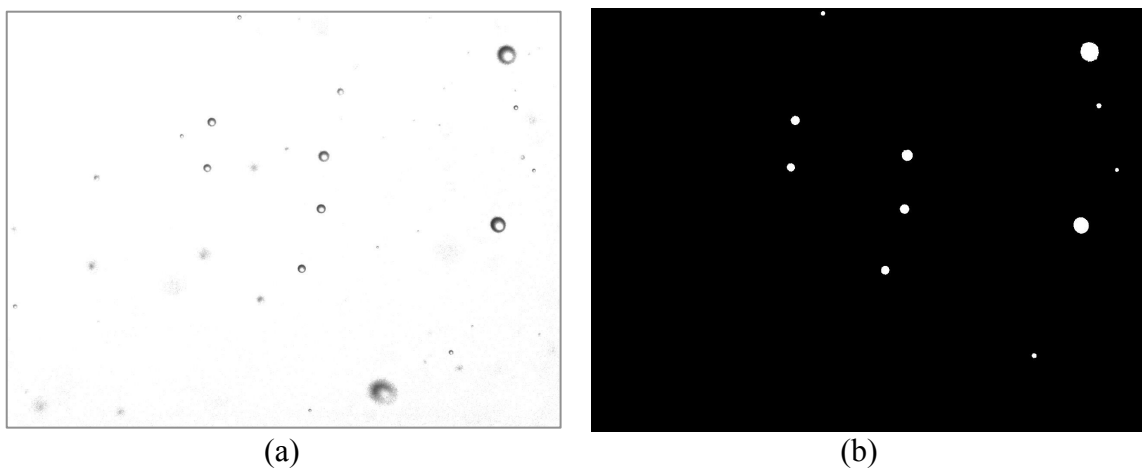


Figure 5.21: Image of liquid particles dispersed in air. (a) acquired raw image, (b) Processed image.

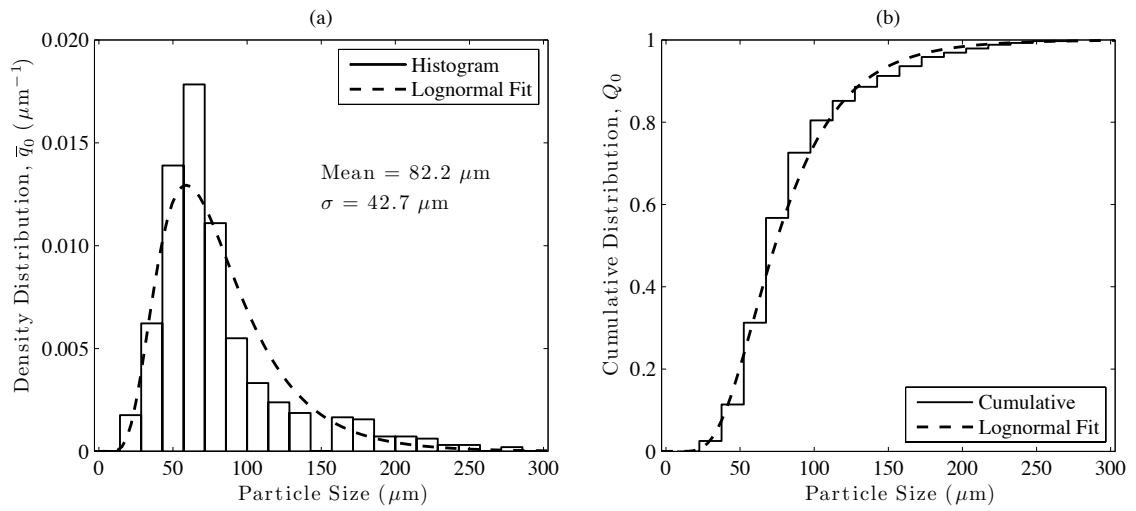


Figure 5.22: Number density and cumulative distribution of spray droplets.

Figure 5.22 to Figure 5.24 report the results of droplets characterised by shadow techniques. About 9700 droplets are detected when plotting the size distribution. These results will be used later for comparison purposes with the direct illumination technique.

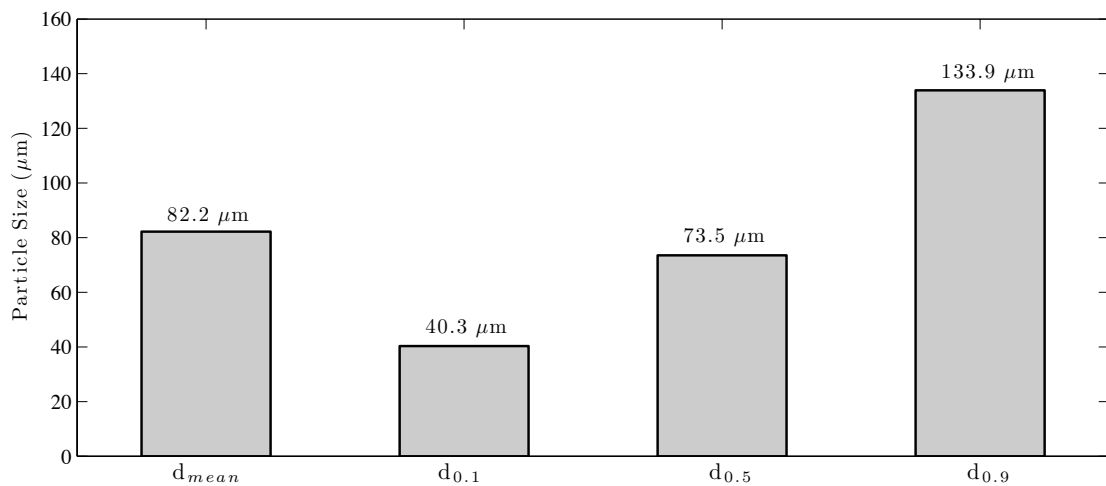


Figure 5.23: Mean size and size at 10, 50 and 90% of cumulative distribution.

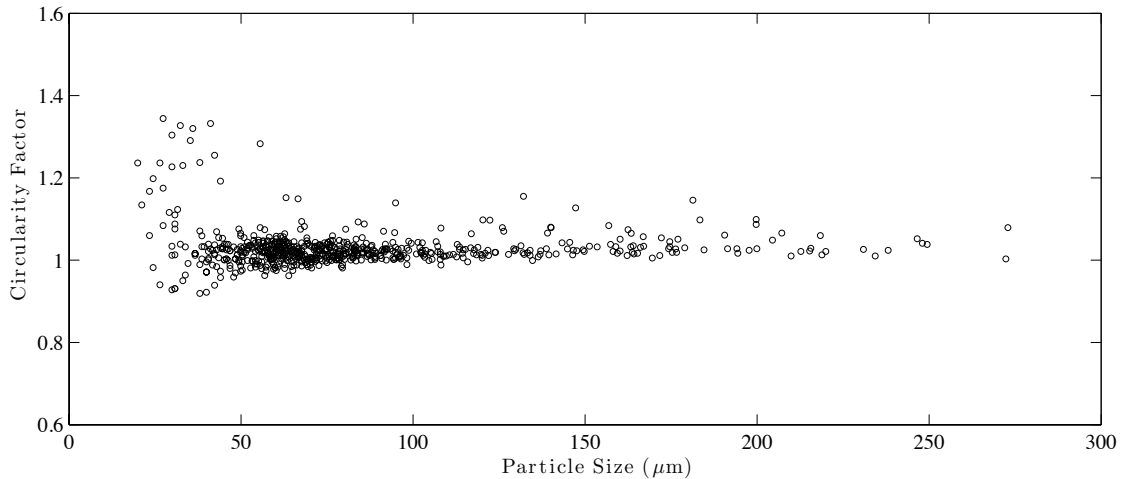


Figure 5.24: Particle shape of spray droplets.

5.5 Parametric Study with the Shadow Technique

Extensive experiments were performed to investigate the effect of parameters on the accuracy of the particle size. The parameters of interest include image magnification factor and a laser intensity. These parameters are important in finding the optimum configuration of the NPS during the image acquisition process. They are two types of known sizes of particles used in this study which are certified microspheres and Fillite particles. The Fillite mean size is determined by SEM machine (Section 5.4.2) while for the certified microsphere is provided by the manufacturer of the particle (Section 5.4.1).

In this parametric experiment, an off-line particle analysis is applied. This is important to investigate the quality of the acquired images before it is processed and analysed. The acquired image should have good contrast in order to clearly show the difference between a particle's image and its background. In order to determine the appropriate contrast and the optimum magnification of the image, the experiment has been designed as depicted in Table 5.4.

Table 5.4: Matrix of experiments to identify the optimum value of IMF and LI.

Laser Intensity (%)	Image Magnification Factor					
	0.4	0.5	0.6	0.8	1.2	1.5
80	yes	yes	yes	yes	-	-
85	yes	yes	yes	yes	yes	yes
90	yes	yes	yes	yes	yes	yes
95	yes	yes	yes	yes	yes	yes
98	-	-	-	-	yes	yes

5.5.1 *Certified Microsphere - Laser Intensity*

The amount of light is essential in acquiring a good image quality. Different laser intensities are applied for each image magnification setup as shown in Table 5.4. The setup of this experiment is similar to Figure 5.8. About 100 images are acquired for each test. All images are then saved on a computer hard disk for off-line analysis.

At each IMF, various LI between 80 to 95% are applied during the image acquisition process. It is found that different values of LI produce dissimilar acquired images. As depicted in Figure 5.25, 80% of LI produces a poor image contrast compared to 85, 90 or 95%. The image background is too low and it is not bright enough to differentiate between particles and background. LI at 90% produces a good acquired image with clear contrast. This generates better processed image by the developed software.

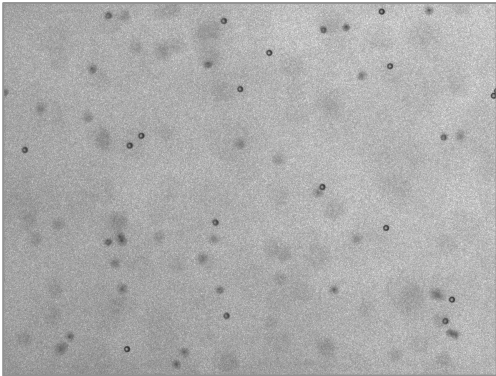
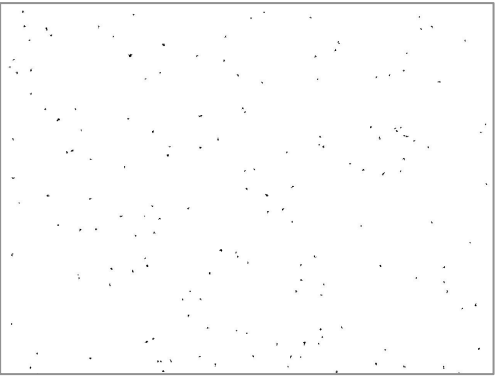
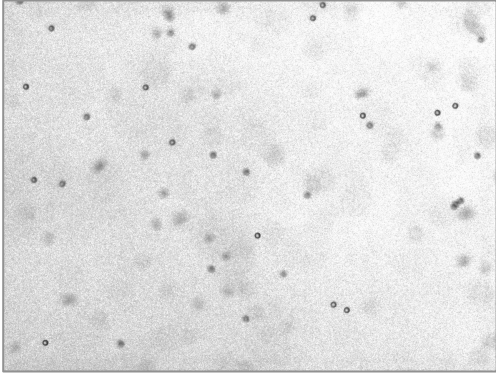
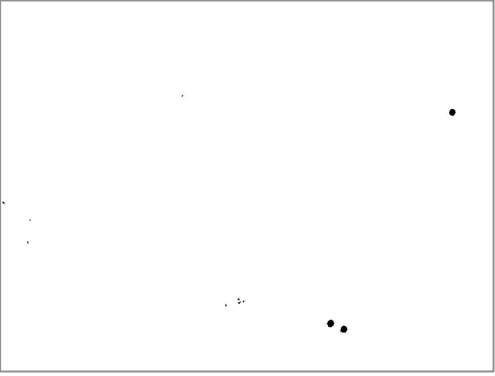
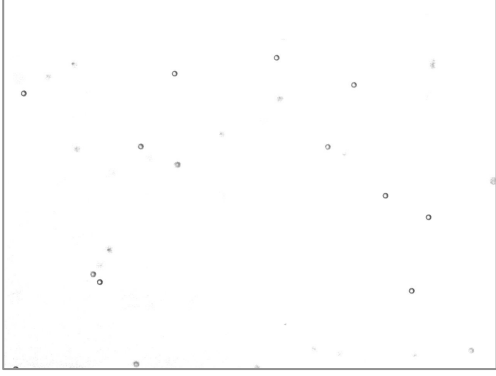
LI	Acquired Image	Processed Image
80%		
85%		
90%		
95%		

Figure 5.25: Acquired and processed images of the certified microsphere for IMF = 0.8 at different LI.

At 95% of LI, it is too high for IMF of 0.8. This is not recommended as the light starts to overcome the particles and make the shadow of the particles become smaller. Therefore, an optimum LI is required to produce well contrast of acquired image.

Figure 5.26 shows the size distribution of certified microsphere for IMF of 0.8 at different LI. It clearly shows that the distributions at 90 and 95% of LI are almost similar. For 80% of LI, it produces narrow distribution while 85% of LI depicts wide distribution. In terms of the mean size, LI at 90% produces a very close value compared to the data provided the particle's manufacturer (Figure 5.27). Therefore, at an IMF of 0.8, the optimum LI is found at 90%. Similar experiments are also performed for the rest of the IMF. The optimum LI found for each IMF is illustrated in Figure 5.28.

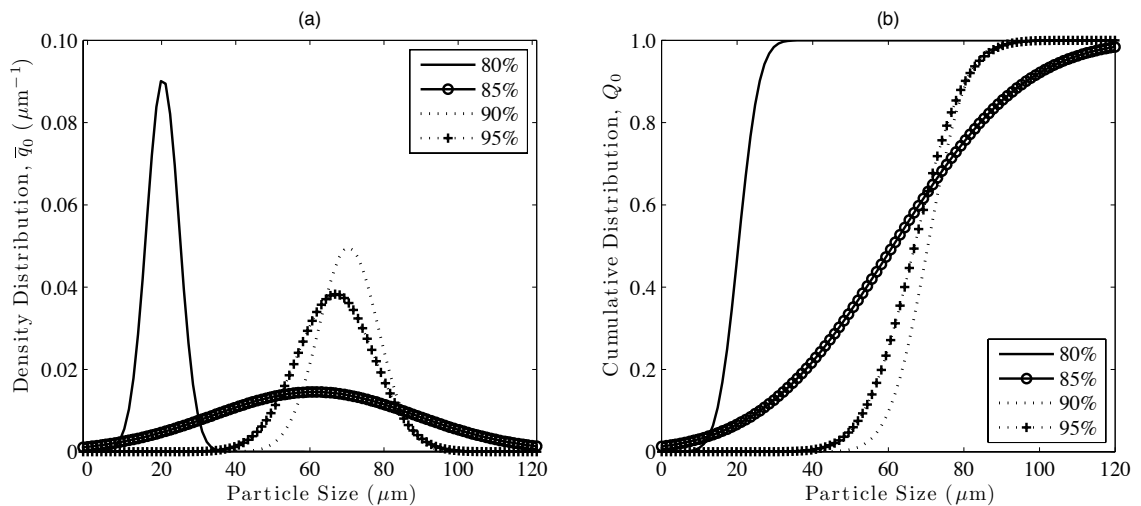


Figure 5.26: Numbered density and cumulative size distribution of the certified microspheres for IMF = 0.8 at different LI.

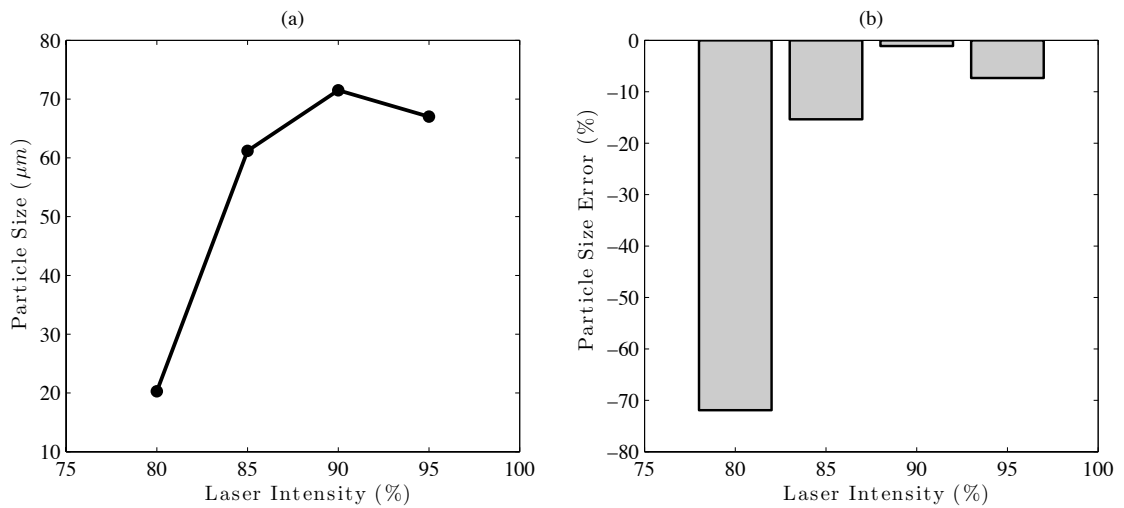


Figure 5.27: Mean sizes of the certified microspheres and their errors for IMF = 0.8 at different LI.

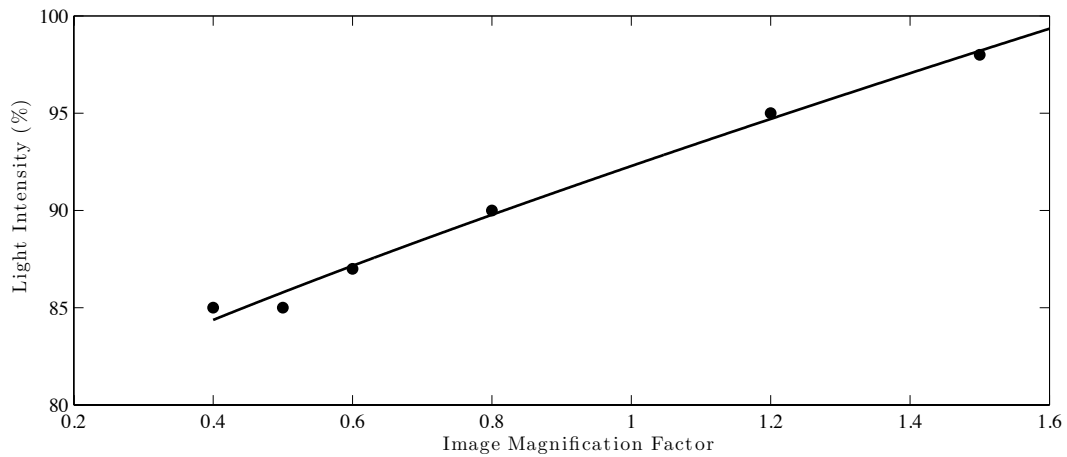


Figure 5.28: Optimum LI of the certified microspheres at different IMF

5.5.2 Certified Microsphere - Image Magnification

In the image analysis method, a small particle has to be magnified in order to accurately determine its size. Appropriate optical configurations are required to ensure the right factor of image magnification for each measurement. In this experiment, the certified microspheres are measured at different image magnification factor values as stated in Table 5.4. The setup of this experiment is similar to Figure 5.8. About 100 images are acquired on each test. All images are then saved in a computer hard disk for off-line analysis.

At each LI, various IMF between 0.4 and 1.5 are applied during the image acquisition process. The setup of the experiment is similar to that in Figure 5.8. The magnification of the image is increased by increasing the distance between the camera and the lens using bellows. For this IMF study, the processed of acquired images are performed for IMF between 0.4 and 1.5 at optimum LI only (Figure 5.28).

Figure 5.29(a) gives a wide spread distribution with low peaks is recorded at lower IMF values while narrow distributions with higher peak at higher IMF values are obtained. It clearly shows that the NPS with higher IMF produces very steep cumulative distribution as illustrated in Figure 5.29(b). This concludes that with higher IMF values, the NPS detects lower standard distribution and nearer mean size to the data provided by the manufacturer (Figure 5.30). Figure 5.31 shows the mean size and its standard distribution error compares favourably to the data in Table 5.2. It shows that the mean size error is less than 5% for IMF between 0.5 and 1.5. However, the standard distribution error records more than 100% error for IMF below 0.8.

The NPS is able to detect the shape of the particle whether it is spherical in shape or not. Figure 5.32(a) displays the higher the IMF where nearer to the range is to 1.0 represent a spherical shape. The numbers of detected particles decrease when the NPS is set at higher IMF as shown in Figure 5.32(b). This is due to the smaller FOV of the acquired image.

It is also found that the accuracy of mean size measurement increases when IMF increased. This is due to the number of pixels that represent a single particle area is increased (Figure 5.33(a)). Also, the calibration dimension of single pixels size is

become smaller when IMF value is increased (Figure 5.33(b)). Based on all these results, the optimum IMF for NPS is 0.8. This selection is made based on the lower error of mean size which is below 1% and the number of particles detected is larger than IMF of 1.5. Large numbers of the detected particles are necessary in plotting size distribution of the particles.

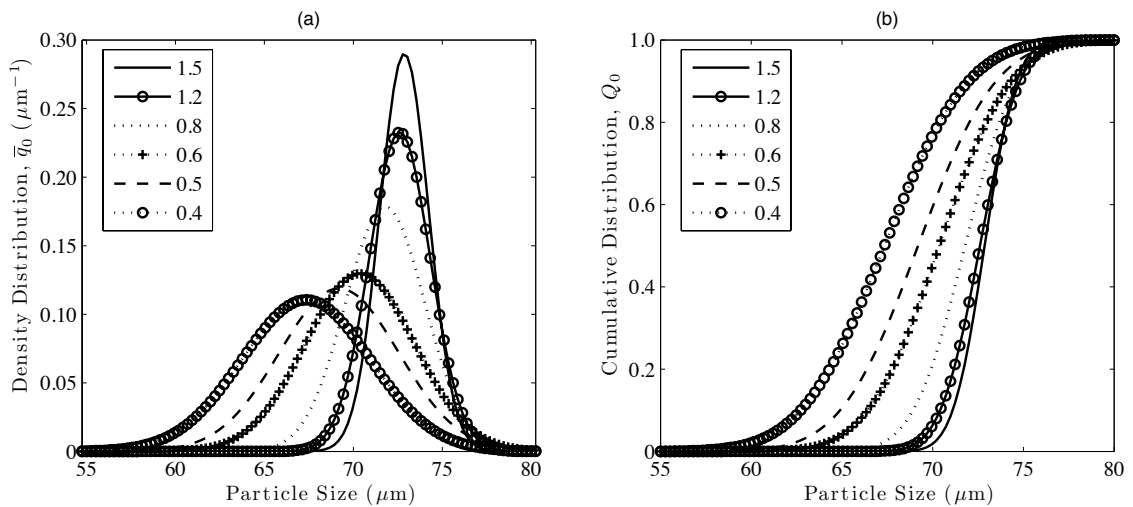


Figure 5.29: Numbered density and cumulative size distribution of the certified microspheres for optimum LI at different IMF.

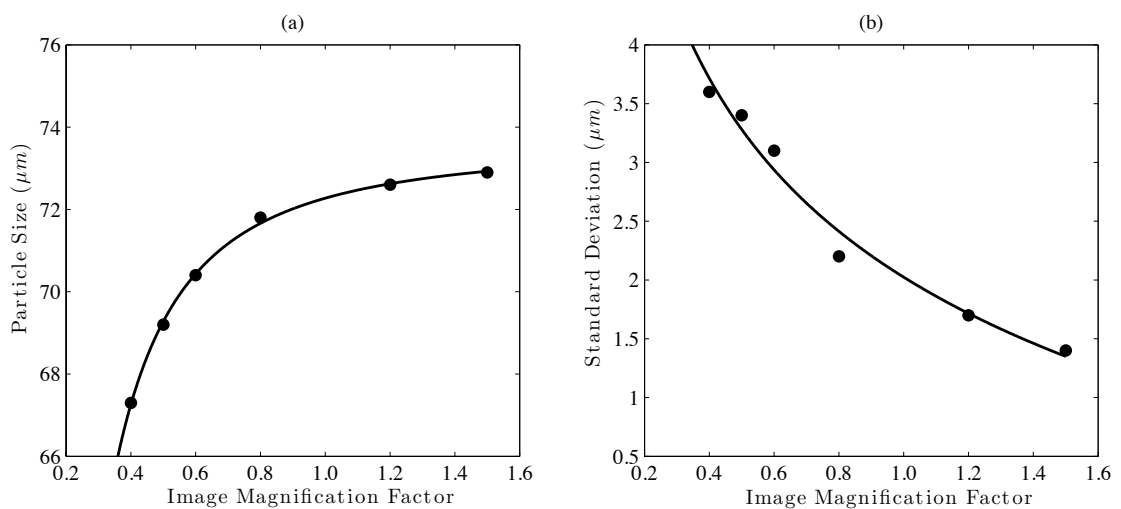


Figure 5.30: Mean sizes of the certified microspheres and their standard distribution for optimum LI at different IMF.

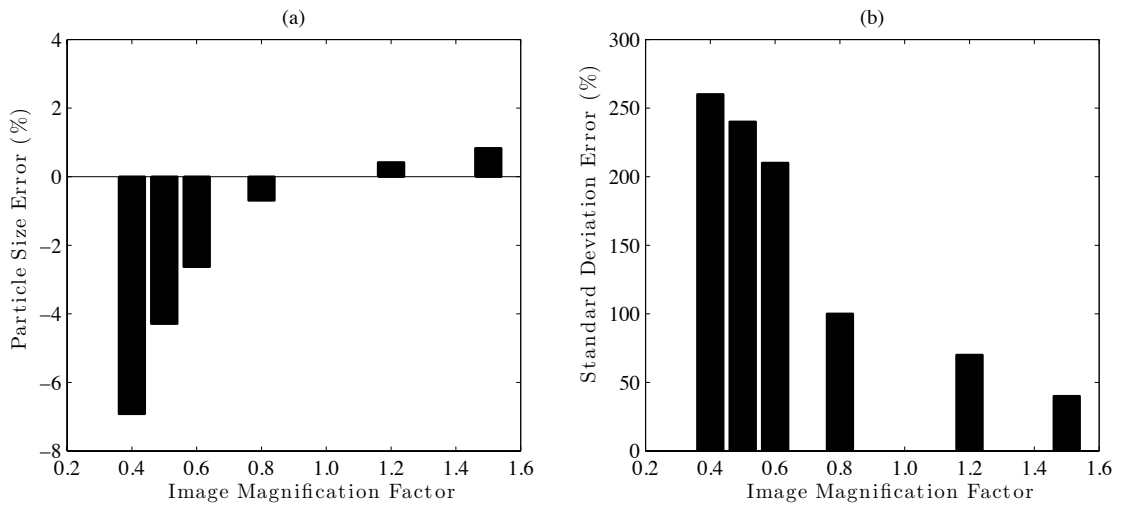


Figure 5.31: Mean size errors of the certified microspheres and their standard deviation errors for optimum LI at different IMF.

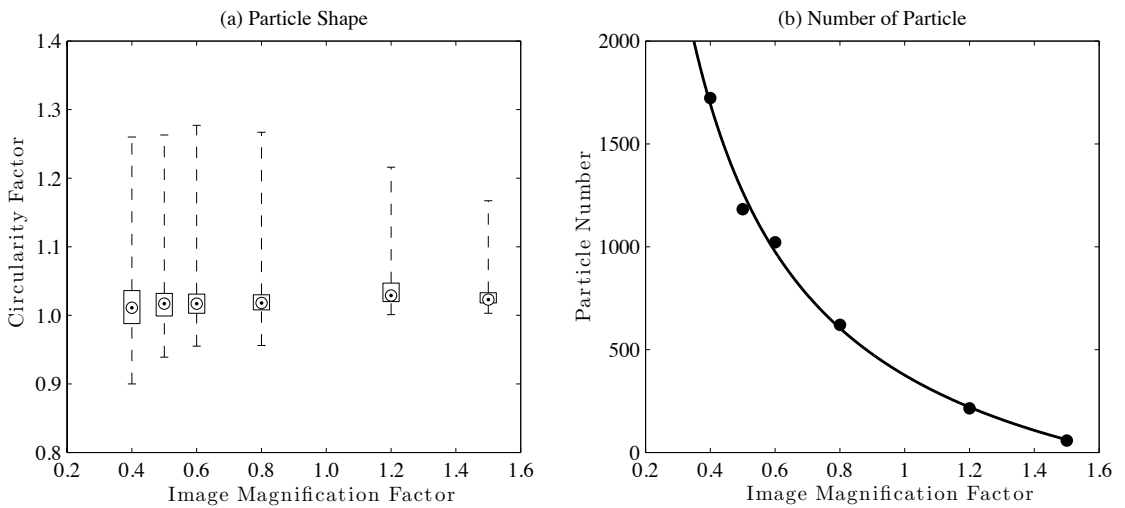


Figure 5.32: Particle shape and detected number of particle of the certified microspheres.

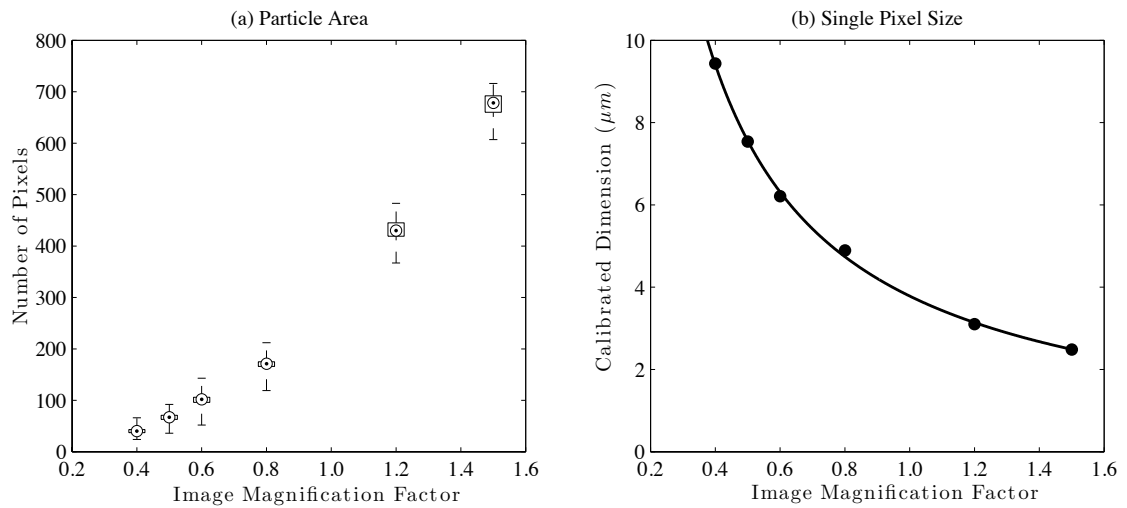


Figure 5.33: Particle area in pixels and the dimension of single pixels size of the certified microspheres.

5.5.3 *Fillite Particles - Laser Intensity*

The Fillite particles are used to investigate the effect of laser intensity on the accuracy of the size. This experiment is similar to the Section 5.5.1 except for the particles in the transparent container which are replaced to the Fillite.

For each IMF value, various LIs ranging between 80 to 95% are applied during the image acquisition process. It is found that different LIs produce dissimilar images, where the higher the LI, the better the image contrast (Figure 5.34). This similar behaviour is also found when acquiring the certified microsphere in section 5.5.1.

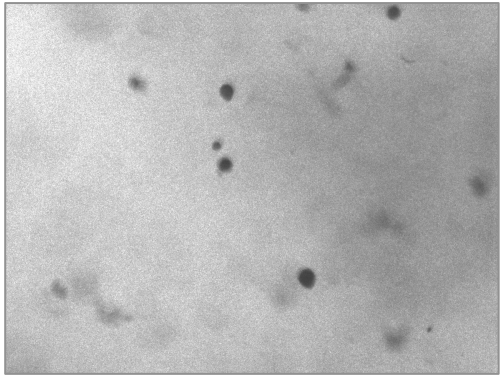
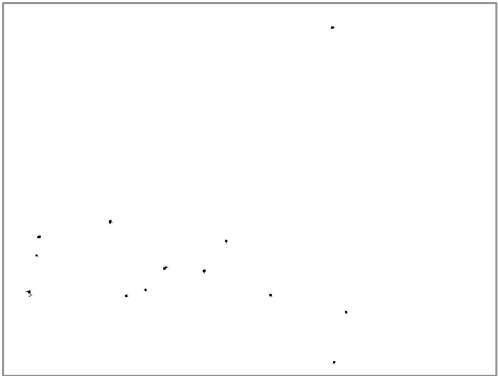
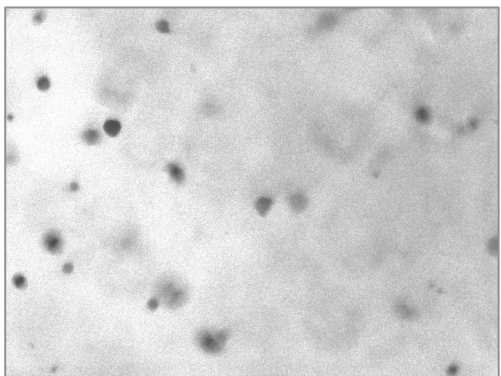
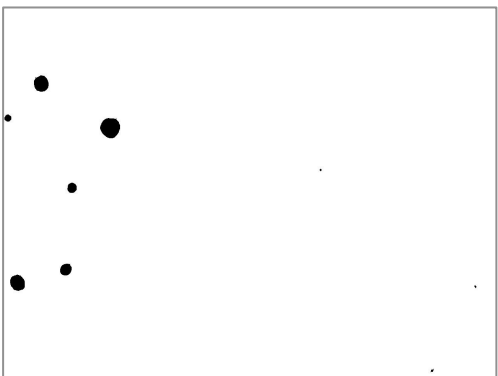
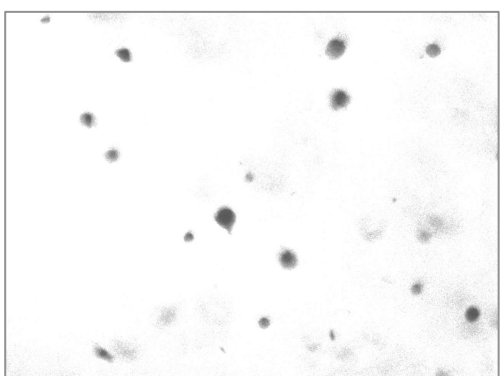
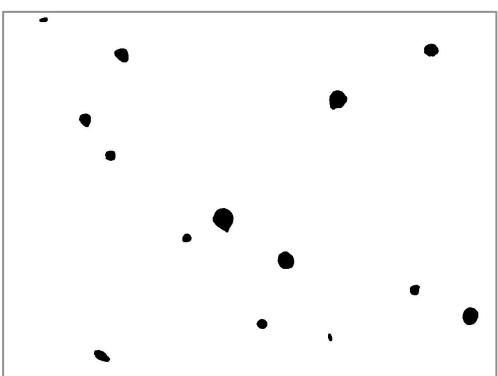
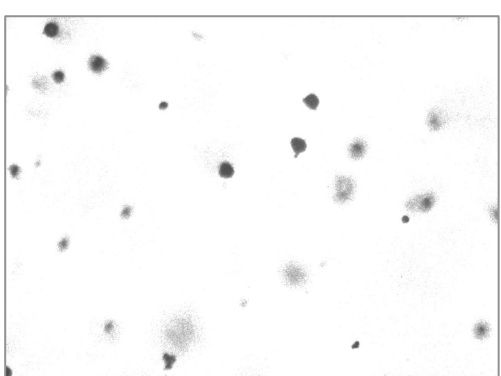
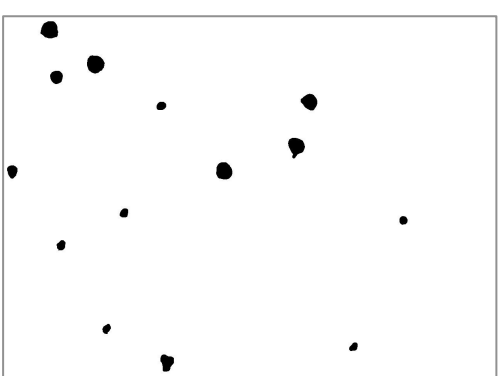
LI	Acquired Image	Processed Image
80%		
85%		
90%		
95%		

Figure 5.34: Acquired and processed images of the Fillite particles for IMF of 0.8 at different LI.

Figure 5.35 shows the size distribution of Fillite particles for IMF of 0.8 for varying LIs. It is clearly shows that the distributions at 90 and 95% of LI are almost similar. For 80% of LI, it produces narrow distribution while 85% of LI depicts wide distribution. In term of the mean size, LI at 90% produces very close value compared to the data provided the particle's manufacturer (Figure 5.36). Therefore, at the IMF of 0.8, the optimum LI is found at 90%. Similar experiments are also performed for the rest of the IMF. The optimum LI found for each IMF is illustrated in Figure 5.37.

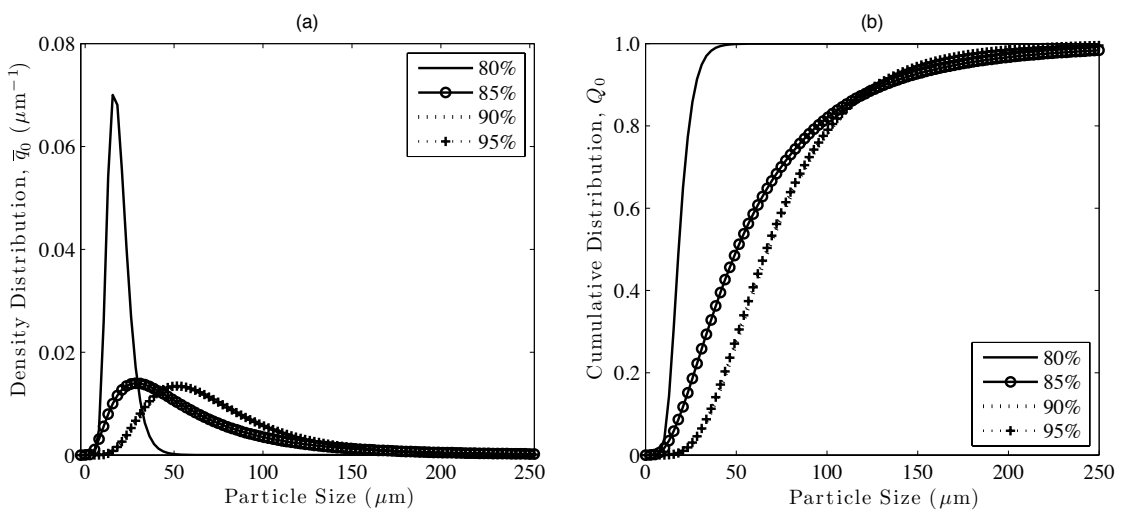


Figure 5.35: Numbered density and cumulative size distribution of Fillite for IMF of 0.8 at different LI.

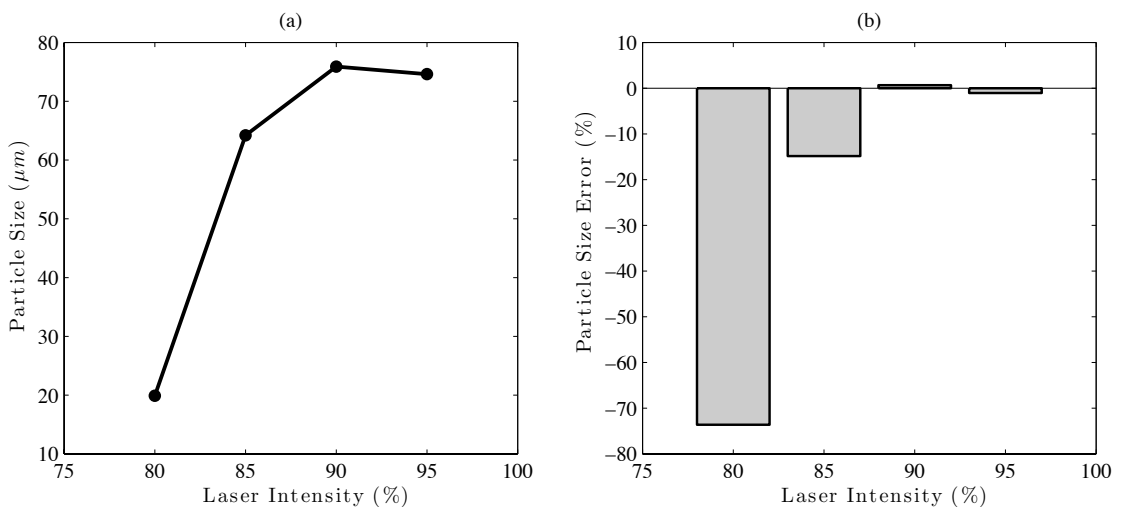


Figure 5.36: Mean sizes of the Fillite and their errors for IMF = 0.8 at different LI.

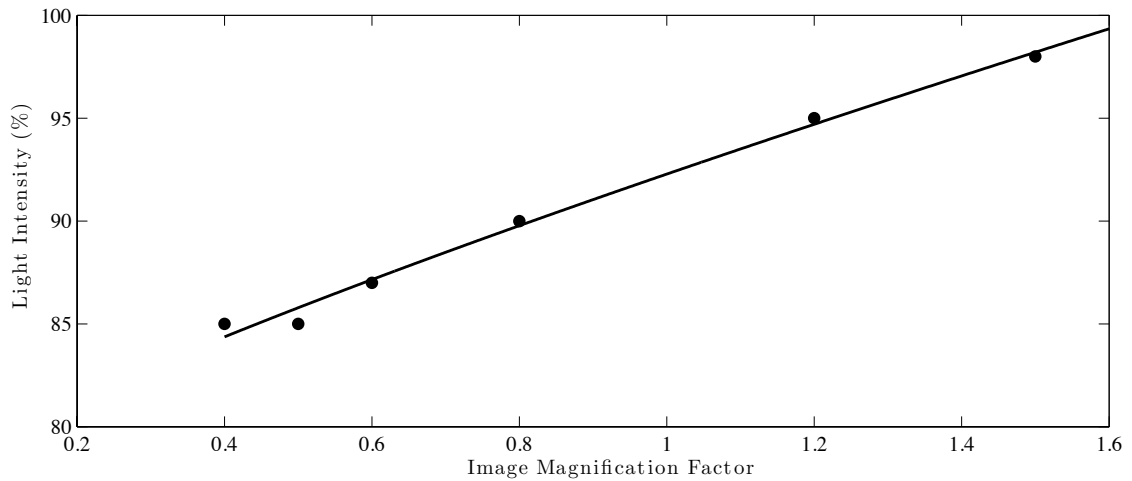


Figure 5.37: Optimum LI of the Fillite at different IMF.

5.5.4 *Fillite Particles - Image Magnification*

The proper image magnification for acquiring a raw image is essential to ensure the accuracy of sizing the particles. In this experiment, the effect of IMF on the accuracy of Fillite particles is performed. Different values of IMF are applied in this off-line measurement and the results are listed in Table 5.4. The setup of the experiments is similar to the Section 5.5.2. Acquired images at optimum LI are processed and analysed and the results depicted in Figure 5.38 to Figure 5.42.

It is found, as shown in Figure 5.39(a), that the mean size of Fillite particle is about 75 micron at the IMF between 0.6 and 1.5. This contributes to the mean size errors of less than 5% (Figure 5.40(a)) when compared it to SEM results as explained in section 5.4.2. The standard distribution shows errors of less than 5% for IMF of 0.8 to 1.5 as illustrated in Figure 5.40(b).

The circularity factor (CF) of the Fillite particles at higher IMFs shows that the particles are spherical in shape where the ranges of value are nearly 1.0 (Figure 5.41(a)).

However, lower IMF depicts slightly non-spherical shape where the circularity factor is far from 1.0. This is due to the lower IMF produces smaller image of particles and has limitation in recognising the circular shape of Fillite. Figure 5.41(b) shows the number of particles detected by NPS at different IMF. The lower the IMF, the larger number of particles detected due to the bigger FOV of the image.

It is found that the accuracy of mean size measurement increases when IMF increases. This is due to the increase in the number of pixels that represent a single particle area (Figure 5.42(a)). Also, the calibration dimension of single pixels size becomes smaller when IMF is increased (Figure 5.42(b)). Based on all these results, the optimum IMF for NPS is 0.8. This selection is made based on the lower error of mean size which is below 5% and a number of particles detected is larger than IMF of 1.5. The large number of detected particles is necessary to plot the size distribution of the particles.

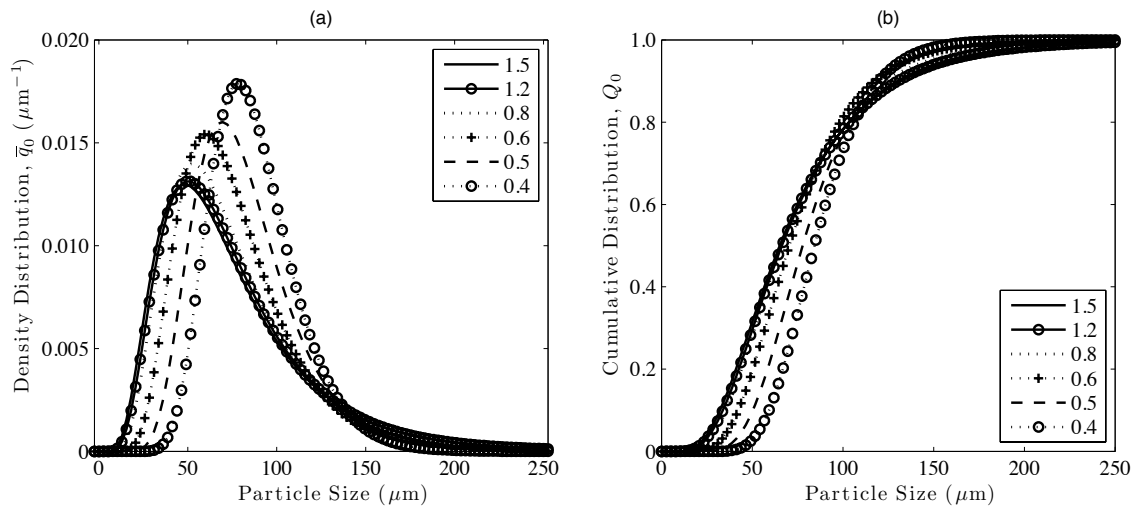


Figure 5.38: Numbered density and cumulative size distribution of the Fillite particles for optimum LI at different IMF.

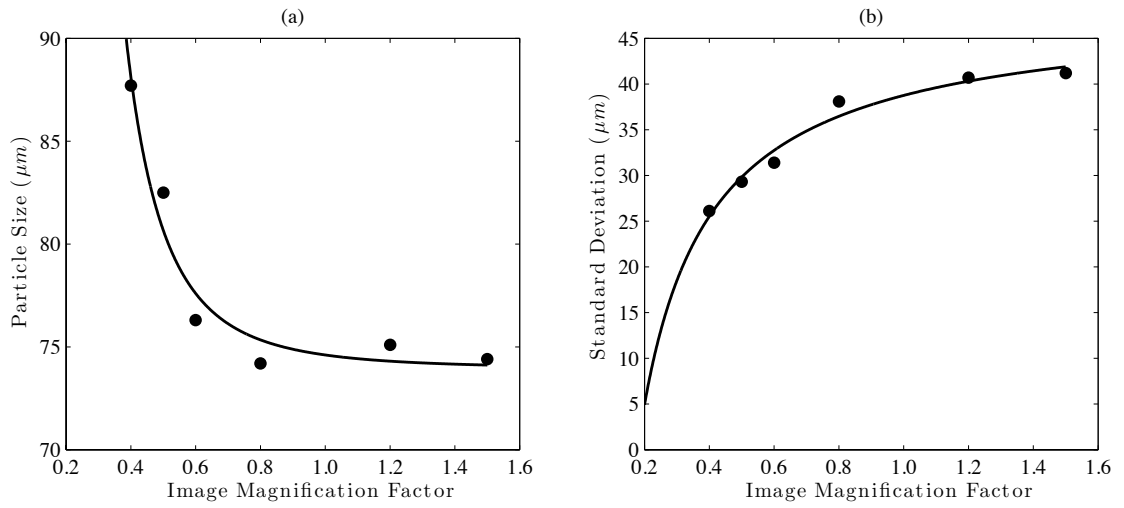


Figure 5.39: Mean sizes of the Fillite particles and their standard distribution for optimum LI at different IMF.

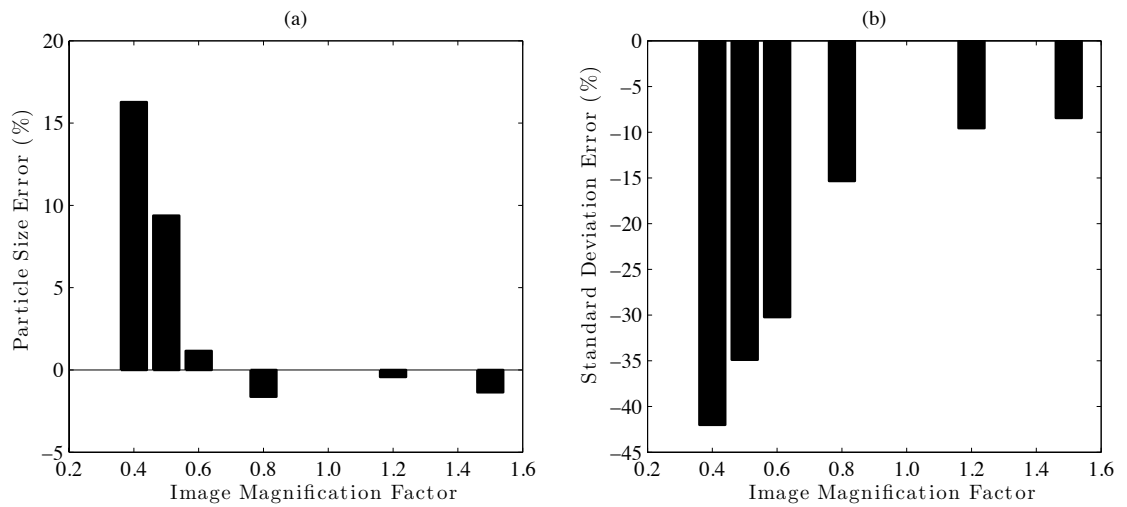


Figure 5.40: Mean size errors of the Fillite particles and their standard deviation errors for optimum LI at different IMF.

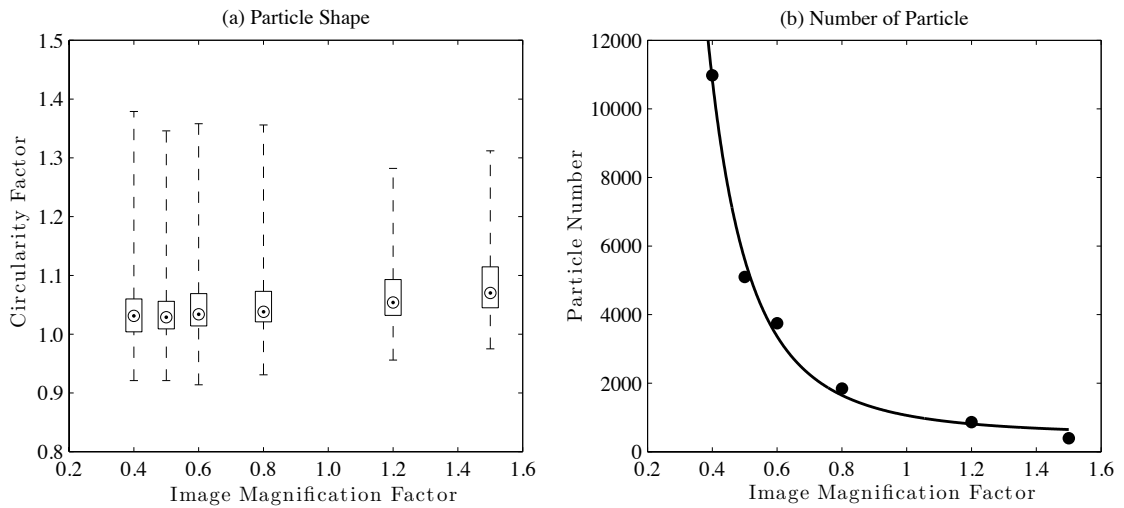


Figure 5.41: Particle shape and detected number of particle of the Fillite particles.

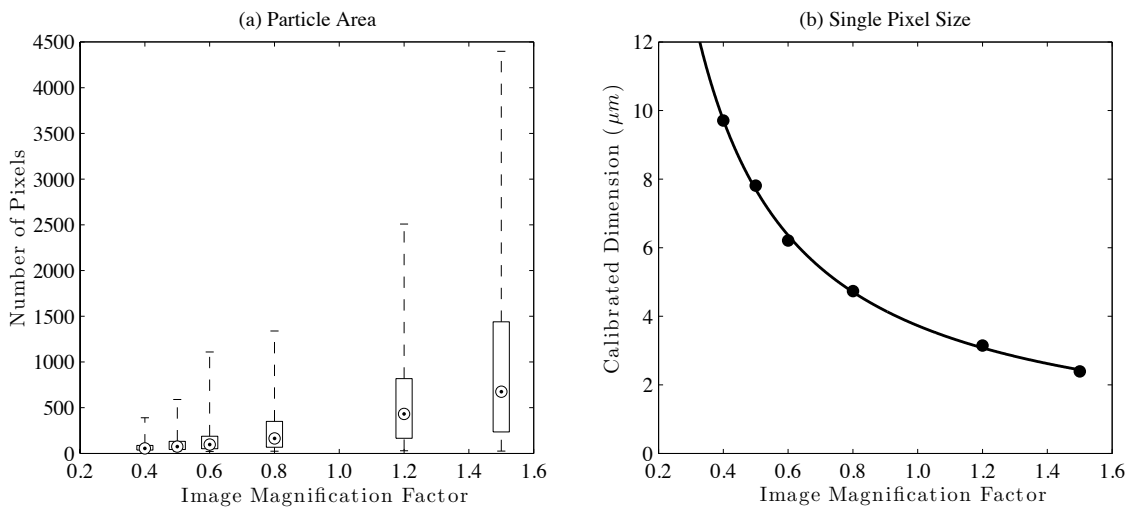


Figure 5.42: Particle area in pixels and dimension of single pixels size of the Fillite particles.

5.6 Particle Sizing by Direct Illumination Technique

This is an alternative technique for the measurement of particles sizes. The working principle of the NPS employed is similar to that of the Section 5.2.2. The only difference is the way the particles are illuminated and the algorithms used for image processing. This technique is based on the acquisition of images of scattered light from

particles and on extracting useful information from the images. The setup of the NPS that applied the DI technique is shown in Figure 5.43.

In this setup, the pulsed beam is fired from the laser unit and converted to a laser sheet by a cylindrical lens. The camera is positioned perpendicular to the laser sheet which is set at a scattering angle (SA) of 90° and focused at the plane inside the light sheet. The particles inside the container are illuminated by the laser sheet. The light scattered by these particles is recorded using a digital camera as a sequence of frames. Once an image of dispersed particles is acquired, it is processed and analysed by the software as described in details in Chapter 4.

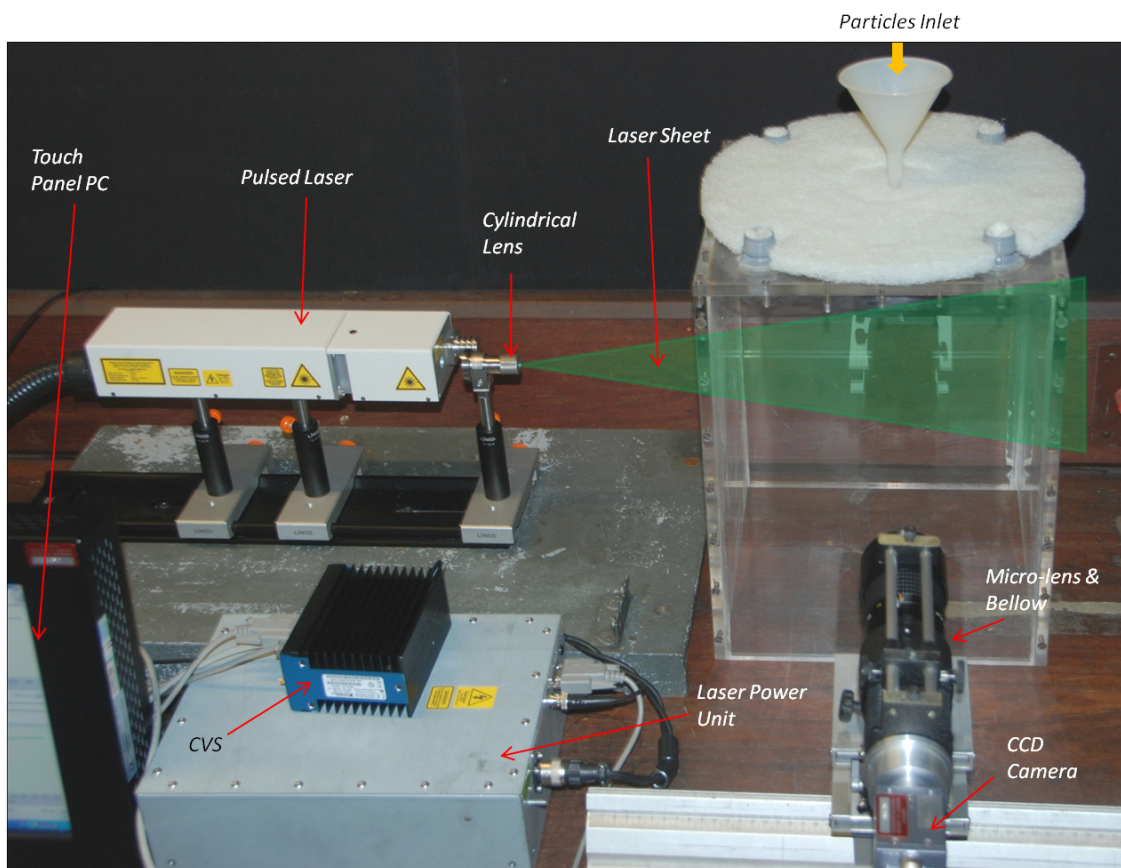


Figure 5.43: NPS setup for the direct illumination technique.

Figure 5.44(a) shows an example of a free-flow of solid particles (opaque) in the air while Figure 5.44(b) is a water droplet (transparent) dispersed in air produced by a spray atomiser. The acquired images produce dark background and bright images for a solid particle, while for a liquid, a dark background and two bright spots that represent single droplets are produced.

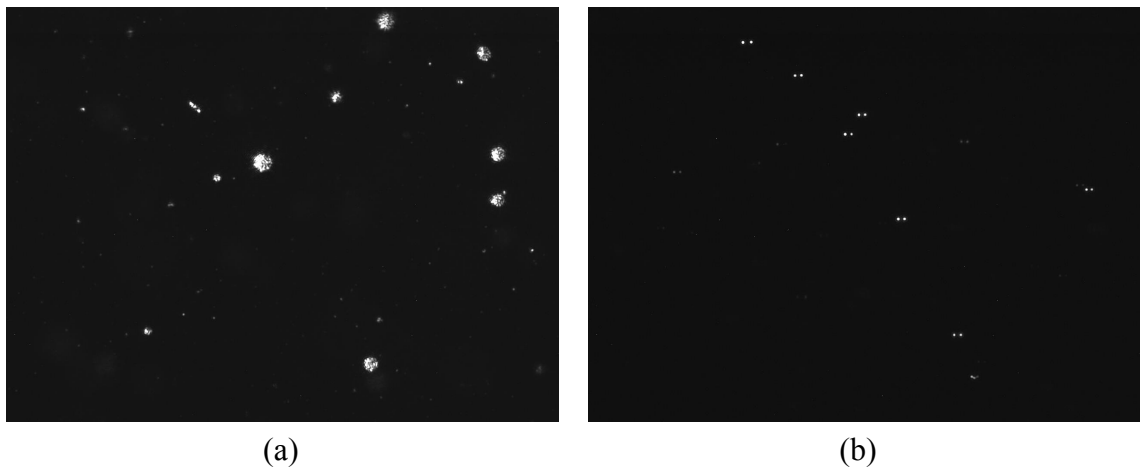


Figure 5.44: Examples of acquired raw images by DI technique. (a) solid particles dispersed in air ($SA = 90^\circ$), (b) liquid particles dispersed in air ($SA = 70^\circ$).

5.7 Parametric Study on DI Technique

In this study, two parameters are investigated to determine their influence on the accuracy of particle sizes. The parameters include the laser intensity (LI) and the scattering angle. As discussed before, the DI technique is based on scattered light by the particles when the light hit them. So, the intensity of direct hit on particles surface may affect the size of actual particles. The scattering angle may also contributes to the accuracy of the particle size due to the different behaviour of transparent particles when the incident light passing through them. So, Table 5.5 is designed to investigate these parameters on the accuracy of particle size.

As described in section 5.5.2 and 5.5.4, an IMF of 0.8 is the optimum setting to acquire the particle image. At this setting, it produces good accuracy and captured bigger field of view. Therefore it detects more particles compare to 1.2 and 1.5. Based on this finding, the IMF of 0.8 has been set for the experiment in Table 5.5.

Table 5.5: Matrix of experiments to identify the optimum value of LI and SA.

Laser Intensity (%)	Scattering Angle (degree)			
	30	50	70	90
80	yes	yes	yes	yes
85	yes	yes	yes	yes
90	yes	yes	yes	yes
95	yes	yes	yes	yes

5.7.1 *Fillite Particles - Laser Intensity*

The Fillite particles are used to investigate the effect of laser intensity on the accuracy of the size. This experiment is similar to that in section 5.5.1 except for the particles in the transparent container which are replaced by the Fillite.

At each scattering angle, various LI from 80 to 95% are applied during the image acquisition process. The experimental setup of this study is illustrated in Figure 5.45. It is found that different LI produce dissimilar acquired image, where the higher the LI, the more scattered light is recorded (Figure 5.46).

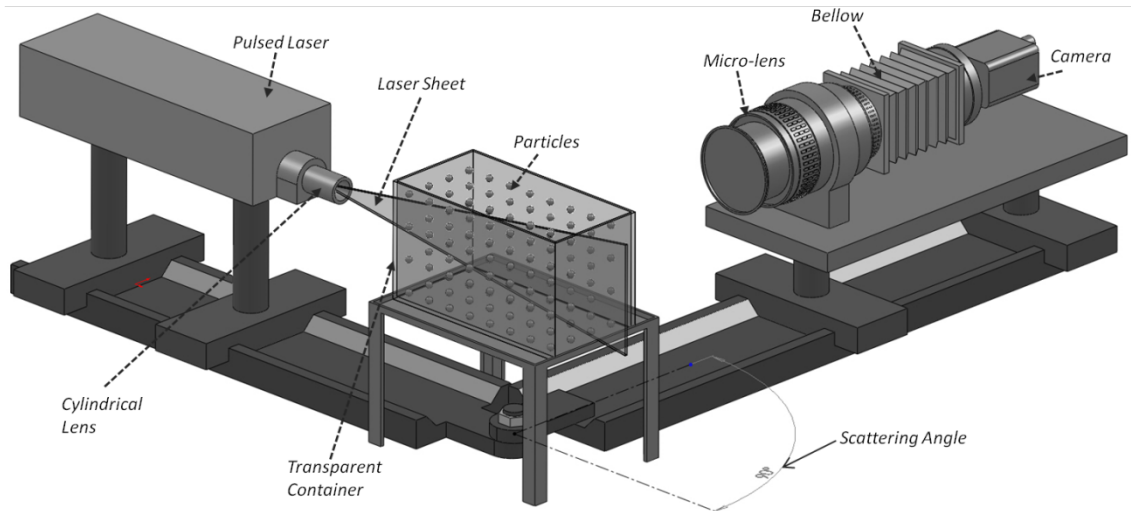


Figure 5.45: Experimental setup of size measurement for particles suspended in water using DI technique.

An acquired image at 80% of LI produces the lowest scattered light. It seems that the intensity is not good enough to illuminate the particles. It is found that the processed image produces smaller shape of particles compared to acquired image. This contributes to lower mean particle size with 9% error at 80% of LI as depicted in Figure 5.47.

It is recorded that the mean size increases with an increase of LI. Almost similar mean size are recorded at 85, 90 and 95% with an error below 5%. The particle diameter at 10, 50 and 90% of size distribution is plotted in Figure 5.48. It clearly shows that 80 and 85% of LI recorded more than 20% error at $d_{0.1}$. At this intensity, a smaller particle scatter low light and it is difficult to be seen by a camera.

At 90% of LI, the diameter of $d_{0.5}$ gives lower errors which are below 3%. Also, at this intensity, a lower error is recorded for the mean particle size. Therefore, the optimum LI of this DI technique in measuring opaque particles is found at 90%.

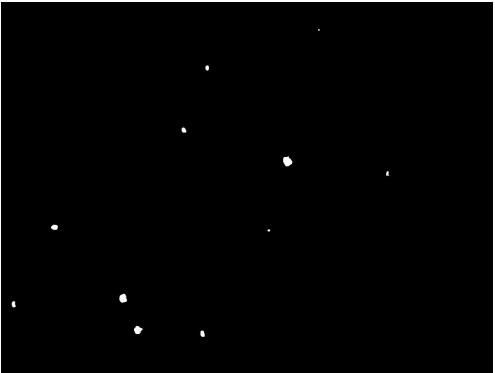
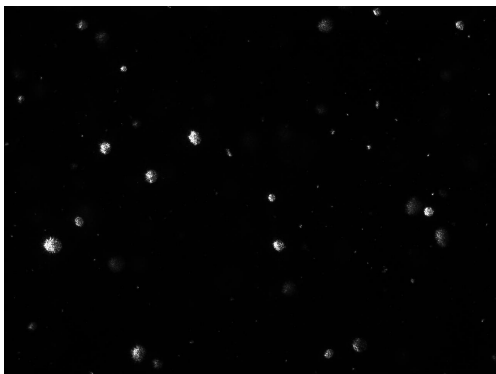
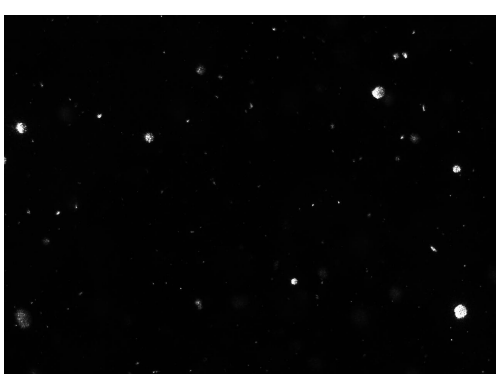
LI	Acquired Image	Processed Image
80%		
85%		
90%		
95%		

Figure 5.46: Acquired and processed images of the Fillite particles for IMF = 0.8 at different LI.

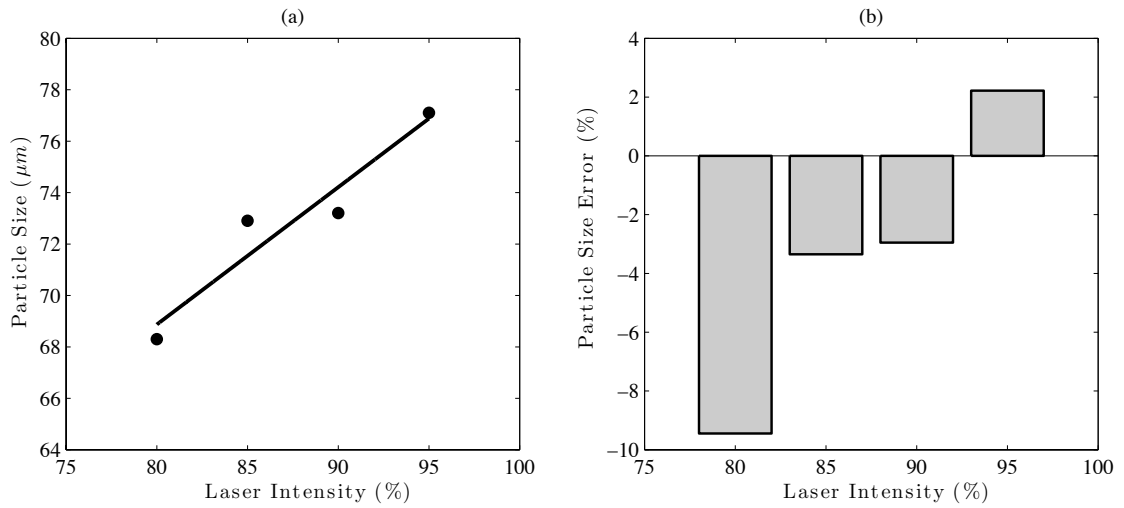


Figure 5.47: Mean particle size and its error at different LI.

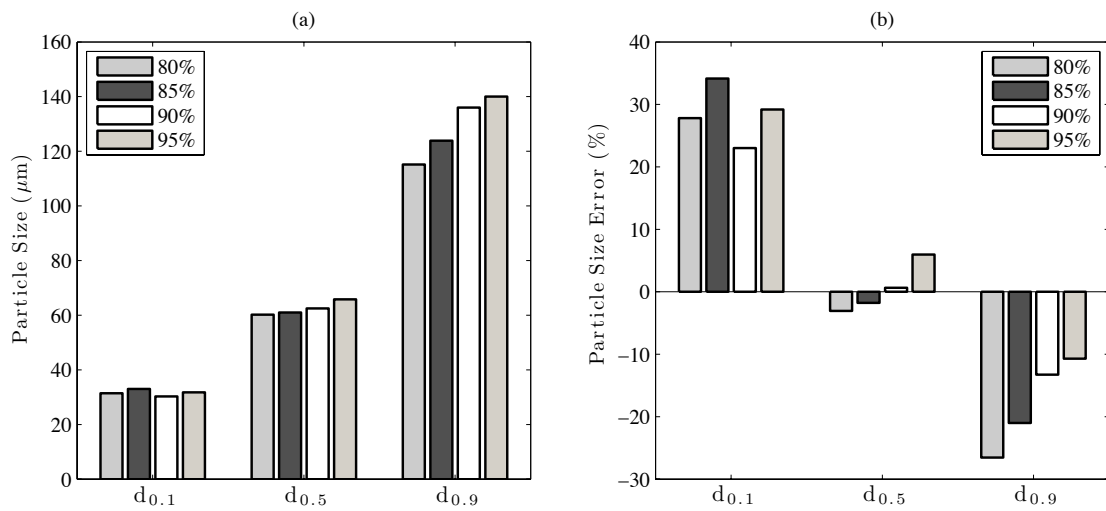


Figure 5.48: Particle size and its error at 10, 50 and 90% of cumulative distribution.

5.7.2 Fillite Particles - Scattering Angle

In this section, the objective is to investigate the effect of SA on the particle size. The similar experimental setup in Figure 5.45 is utilised. However, the SA is varied at 30, 50, 70 and 90°. In this experiment, the LI is set to 90% which is an optimum setting as determined in Section 5.7.1.

It is found that by varying SA between 30 and 90⁰, the value of mean particle size does not change significantly. This is clearly depicted in Figure 5.49(a) where the measured mean size by DI and SEM are in agreement showing an error of less than 5% (Figure 5.49(b)). All the measured results from 30 to 90⁰ show that 90% of the particles is passing 125 μm with errors below 2%. This shows that the SA does not affect significantly the accuracy of the particle size measurement (Figure 5.50).

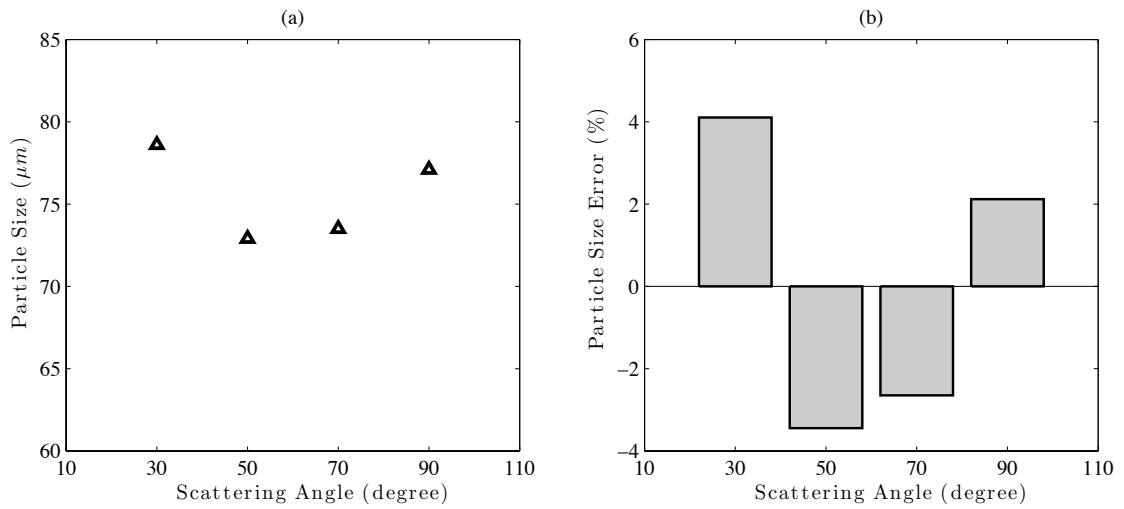


Figure 5.49: Mean particle size and its error at different SA.

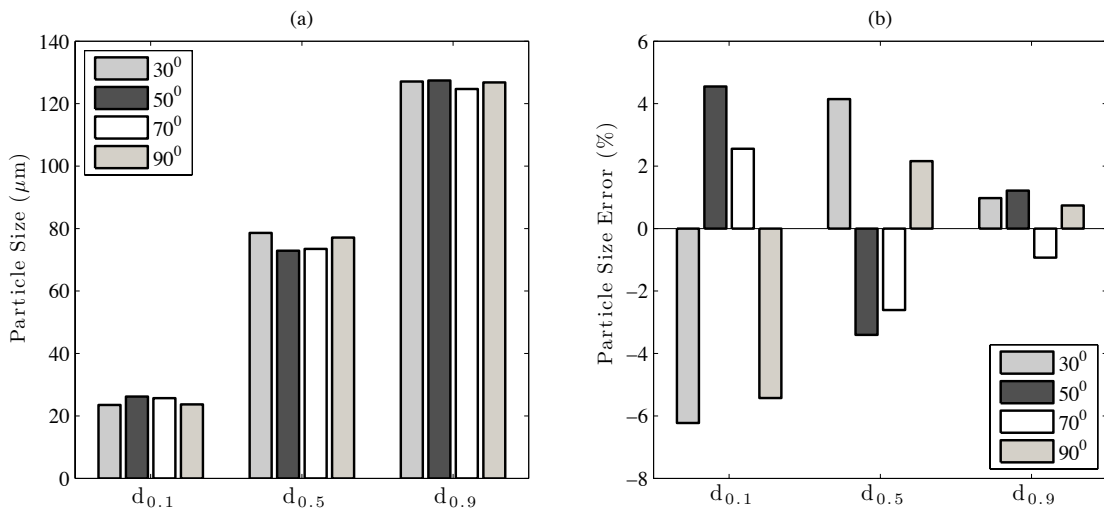


Figure 5.50: Particle size and its error at 10, 50 and 90% of cumulative distribution.

5.7.3 Liquid Particles - Laser Intensity

By applying a similar technique as given in Section 5.7.1, the NPS is used for the sizing of the liquid particles or droplets dispersed in air (Figure 5.51). The droplets are water based and produced by a spray atomiser. The scattering angle of the setup is set to about 70° in order to produce two glare points of single particle (Section 5.7.4). This study reports the effect of LI on the accuracy of the liquid particles size.

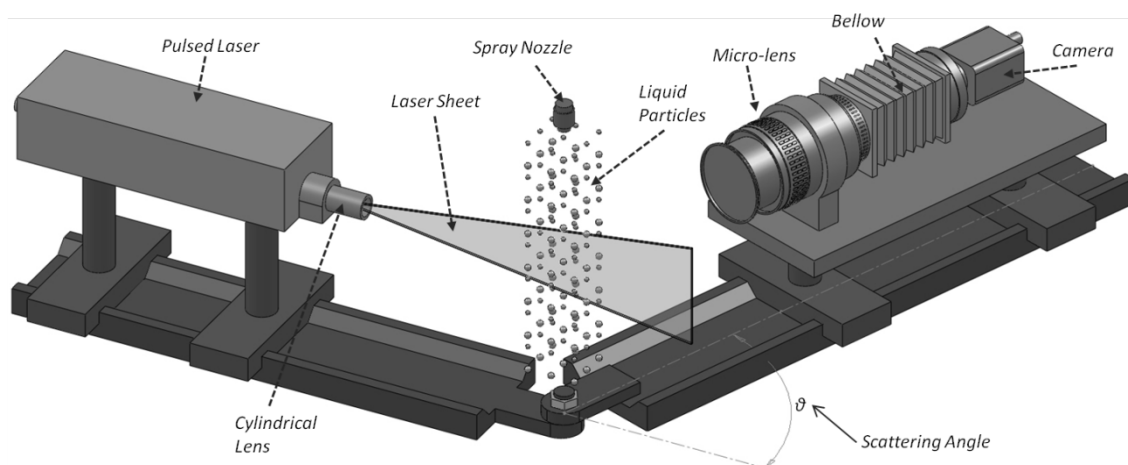


Figure 5.51: Experimental setup of droplet sizing by DI technique.

It is found that the LI in DI technique affect the accuracy of the particle sizes. In Figure 5.52, it is clearly shown that the higher the LI applied to the particles, the brighter the scattered light captured by camera. This contributes to the larger mean size at higher LI (Figure 5.53). The mean sizes of this experiment are compared to the reference data measured by shadow technique (Section 5.4.3). With the current setup, DI technique has limitation in determining smaller particle size. This is depicted in Figure 5.54(b), where the error on $d_{0.1}$ is very high (about 130%) compared to result from shadow technique. Smaller droplets scatter few lights at lower LI and more light at higher LI. With few scattered light, it is hard to be visible by the camera.

LI	Acquired Image	Processed Image
80%		
85%		
90%		
95%		

Figure 5.52: Acquired and processed images of the liquid particles for $IMF = 0.8$ at different LI.

At a high scattered light, both glare points overlap each other and this will be rejected by the developed software to ensure the accuracy of the results (Chapter 4). Therefore, based on the mean and size distribution results, the optimum LI of the droplets with DI is 90%.

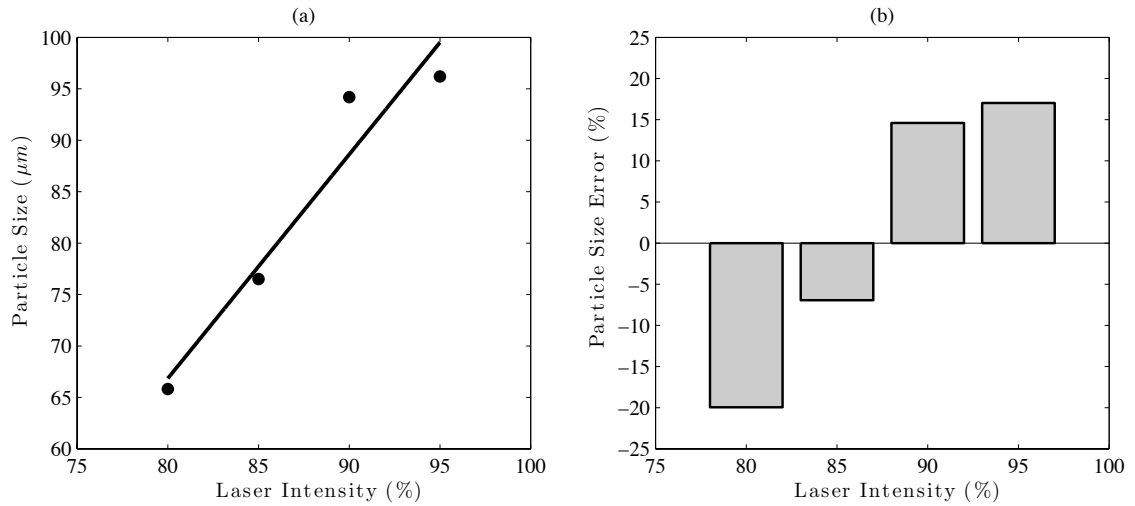


Figure 5.53: Mean particle size and its error at different LI.

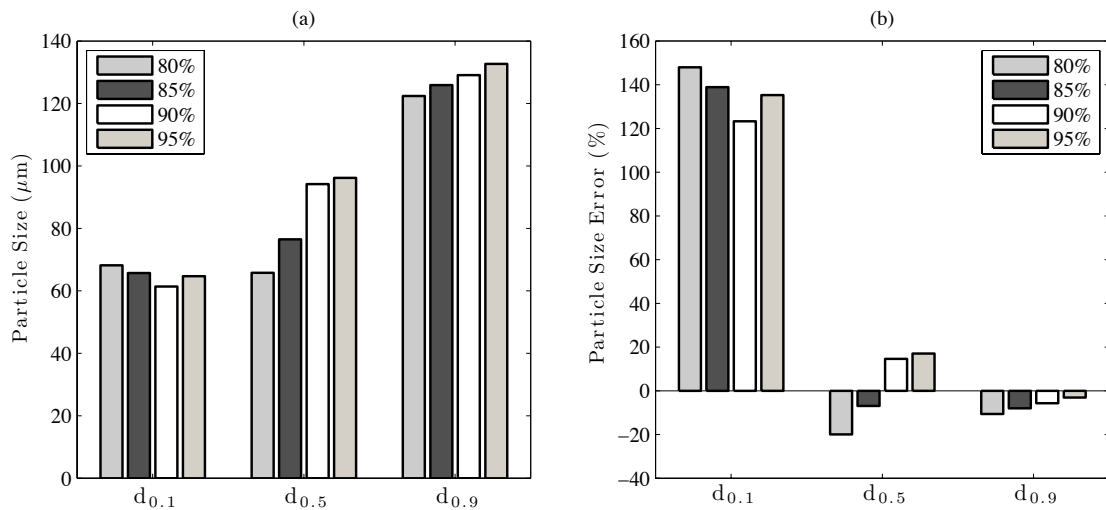


Figure 5.54: Particle size and its error at 10, 50 and 90% of cumulative distribution.

5.7.4 *Liquid Particles - Scattering Angle*

In this study, the effect of scattering angle on the grey level of scattered light by a droplet was investigated. This is to identify the correct scattering angle (SA) for image acquisition for the droplet. Figure 5.56 shows an in-focus image of the droplet that consists of projected separation of two glare points [47]. These points refer to the reflection and refraction and the distance between the two points will be directly related to the droplet size [28]. In this experiment, the images are taken at different scattering angles using the setup configuration as shown in Figure 5.55. In-focus images of a droplet are captured at 30° , 50° , 70° and 90° scattering angle. The images and the greyscale plots are shown Figure 5.57. The plots are referred in greyscale values which represent from 0 to 255. The higher the intensity, the higher the value of greyscale.

Figure 5.57 shows the in-focus image of a single droplet at different scattering angles and their greyscale plots. Each image consists of two glare points which refer to reflection (a) and refraction (b). The greyscale of reflection is lower than refraction point for 30° and 50° . However, at 90° , the reflection recorded a higher intensity compared to the refraction point. Almost similar greyscale intensity for both points is found at 70° scattering angle. The ratios of greyscale between the reflection and refraction points are plotted in Figure 5.58. Based on the plot, it is clearly seen that the scattering angle at about 72° produces the intensity ratio equal to one. Therefore, for this study, the size measurement of DI method is selected at 72° to obtain the consistency of the results.

Figure 5.59 depicts the size distribution measured by DI technique. The experiments are performed at 72° SA and 90% LI. The measured results are compared to the shadow

technique as described in Section 5.4.3 and also to the work done by Hess [48]. The relationship between the separation of the glare point and the droplet size is given in Equation 5.1 [48].

$$d = 2GP \left[\cos \frac{\vartheta}{2} + \frac{RI \sin \frac{\vartheta}{2}}{\sqrt{RI^2 + 1 - 2RI \cos \frac{\vartheta}{2}}} \right]^{-1} \quad 5.1$$

where;

- d Droplet diameter
- GP Separation between glare points
- ϑ Scattering angle
- RI Refractive index of the droplet

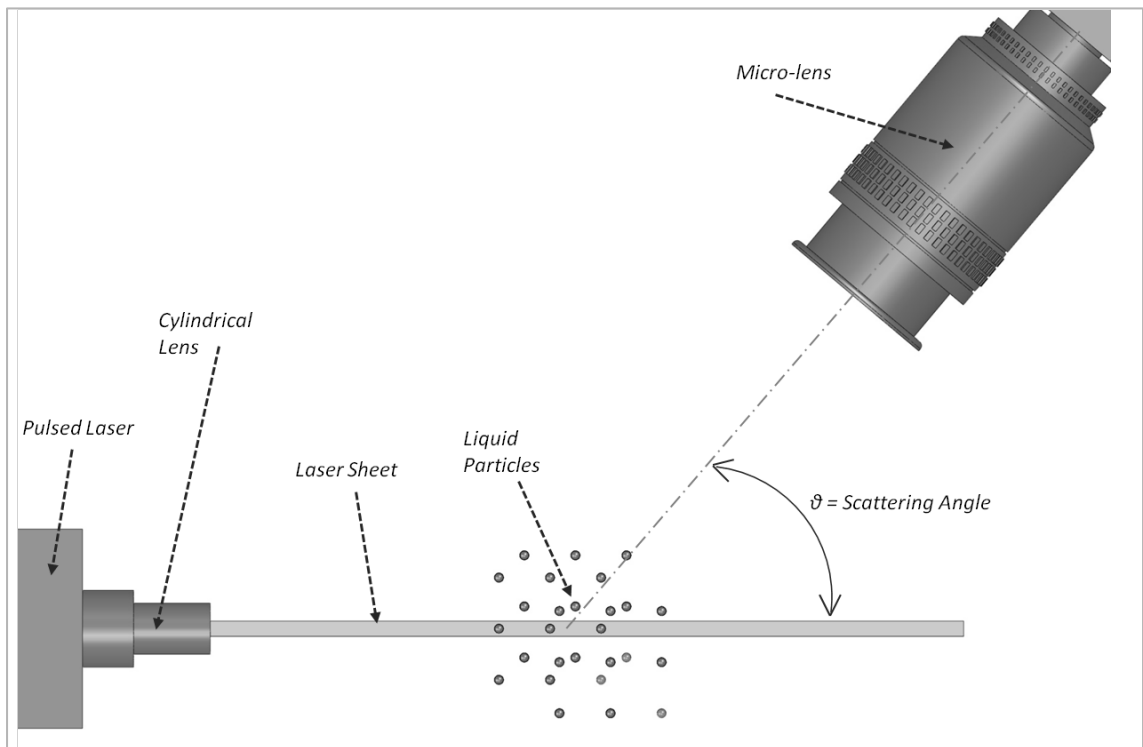


Figure 5.55: Schematic configuration of the DI method

It is found that all techniques record 100% of the droplets below 200 μm . A good agreement is found between shadow and Hess. In addition, the spread and shape of the size distribution measured by DI are almost similar to the Hess (Figure 5.59). However, the results obtained by DI are shifted to the larger size of the distribution plots.

As shown in Figure 5.60(a), the DI overestimates the mean size by a factor of 1.2, which contributes to large error as depicted in Figure 5.60(b). This is believed due to the contribution of scattered light produced by the glare points.

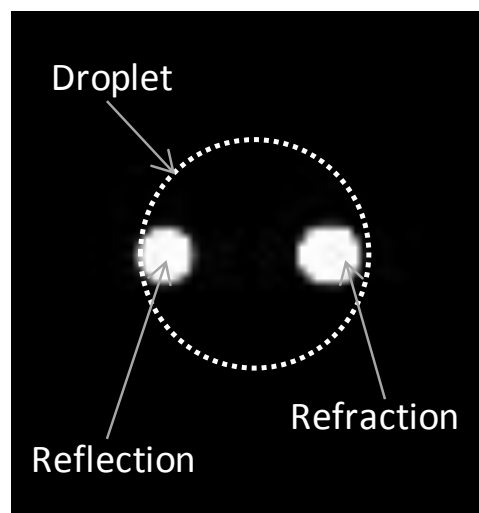


Figure 5.56: In-focus image of two glare points of a droplet

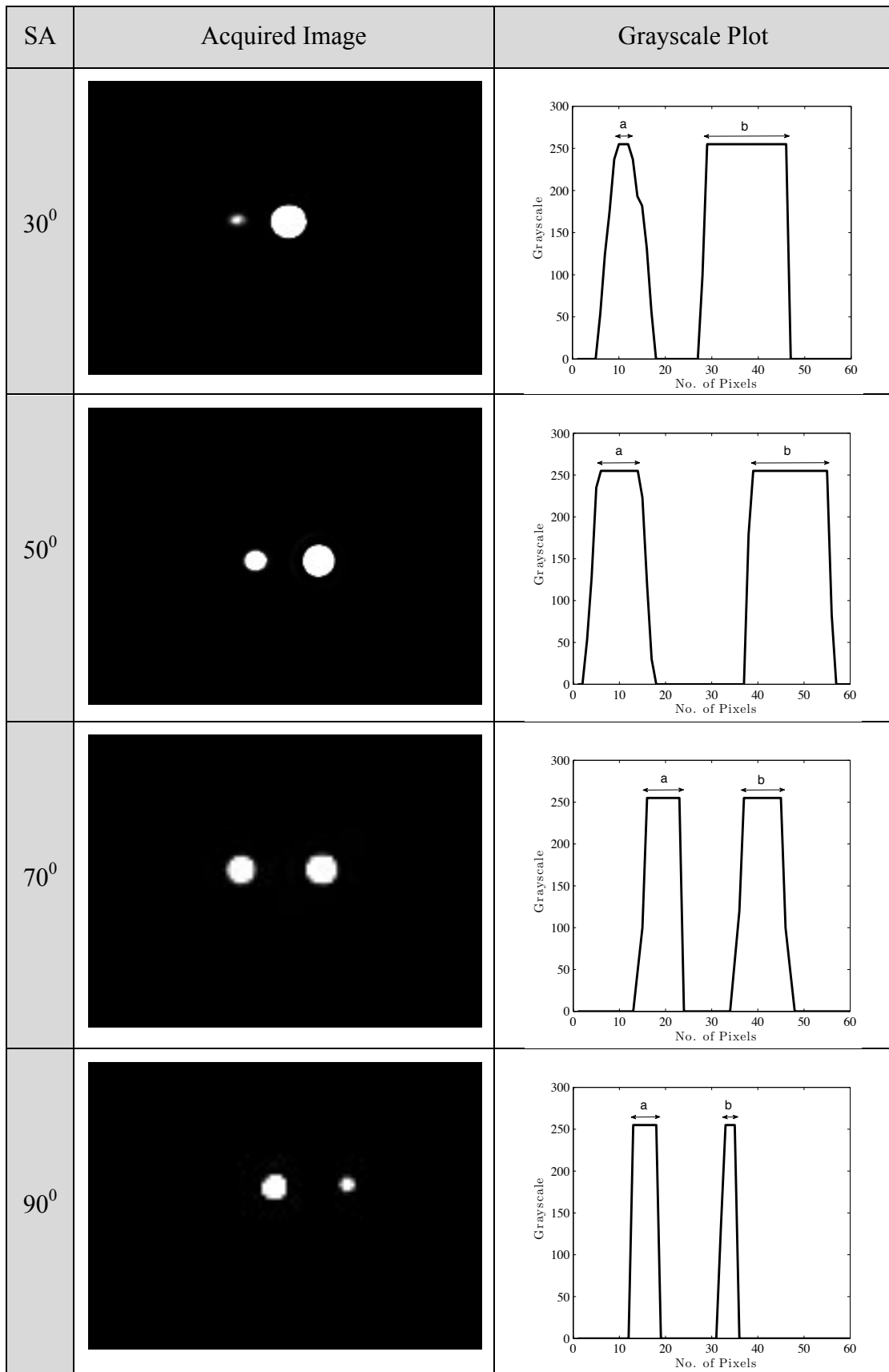


Figure 5.57: Acquired images and greyscale plots of liquid particles at 30⁰, 50⁰, 70⁰ and 90⁰ scattering angle.

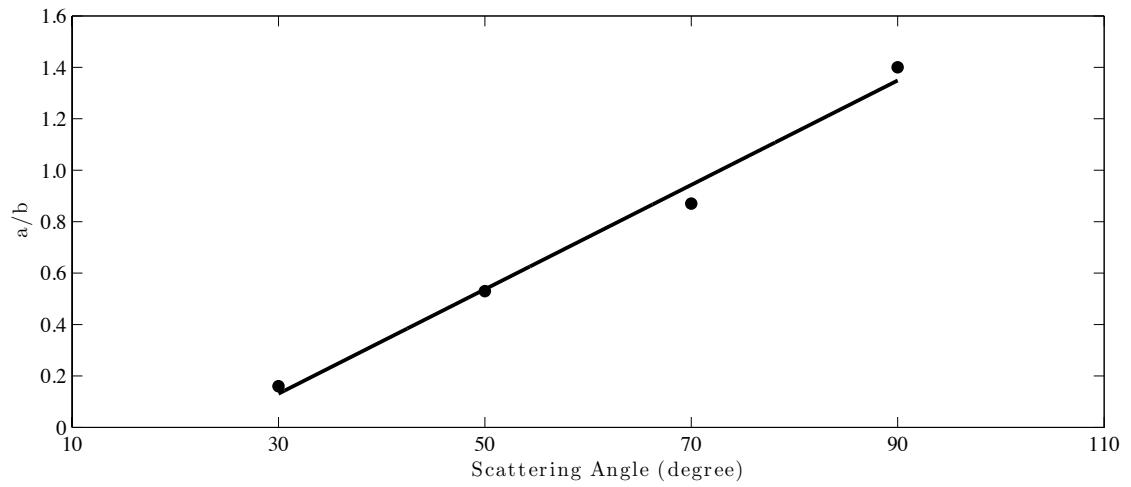


Figure 5.58: Greyscale ratio between reflection and refraction points

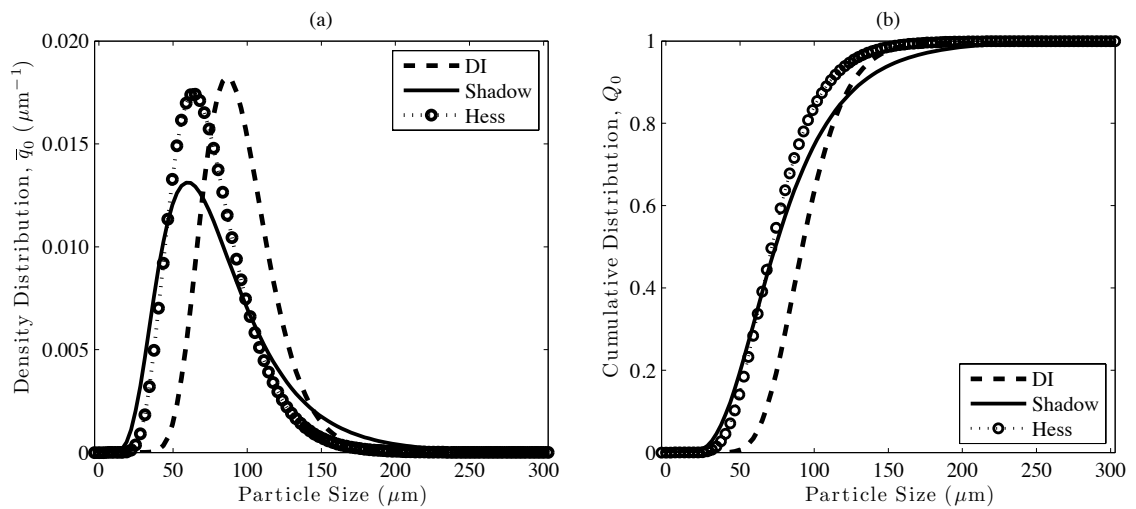


Figure 5.59: Comparison of numbered size distribution between DI, Shadow and work done by Hess [48] using Equation 5.1.

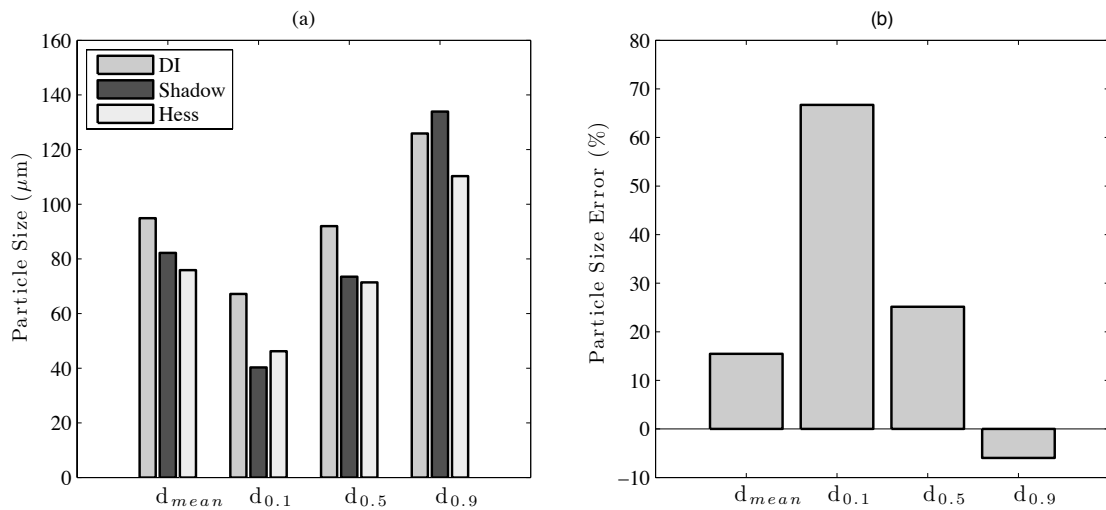


Figure 5.60: (a) Particle size at 10, 50 and 90% of cumulative distribution obtained DI, Shadow and work done by Hess [48] using Equation 5.1. (b) Particle size error obtained by DI compared to the shadow technique.

5.8 Characterisation of Solid and Liquid Particles Dispersed in Air

NPS is designed to have the ability to perform an automated particle sizing of solid and also liquid particles. Experiments are also carried out to characterise the flow consisting of these mixtures. To achieve this, a novel technique called the Particle Mixture Shadow (PMS) is developed.

This technique is based on the shadow sizing technique described in Section 5.4, where the camera acquires shadow images of particles and the developed software used to produce the particle size distribution. However, the acquired raw images and algorithms for image processing steps are different. An acquired image of this technique may consist of solid and liquid particles as depicted in Figure 5.61.

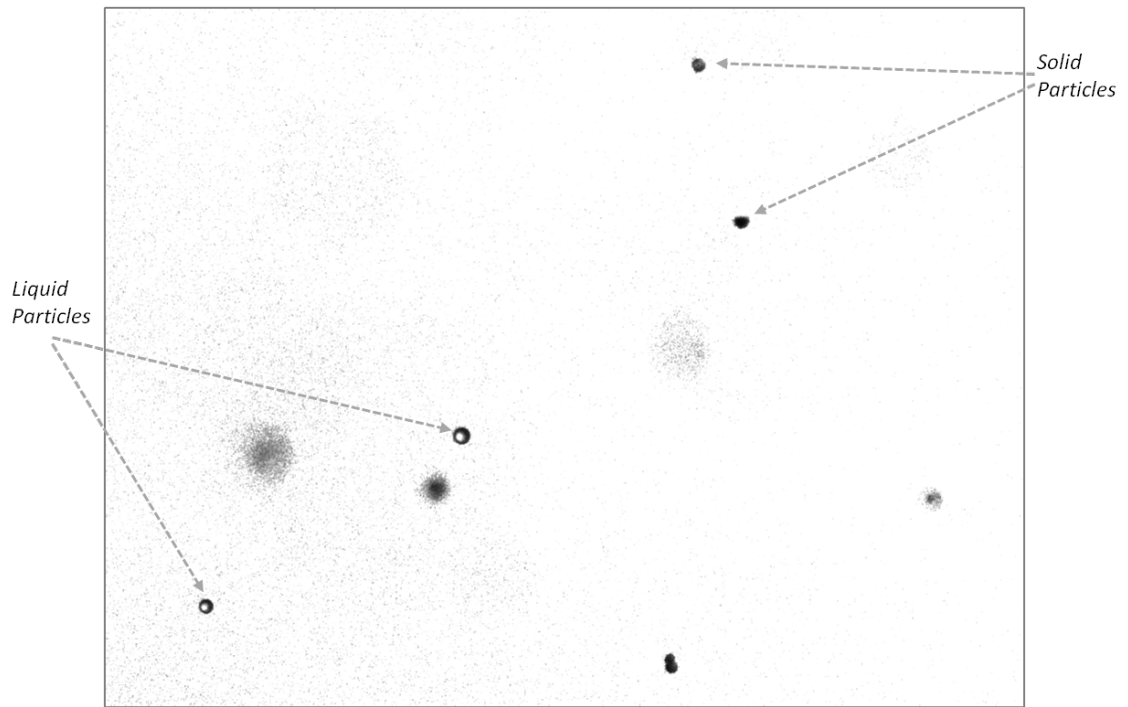


Figure 5.61: Acquired image by PMS technique that contain solid and liquid particles.

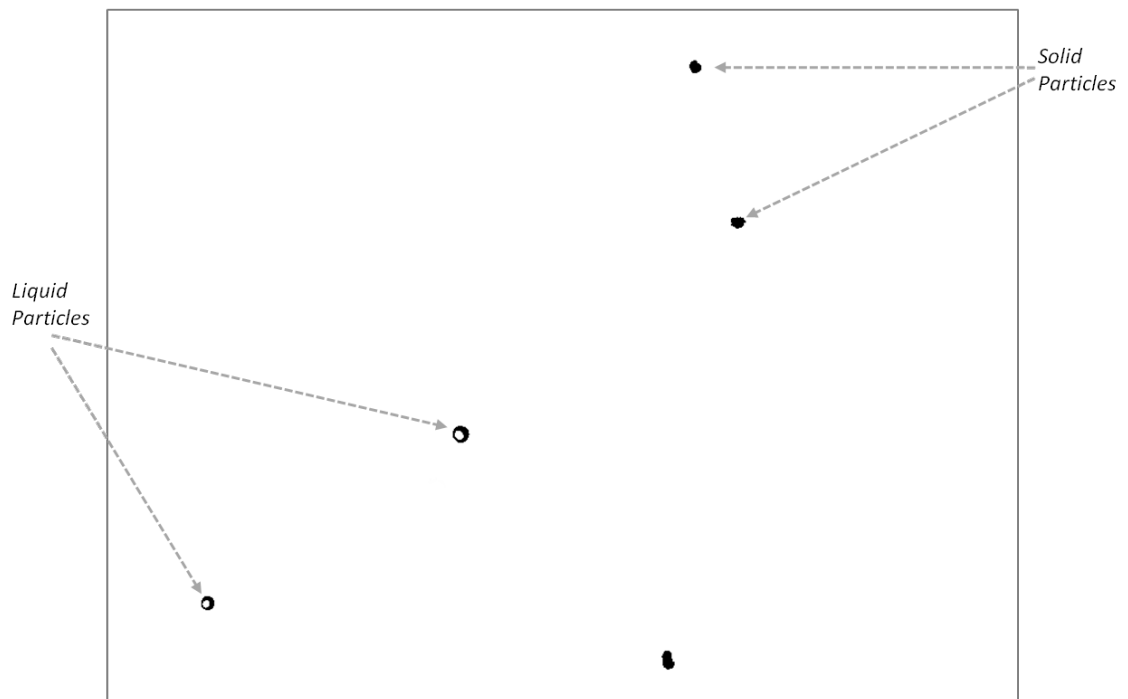


Figure 5.62: Processed image by PMS technique that contain solid and liquid particles.

The setup of this experiment is similar to that of Section 5.4. The particles are back-lighted with a light source which the camera acquiring the shadow image of the objects. The solid particles which are the Fillite particles are introduced from the top while liquid particles are produced by a spray atomiser and sprayed from the side. The images acquired by this technique produce dark images of a solid particles as depicted in Figure 5.61. For a liquid particles, they produce dark images with a bright spot in the middle of it.

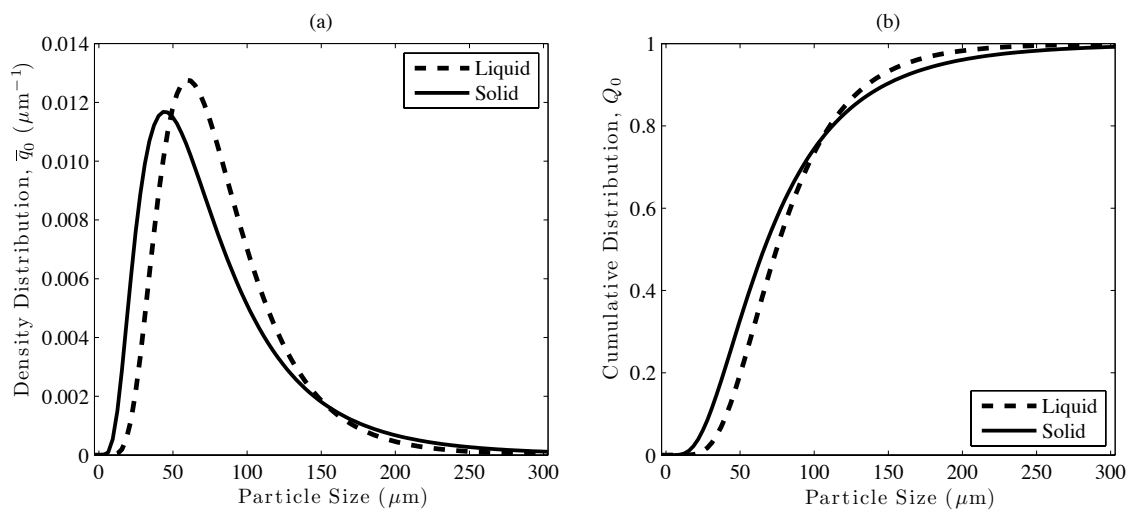


Figure 5.63: Size distribution of liquid and solid particles dispersed in air measured by PMS technique.

Image analysis is applied to process the acquired images in order to determine on-line droplet size distributions using the custom developed software. Figure 5.62 shows the processed image of solid and liquid particles dispersed in air. Only in-focus images of particles are selected for the processing to ensure the accuracy of the size measurement. Different algorithms are designed to differentiate both phases and have been described in details in Chapter 4. They process the respective image to determine size distribution of each phases (solid/liquid) as illustrated in Figure 5.63.

A number of experiments are performed to obtain the optimum setting of the image acquisition when acquiring raw images of solid and liquid particles mixtures. These investigations are very important in determining the sensitivity of the LI and IMF in the accuracy of particles sizes as described in Section 5.5. The proper amount of light is important in producing better contrast of the acquired image. It also produces a bright spot in the middle of the transparent particle (Figure 5.61). This feature has been used as a criterion to distinguish between opaque and transparent particles. A %Area is introduced in this study as a parameter to represent the solid and liquid particle. The values between 1 to 64% are used to represent solid, while 65 to 95% are for the liquid particles (Figure 5.64). The details discussion about %Area is given in Chapter 4.

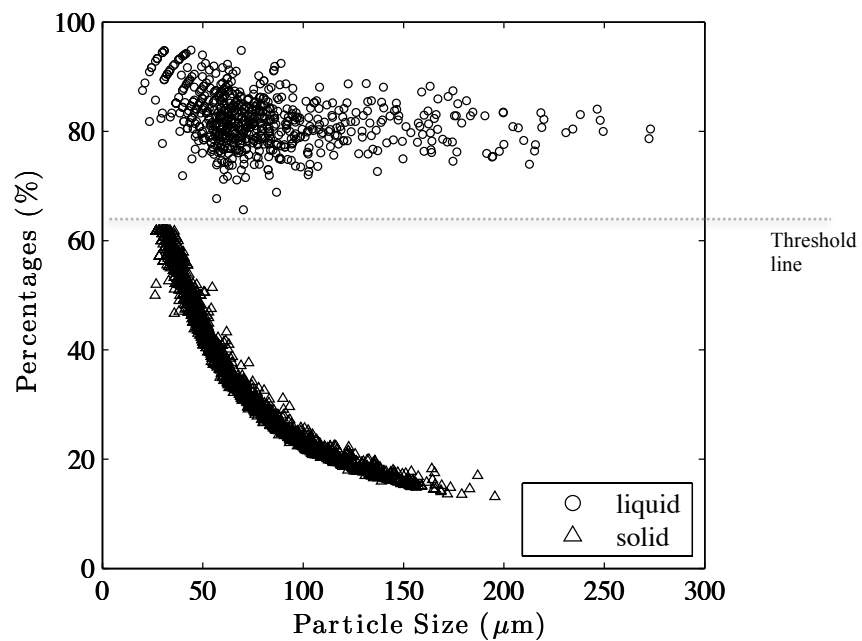


Figure 5.64: %Area that represents solid and liquid particles.

5.9 Conclusions

This chapter has described the operating principle of NPS in sizing the particles that are dispersed in air and in water. The NPS has the ability to size the particles using the

shadow and DI techniques. The particle size results of the NPS were validated using the certified microsphere particle size standard as reported in Section 5.4.1. It was found that measured particles size agrees well with the data provided by the manufacturer of the certified particles. Comparisons of Fillite particle size between NPS and SEM were carried out. A good agreement between both results was found which means that the NPS produced very good accuracy in sizing the particles. The measurement of droplets size produced by a spray atomiser was also performed. The comparison between the shadow and the DI techniques were produced. Parametric studies were carried out to determine an optimum setting of image acquisition of the NPS. The effect of parameters such as IMF, LI and SA on particle sizing were investigated to ensure the accuracy of the measurements.

A novel technique called PMS was developed. The technique can be applied if the measured particles are solids or liquid or a mixture of solids and liquids. The NPS device was used in characterising a mixture of solid and liquid particles dispersed in air. It can be concluded that PMS which is based on shadow technique has been successfully developed and applied to the mixture of solid liquid particle. However, at present, the PMS has to be used in a well dispersion particles to prevent them from overlap. The PMS technique may not operate well in high dense mixture of solid and liquid flows.

Chapter 6

Conclusions and Suggestions for Future Work

6.1 Conclusions

A particle size measurement device called Non-intrusive Particle Sizer has been successfully developed. It can operate using three different techniques; shadow sizing, direct illumination and particle mixture shadow. The NPS is designed to provide nonintrusive on-line measurements of solid and liquid particles which are dispersed in a fluid medium. The NPS is based on imaging techniques, where the acquired images are processed and analysed to determine the required information. The main results and achievements of this thesis are summarised as follows:

- A new technique for measuring particle size that involves a mixture of solid and liquid particles has been developed. This technique, called PMS, is based on the shadow sizing technique. With an appropriate setting of the laser intensity and the image magnification factor, the acquired image of a mixture of opaque and transparent particles can be clearly visible. However, the particles have to be well dispersed to prevent the collision between solid and liquid particles. Also, the PMS is only limited to the particles which are fully transparent and opaque.
- Image processing software has been designed by applying algorithms to process and analyse all the acquired images. For PMS technique, the %Area has been introduced to distinguish between opaque and transparent particles. The use of %Area parameter

in characterising a mixture of solid and liquid particles is a key contribution in broadening the particle sizing measurement based on shadow technique.

- The sensitivity of image magnification factor (IMF) and laser intensity (LI) on the accuracy of particle size has been studied. Proprietary and certified microsphere particles are measured using shadow sizing techniques. It is found that the higher the IMF, the better accuracy can be achieved. The optimum setting of 0.8 for IMF has been used due to the lower mean error (<2%) and it can detect greater number of particles. In terms of LI, the setting of 90% is the best to produce a good image contrast. By implementing these optimum settings, the NPS has been validated against the certified microsphere particles. The results demonstrate excellent agreement for all the required calibration tests.
- Comparison between shadow technique and Scanning Electron Microscopy (SEM) results has shown good agreement for the measurement of Fillite particles. The discrepancy on the mean size found to be less than 5%. The measured particles shape recorded the value nearly 1.0, which is circular shape. This circular shape of Fillite particles is similar to the image captured by SEM.
- In DI technique, it is found that the size of opaque particle does not change at different scattering angle. The camera can be set at any scattering angle between 30° to 90° . However, transparent particle behave differently when it hits by incident light. Equal intensity of two glare points has been found at a scattering angle of around 70° . The equation of mean droplet size is introduced, where the distance of 2 glare points and their areas are measured. The equation does not require the value of

droplet refractive index (RI). The measured mean size was found to be larger by a factor of 1.2 compared to shadow technique. The drawback of this DI technique in measuring transparent particles is it can only operate at scattering angle around 70° , where both glare points are similar intensities.

- Generally, the NPS is designed to operate as a standalone device. It works best in measuring the sizes between $5\ \mu\text{m}$ to several millimetres depending on the optical configurations. The measured results are able to produce both number and volume size distributions. Instead of the sizes, the shape and the particle concentration are displayed in the developed software. However, the NPS may produce large error if the particles are overlapped. The NPS is designed without algorithms to analyse overlap particles due to the time consuming of the process. This is to ensure that the NPS can process and analyse the images in real-time.

To the author's knowledge, no previous attempt has been made to develop a technique to measure a mixture of opaque and transparent particles dispersed in air. This attempt has been successfully completed in this project showing that the ability of NPS in measuring these particles can be achieved using PMS technique.

6.2 Recommendations for further work:

A number of suggestions have been identified as ways in which the software may be improved:

- Further improvements on the PMS technique may be performed such as improvements related to the detection of a mixture of solid and liquid particles that are attached together. Methods to characterise the overlapped or attached particles may be studied to improve the technique.
- In DI technique, the captured images of liquid and solid particles appear to be different. Particles mixture characterisation may be possible by implementing DI technique. More studies may be conducted to acquire knowledge to distinguish these particles.
- This study is only concentrated on the measurement of opaque and transparent particles. Different refractive index of particles may affect the accuracy of the measurement. Detailed studies may be performed to investigate this behaviour.
- The purpose of the NPS may be extended to measure particles velocity. High repetition of pulsed laser and better image algorithms are required and further developments may be produced.

References

- [1] A. H. Lefebvre, *Atomization and sprays*: CRC Press, 1989.
- [2] H. G. Merkus, *Particle size measurements: fundamentals, practice, quality*: Springer, 2009.
- [3] C. T. Crowe, M. Sommerfeld, and Y. Tsuji, *Multiphase flows with droplets and particles*: CRC Press, 1998.
- [4] G. G. Nasr, A. J. Yule, and L. Bendig, *Industrial sprays and atomization: design, analysis and applications*: Springer Verlag, 2002.
- [5] T. Allen, *Particle size measurement*: Chapman & Hall, 1997.
- [6] M. Rhodes, *Introduction to particle technology*: Wiley, 2008.
- [7] B. Standard, "Particle size analysis-image analysis methods–Part 1," in *Static Image Analysis Methods* vol. 13322-1. London: British Standard, 2004.
- [8] R. Carter and Y. Yan, "Measurement of particle shape using digital imaging techniques," *Journal of Physics: Conference Series*, vol. 15, p. 177, 2005.
- [9] C. Tropea, "Optical particle characterization in flows," *Annual Review of Fluid Mechanics*, vol. 43, pp. 399-426, 2011.
- [10] W. Lauterborn and A. Vogel, "Modern optical techniques in fluid mechanics," *Annual Review of Fluid Mechanics*, vol. 16, pp. 223-244, 1984.
- [11] S. Thoroddsen, T. Etoh, and K. Takehara, "High-speed imaging of drops and bubbles," *Annu. Rev. Fluid Mech.*, vol. 40, pp. 257-285, 2008.
- [12] D. Lee Black, M. Q. McQuay, and M. P. Bonin, "Laser-based techniques for particle-size measurement: a review of sizing methods and their industrial applications," *Progress in Energy and Combustion Science*, vol. 22, pp. 267-306, 1996.

- [13] W. D. Bachalo, "Droplet analysis techniques: their selection and applications," *Liquid Particle Size Measurement Techniques: A Symposium*, 1984.
- [14] A. Jones, "A review of drop size measurement--the application of techniques to dense fuel sprays," *Progress in Energy and Combustion Science*, vol. 3, pp. 225-234, 1977.
- [15] D. S. Mahler and D. E. Magnus, "Hot-wire technique for droplet measurements," *Liquid Particle Size Measurement Techniques: A Symposium*, 1984.
- [16] K. May, "The cascade impactor: an instrument for sampling coarse aerosols," *Journal of Scientific Instruments*, vol. 22, p. 187, 1945.
- [17] K. Kim and W. R. M. JR, "Drop-size distributions from pneumatic atomizers," *AIChE Journal*, vol. 17, pp. 575-584, 1971.
- [18] K. May, "The measurement of airborne droplets by the magnesium oxide method," *Journal of Scientific Instruments*, vol. 27, p. 128, 1950.
- [19] H. C. Hulst and H. van de Hulst, *Light scattering by small particles*. New York: Dover Publications, 1981.
- [20] F. Durst, A. Melling, and J. Whitelaw, *Principles and practice of laser-doppler anemometry*. London: Academic Press 1976.
- [21] A. Tinke, K. Vanhoutte, F. Vanhoutte, M. De Smet, and H. De Winter, "Laser diffraction and image analysis as a supportive analytical tool in the pharmaceutical development of immediate release direct compression formulations," *International Journal of Pharmaceutics*, vol. 297, pp. 80-88, 2005.
- [22] A. Hewitt, "Droplet size spectra classification categories in aerial application scenarios," *Crop Protection*, vol. 27, pp. 1284-1288, 2008.
- [23] A. Tinke, A. Carnicer, R. Govoreanu, G. Scheltjens, L. Lauwerysen, N. Mertens, K. Vanhoutte, and M. Brewster, "Particle shape and orientation in laser

diffraction and static image analysis size distribution analysis of micrometer sized rectangular particles," *Powder Technology*, vol. 186, pp. 154-167, 2008.

- [24] E. Berrocal, "Multiple scattering of light in optical diagnostics of dense sprays and other complex turbid media," PhD, School of Engineering, Cranfield University, Cranfield, 2006.
- [25] M. Farooq, R. Balachandar, D. Wulfsohn, and T. Wolf, "PA--Precision Agriculture:: Agricultural sprays in cross-flow and drift," *Journal of Agricultural Engineering Research*, vol. 78, pp. 347-358, 2001.
- [26] E. Mulugeta and M. Geyer, "Characterising the washing processes of vegetables and potatoes," *Biosystems Engineering*, vol. 91, pp. 441-453, 2005.
- [27] D. Nuyttens, K. Baetens, M. De Schampheleire, and B. Sonck, "Effect of nozzle type, size and pressure on spray droplet characteristics," *Biosystems Engineering*, vol. 97, pp. 333-345, 2007.
- [28] H. E. Albrecht, *Laser doppler and phase doppler measurement techniques*: Springer Verlag, 2003.
- [29] S. Sankar, B. Weber, D. Kamemoto, and W. Bachalo, "Sizing fine particles with the phase Doppler interferometric technique," *Applied Optics*, vol. 30, pp. 4914-4920, 1991.
- [30] W. Bachalo, "Method for measuring the size and velocity of spheres by dual-beam light-scatter interferometry," *Applied Optics*, vol. 19, pp. 363-370, 1980.
- [31] Y. Liu and P. Daum, "The effect of refractive index on size distributions and light scattering coefficients derived from optical particle counters," *Journal of Aerosol Science*, vol. 31, pp. 945-957, 2000.
- [32] V. Leemans, H. Magein, and M. F. Destain, "AE--Automation and Emerging Technologies:: On-line fruit grading according to their external quality using machine vision," *Biosystems Engineering*, vol. 83, pp. 397-404, 2002.

- [33] J. B. Blaisot and J. Yon, "Droplet size and morphology characterization for dense sprays by image processing: application to the Diesel spray," *Experiments in Fluids*, vol. 39, pp. 977-994, 2005.
- [34] A. Aroussi, N. Lad, M. F. Muhamad Said, D. Adebayo, and M. Al-Atabi, "The interaction of a cold atomised spray with a circular cylinder," *Journal of Engineering Science and Technology*, vol. 5, pp. 361-372, 2010.
- [35] N. Fujisawa, A. Hosokawa, and S. Tomimatsu, "Simultaneous measurement of droplet size and velocity field by an interferometric imaging technique in spray combustion," *Measurement Science and Technology*, vol. 14, pp. 1341-1349, 2003.
- [36] R. M. Carter and Y. Yan, "On-line particle sizing of pulverized and granular fuels using digital imaging techniques," *Measurement Science and Technology*, vol. 14, pp. 1099-1109, 2003.
- [37] M. Butler Ellis, T. Swan, P. Miller, S. Waddelow, A. Bradley, and C. Tuck, "PM--Power and Machinery:: Design factors affecting spray characteristics and drift performance of air induction nozzles," *Biosystems Engineering*, vol. 82, pp. 289-296, 2002.
- [38] N. Lad, M. F. Muhamad Said, A. Aroussi, and D. Adebayo, "Experimental and computational characterisation of atomised spray flow around a circular cylinder," *Progress in Computational Fluid Dynamics, An International Journal*, vol. 10, pp. 232-238, 2010.
- [39] J. S. Rudolf, "Spray technology reference guide: understanding drop size," Spraying Systems Co.2006.
- [40] J. T. Kashdan, J. S. Shrimpton, and A. Whybrew, "A digital image analysis technique for quantitative characterisation of high-speed sprays," *Optics and Lasers in Engineering*, vol. 45, pp. 106-115, 2007.
- [41] J. T. Kashdan, J. S. Shrimpton, and A. Whybrew, "Two-phase flow characterization by automated digital image analysis. Part 2: Application of PDIA for sizing sprays," *Part. Part. Syst. Charact*, vol. 21, p. 23, 2004.

- [42] A. Lecuona, P. Sosa, P. Rodriguez, and R. Zequeira, "Volumetric characterization of dispersed two-phase flows by digital image analysis," *Measurement Science and Technology*, vol. 11, p. 1152, 2000.
- [43] J. T. Kashdan, J. S. Shrimpton, and A. Whybrew, "Two-phase flow characterization by automated digital image analysis. Part 1: Fundamental principles and calibration of the technique," *Part. Part. Syst. Charact*, vol. 20, p. 397, 2003.
- [44] W. Witt, U. Köhler, and J. List, "Direct imaging of very fast particles opens the application of powerful (dry) dispersion for size and shape characterisation," 2004.
- [45] K. P. Sudheer and R. K. Panda, "Digital image processing for determining drop sizes from irrigation spray nozzles," *Agricultural Water Management*, vol. 45, pp. 159-167, 7 2000.
- [46] R. Carter, Y. Yan, and S. Cameron, "On-line measurement of particle size distribution and mass flow rate of particles in a pneumatic suspension using combined imaging and electrostatic sensors," *Flow Measurement and Instrumentation*, vol. 16, pp. 309-314, 2005.
- [47] H. C. Van de Hulst and R. T. Wang, "Glare points," *Applied Optics*, vol. 30, pp. 4755-4763, 1991.
- [48] C. F. Hess and D. L'Esperance, "Droplet imaging velocimeter and sizer: a two-dimensional technique to measure droplet size," *Experiments in Fluids*, vol. 47, pp. 171-182, 2009.
- [49] M. F. Muhamad Said and A. Aroussi, "On-Line Measurement of Droplet Size using Digital Imaging Analysis Techniques," in *The 14th International Symposium on Flow Visualization (ISFV14)*, EXCO, Daegu, South Korea, 2010.
- [50] M. Maeda, T. Kawaguchi, and K. Hishida, "Novel interferometric measurement of size and velocity distributions of spherical particles in fluid flows," *Measurement Science and Technology*, vol. 11, p. L13, 2000.

- [51] A. Glover, S. Skippon, and R. Boyle, "Interferometric laser imaging for droplet sizing: a method for droplet-size measurement in sparse spray systems," *Applied Optics*, vol. 34, pp. 8409-8421, 1995.
- [52] G. König, K. Anders, and A. Frohn, "A new light-scattering technique to measure the diameter of periodically generated moving droplets," *Journal of Aerosol Science*, vol. 17, pp. 157-167, 1986.
- [53] R. Ragucci, A. Cavaliere, and P. Massoli, "Drop sizing by laser light scattering exploiting intensity angular oscillation in the mie regime," *Particle & Particle Systems Characterization*, vol. 7, pp. 221-225, 1990.
- [54] N. Damaschke, H. Nobach, T. Nonn, N. Semidetnov, and C. Tropea, "Multi-dimensional particle sizing techniques," *Experiments in Fluids*, vol. 39, pp. 336-350, 2005.
- [55] A. Grabmann and F. Peters, "Size measurement of very small spherical particles by mie scattering imaging (msi)," *Particle & Particle Systems Characterization*, vol. 21, pp. 379-389, 2004.
- [56] K. Hesselbacher, K. Anders, and A. Frohn, "Experimental investigation of Gaussian beam effects on the accuracy of a droplet sizing method," *Applied Optics*, vol. 30, pp. 4930-4935, 1991.
- [57] P. Lemaitre, E. Porcheron, A. Nuboer, and G. Grehan, "Interferometric laser imaging development for droplets sizing (ILIDS) in hostile environment," *ICLASS, Kyoto, Japan. Aug, 2007*.
- [58] C. Mounaïm-Rousselle and O. Pajot, "Droplet sizing by Mie scattering interferometry in a spark ignition engine," *Particle & Particle Systems Characterization*, vol. 16, pp. 160-168, 1999.
- [59] M. Maeda, Y. Akasaka, and T. Kawaguchi, "Improvements of the interferometric technique for simultaneous measurement of droplet size and velocity vector field and its application to a transient spray," *Experiments in Fluids*, vol. 33, pp. 125-134, 2002.

- [60] N. Roth, K. Anders, and A. Frohn, "Refractive-index measurements for the correction of particle sizing methods," *Applied Optics*, vol. 30, pp. 4960-4965, 1991.
- [61] B. Mulhem, G. Schulte, and U. Fritsching, "Solid-liquid separation in suspension atomization," *Chemical Engineering Science*, vol. 61, pp. 2582-2589, 2006.
- [62] U. Fritsching, B. Mulhem, O. Kurt, and G. Schulte, "Influence of suspended solid particles on suspension atomization processes."
- [63] D. Fernández Alonso, J. Gonçalves, B. Azzopardi, and J. Coury, "Drop size measurements in Venturi scrubbers," *Chemical Engineering Science*, vol. 56, pp. 4901-4911, 2001.
- [64] M. Honkanen, P. Saarenrinne, T. Stoor, and J. Niinimäki, "Recognition of highly overlapping ellipse-like bubble images," *Measurement Science and Technology*, vol. 16, p. 1760, 2005.
- [65] X. Zabulis, M. Papara, A. Chatziargyriou, and T. Karapantsios, "Detection of densely dispersed spherical bubbles in digital images based on a template matching technique:: Application to wet foams," *Colloids and Surfaces A: Physicochemical and Engineering Aspects*, vol. 309, pp. 96-106, 2007.
- [66] BS-ISO, "Representation of results of particle size analysis—Part 1," in *Graphical representation* vol. 9276-1. London: British Standard, 1998.
- [67] BS, "Methods for determination of particle size distribution - Part 4," in *Guide to microscope and image analysis methods* vol. 3406-4. London: British Standard, 1993.
- [68] S. Allaire and L. E. Parent, "Size guide number and Rosin-Rammler approaches to describe particle size distribution of granular organic-based fertilisers," *Biosystems Engineering*, vol. 86, pp. 503-509, 2003.

- [69] BS-ISO, "Representation of results of particle size analysis—Part 2," in *Calculation of average particle sizes / diameters and moments from particle size distributions* vol. 9276-2. London: British Standard, 2001.
- [70] A. Ryer, *Light measurement handbook*: International Light Inc., 1998.
- [71] <http://www.antonine-education.co.uk>.
- [72] SONY, *Digital Camera Module - Technical Manual*: SONY Corporation, 2007.
- [73] M. Csele, *Fundamentals of light sources and lasers*: Wiley Interscience, 2004.
- [74] NI, *NI Vision Concept Manual*: National Instruments, 2007.
- [75] M. Petrou and P. Bosdogianni, *Image processing: the fundamentals*: Wiley, 1999.
- [76] B. Standard, "Particle size analysis-image analysis methods—Part 2," in *Dynamic Image Analysis Methods* vol. 13322-2. London: British Standard, 2006.

Appendix A

Publications, Recognitions, Conferences

A.1 Recognitions

- 1) June 2009: Top 10 for poster presentation at the Festival of Postgraduate Research in University of Leicester, UK (Title: Taming the Droplets)
- 2) July 2009: Selected to represent the University of Leicester in poster presentation at the Vitae's Regional Competition, University of Nottingham, UK (Title: Taming the Droplets)

A.2 List of Journal Publications

- 1) N. Lad, A. Aroussi, **M.F. Muhamad Said**. Droplet Size Measurement for Liquid Spray using Digital Image Analysis Technique. Journal of Applied Sciences, ISSN 1812-5654, 2011.
- 2) Aroussi, N. Lad, **M.F. Muhamad Said**, D. Adebayo, M. Al-Atabi. The Interaction of a Cold Atomised Spray with a Circular Cylinder. Journal of Engineering Science and Technology, vol. 5, pp. 361-372, 2010.
- 3) N. Lad, **M.F. Muhamad Said**, A. Aroussi, D. Adebayo. Experimental and Computational Characterisation of Atomised Spray Flow Around a Circular Cylinder. Progress in Computational Fluid Dynamics, An International Journal. vol. 10, pp. 232-238, 2010.

A.3 List of Proceeding Publications

- 1) Norasikin Mat Isa, **M.F. Muhamad Said**, A. Aroussi. A Particulate Monitor for Carbon Beneficiation Enhancement. International Symposium on Environment Friendly Energies in Electrical Applications (EFEEA). Ghardaia, Algeria, 2010.
- 2) **M.F. Muhamad Said** and A. Aroussi. On-Line Measurement of Droplet Size using Digital Imaging Analysis Techniques. The 14th International Symposium on Flow Visualization. Daegu, Korea, 21 ~ 24 June 2010.
- 3) **M.F. Muhamad Said**, A. Aroussi and N. Lad. Droplet Size Measurement for Liquid Spray using Digital Image Analysis Technique. The 2nd International Conference on Plant Equipment and Reliability (ICPER2010). Kuala Lumpur, 15 ~ 17 June 2010
- 4) A. Aroussi, **M.F. Muhamad Said**, and N. Lad. The Design of a Spray Characteriser. 4th Algerian Congress of Process Engineering 2009. Algiers, Algeria, 2009.
- 5) **M.F. Muhamad Said**, N. Lad, and A. Aroussi. Impingement of a Liquid Spray on a Convex Surface. 4th Algerian Congress of Process Engineering 2009. Algiers, Algeria, 2009.
- 6) **M.F. Muhamad Said** and A. Aroussi. An On-Line Particle Characterisation Device. The 3rd International Conference on Mechatronics (ICOM'08). Kuala Lumpur, Malaysia, 2008.
- 7) **M.F. Muhamad Said** and A. Aroussi. A Non-Intrusive Spray Characteriser. The 4th International Symposium on Hydrocarbons and Chemistry. Ghardaia, Algeria, 2008.

A.4 List of Oral Presentations

- 3) 2010: Paper presentation at the 14th International Symposium on Flow Visualization (*Daegu - South Korea*).
- 4) 2009: Paper presentation at the 4th Algerian Congress of Process Engineering (*Algiers - Algeria*).
- 5) 2009: Poster presentation at the 4th Festival of Postgraduate Research at University of Leicester. (*Leicester - UK*).
- 6) 2009: Poster presentation at the Vitae's Regional Competition in University of Nottingham. (*Nottingham - UK*).
- 7) 2008: Paper presentation at the The 4th International Symposium on Hydrocarbons and Chemistry (*Ghardaia - Algeria*).

Appendix B

Dynamic Image Analysis Software

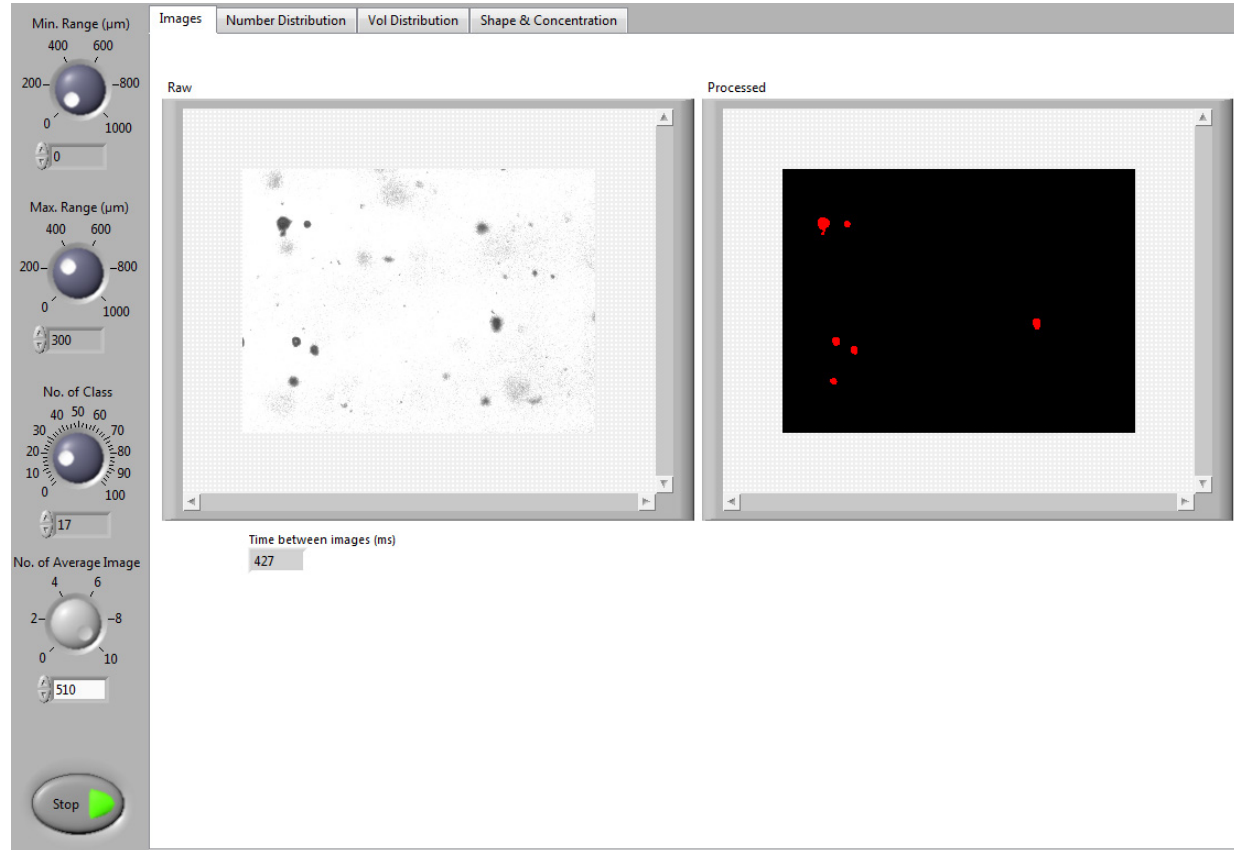


Figure B.1: Front panel of the DIA software shows the captured and processed images.

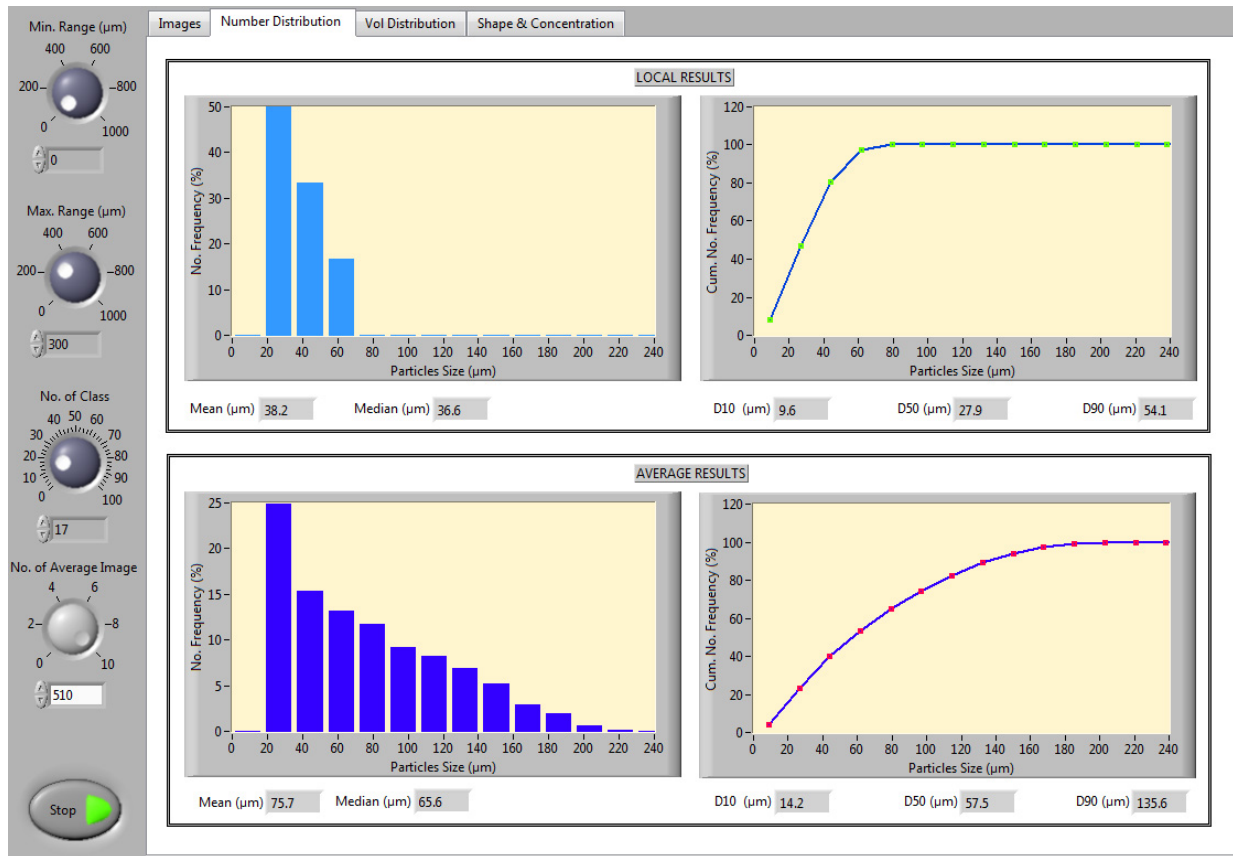


Figure B.2: Front panel of the DIA software shows the size number distribution of local and average values.

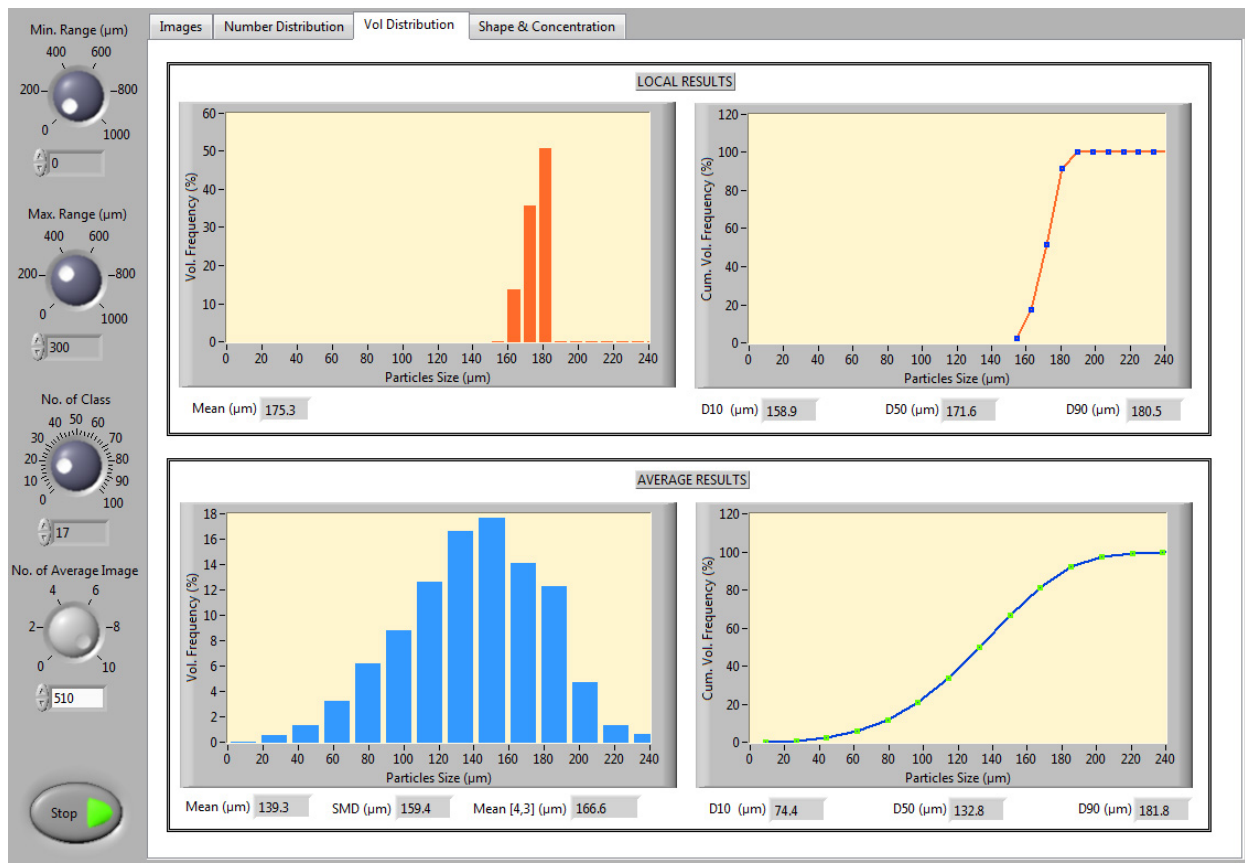


Figure B.3: Front panel of the DIA software shows the size volume distribution of local and average values.

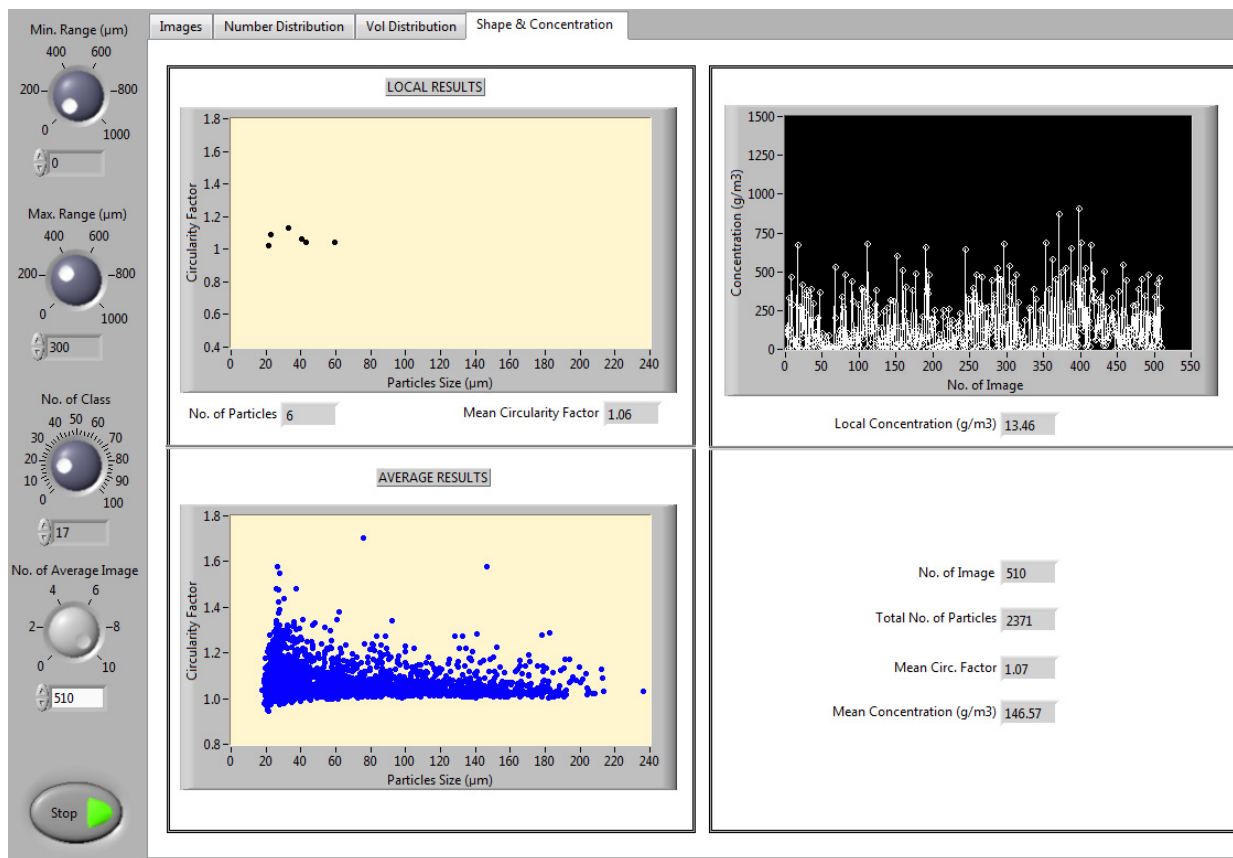


Figure B.4: Front panel of the DIA software shows the distribution of circularity factor and particle concentration for local and average values.

Appendix C

Certificate of Size Calibration

Thermo
SCIENTIFIC

Part of Thermo Fisher Scientific

DUKE STANDARDS™ Microsphere Size Standards NIST Traceable Mean Diameter

1. DESCRIPTION. These particle size standards provide accurate and traceable size calibration for particle size analysis. They are part of a series of polymer microspheres with calibrated mean diameters traceable to the Standard Meter through the National Institute of Standards and Technology (NIST). Diameters from 20 nanometers (nm) to 160 micrometers (µm) are available as aqueous suspensions in dropper-tipped vials, calibrated by photon correlation spectroscopy (PCS), transmission electron microscopy (TEM) or optical microscopy. The aqueous medium has been prepared to promote dispersion and reduce clumping of the particles. The approximate particle concentration in percent solids is given to facilitate dilution for the calibration and validation of particle analyzers. Diameters from 200 µm to 1000 µm are available as dry spheres, calibrated by optical microscopy. The certified mean diameter is traceable to NIST. Other values are for information only and should not be used as calibration values.

2. PHYSICAL DATA	Catalog Number: 4270A, Nominal 70 µm
Certified Mean Diameter:	72.3 µm ± 1.3 µm, k=2
Standard Deviation:	0.9 µm
Coefficient of Variation:	1.2%
Microsphere Composition:	Polystyrene
Microsphere Density:	1.05 g/cm ³
Index of Refraction:	1.59 @ 589 nm
Approximate Concentration:	2.1% solids

- Continued on page 2

CERTIFICATE OF CALIBRATION AND TRACEABILITY

This certifies that the calibrated mean diameter dimension of this product was transferred by optical microscopy from a stage micrometer calibrated by the National Institute of Standards and Technology (SRM 2800 SN411). NIST Standard Reference Materials 1690, 1692, 1960, and 1961 were used to validate the accuracy and traceability of the calibration methods.

Catalog Number:	4270A, Duke Standards™ Microsphere Size Standards
Certification Date:	February 10, 2010
Certified Batch:	4270-004
Production Batch:	4270-009
Certified Mean Diameter:	72.3 µm
Uncertainty:	± 1.3 µm, k=2


Ellen B. Layendecker, Metrology Director
Thermo Fisher Scientific Particle Technology



Packaging Lot # **36878**
Specialty Diagnostics Group

46360 Fremont Blvd.

Expiration Date:
Fremont, CA
94538

(510) 979-5000
(510) 979-5002 fax

APR 10

www.thermo.com/particletechnology

3. MEASUREMENT METHODOLOGY The certified diameter of this product was transferred by optical microscopy from an stage micrometer, a glass slide with a scale with line spacing calibrated by NIST in micrometers. The uncertainty is calculated from the calibration transfer uncertainty and the random error of the measurements per NIST Technical Note 1297. The uncertainty listed is the expanded uncertainty, with a coverage factor of 2 ($k=2$). To validate the accuracy of our optical methods, NIST certified microsphere standards were measured by the same method. The size distribution (standard deviation) was obtained by optical microscopy, electron microscopy or electrical resistance analysis depending on the size of the particles. The coefficient of variation is the standard deviation as a percentage of the mean diameter.

4. CERTIFICATE Except for the purposes of record keeping, this certificate may not be reproduced. Rebottling or relabeling voids the warranty and invalidates the certification and traceability of these products. The Certified Batch is the master batch of material that is measured and certified with a NIST traceable mean diameter. The Production Batch represents the intermediate material from which the final product is made. Several Production Batches can be made from one Certified Batch.

5. OPERATING INSTRUCTIONS For ease of use, standards with mean diameters below 200 μm are packaged in an aqueous suspension. They must be thoroughly dispersed in the bottle to ensure statistically consistent samples. To disperse the particles, gently invert the bottle several times, then immerse in a low power ultrasonic bath (10 seconds). Do not shake the bottle, as the small bubbles formed may introduce statistical artifacts. Before using, clear the tip of residue by dispensing 2 - 3 drops into a waste container. Dispense immediately after dispersion using the dropper tip. Standards 200 μm and larger are dry and should not be shaken as this may produce static, making the particles hard to handle.

6. SAFETY AND HANDLING PRECAUTIONS Avoid aerosol production in the workplace while handling these products, or wear a suitable filter respirator when necessary. Avoid inhalation or ingestion of the particles. These products should only be used by trained scientific personnel. A Material Safety Data Sheet is included with each package.

7. STORAGE AND DISPOSAL Keep the bottle tightly sealed to avoid contamination. Store aqueous standards upright to prevent clogging the tip with particles. Refrigeration is not required for storage. Do not freeze the particles. In case of spills, wash or wipe the area thoroughly. Caution: surfaces covered with dry spheres may be very slippery. Wipe area with damp cloth. Dispose of as normal laboratory waste. There are no special disposal procedures. Each bottle has a limited shelf life and should not be used after its expiration date.

8. LIMITED WARRANTY These products are intended for laboratory use by trained scientific personnel. Determination of their suitability for a specific end-use is the responsibility of the user, who assumes all liability for loss or damage arising out of the use of the product. Rebottling or relabeling voids the warranty and certification. Microgenics Corporation's warranty is limited to replacement of defective products if returned with our authorization within 60 days of purchase date.

THE FOREGOING WARRANTY SHALL BE IN LIEU OF ANY OTHER WARRANTIES, EXPRESS OR IMPLIED, INCLUDING WITHOUT LIMITATION, ANY IMPLIED WARRANTY OF MERCHANTABILITY AND FITNESS FOR A PARTICULAR PURPOSE. IN NO EVENT SHALL MICROGENICS BE LIABLE FOR INDIRECT, SPECIAL, INCIDENTAL OR CONSEQUENTIAL DAMAGES.